

Impacts of Environmental Structure on Resilience of Yeasts to Stress

Harry James Harvey

Thesis submitted to the University of Nottingham (UK)
for the degree of Doctor of Philosophy



**University of
Nottingham**
UK | CHINA | MALAYSIA

School of Life Sciences

2021

ABSTRACT

Ubiquitously, the environments of microorganisms have three-dimensional structure that create heterogeneous distributions of the space in which microorganisms reside. In particular, the soil environment is a complex porous medium inhabited by a vast array of microorganisms, essential for Earth processes like biogeochemical cycling. However, these microorganisms are subject to environmental perturbation. The physiological impacts of environmental stress on microorganisms are well studied, but whether (and to what extent) soil structure impacts exposure and response of microorganisms to stressors remains poorly understood. In this thesis, it was hypothesised that environmental structures could influence the stressor exposure of cells (and hence stressor survival) within them, and that the extent of this protective effect would depend on the type and scale of environmental structure. To examine this overall hypothesis, the influence of environmental structures on microbial response (or survival) to stress were assessed: first in relation to soil aggregation, then within macroscale pores ranging from 0.5 – 2 mm in diameter and last within micrometre scale structures using microfluidic approaches.

A method was developed to manufacture soil aggregates from natural soils with defined quantities of soil yeast in the aggregate exterior or interior. This was used to examine the impact of soil aggregation on microbial survival of a small panel of stressors (anoxia, lead nitrate, and heat stress). Results indicated that yeast cells inside aggregates were protected from acute heat stress relative to cells at the aggregate exterior, whereas effects of aqueous lead nitrate or anoxia were similar on cells at either location. The protective effect against heat stress was compromised after prolonged heat exposure but was accentuated within compacted versions of soil aggregates, providing evidence that soil compaction, a common consequence of agricultural activity, can influence microbial stress resilience.

In further experiments, structured environments with millimetre-scale pores were developed by setting up vessels containing glass beads of different sizes. Yeast

inocula and stressors were introduced to these to explore the relationship between the environmental pore size and stress survival. Here, it was demonstrated that survival of yeast in response to lead nitrate within these structures increased with decreasing average pore size. This trend was reproduced using additively-manufactured (3D-printed) lattice structures, containing pores of similar size ranges to the less-uniform glass bead structures.

Finally, microfluidic devices were used to determine whether structure at the microscale impacted microbial survival of stress. These devices contained either fabricated soil-like structures, or small microspheres to create simplified structures within otherwise homogeneous environments. At this scale, an impact of environmental structure was less clear. However, in the simplified microsphere environments, results suggested that cells within more confined spaces (i.e., more surrounded by protective structures) were less exposed to stressor (copper sulfate), which was introduced as a flowing solution within the microfluidic devices.

Taken together, results from this thesis suggest that environmental structure can determine microbial (exposure to and) survival of stress, at scales of structure ranging from micrometres to millimetres. The new methodologies and results developed within this thesis provide a foundation upon which the relationship between microbial perturbation and environmental structure can be further explored.

PUBLICATIONS

HARVEY, H. J., WILDMAN, R. D., MOONEY, S. J. & AVERY, S. V. 2020. Soil aggregates by design: Manufactured aggregates with defined microbial composition for interrogating microbial activities in soil microhabitats. *Soil Biology and Biochemistry*, **148**, 107870.

HARVEY, H. J., WILDMAN, R. D., MOONEY, S. J. & AVERY, S. V. 2020. Challenges and approaches in assessing the interplay between microorganisms and their physical micro-environments. *Computational and Structural Biotechnology Journal*, **18**, 2860-2866.

HARVEY, H. J., WILDMAN, R. D., MOONEY, S. J. & AVERY, S. V. 2021. Microbial metal resistance within structured environments is inversely related to environmental pore size. Accepted manuscript in *Applied and Environmental Microbiology*.

ACKNOWLEDGEMENTS

Firstly, I would like to express my sincerest gratitude to my supervisor Professor Simon Avery for his valued guidance and support throughout my project. I would also like to thank my co-supervisors, Professor Sacha Mooney and Professor Ricky Wildman for their guidance and multidisciplinary expertise.

I am tremendously grateful to my friends and colleagues in B44 for their support and friendship, both inside and outside of the lab. I would particularly like to thank Matt Kokolski for his technical support and for keeping the lab together in one piece and the seemingly endless library of expertise that is Dr. Cindy Vallieres for her continued advice and discussion. Special thanks also to the D&D gang for all of our fantastical exploits and escapism from the world of academia.

And finally, I would like to thank my loved ones; without them I most certainly not be where I am today. I thank my mum and dad for their constant support throughout my life and academic career and for always encouraging me to persevere and do what makes me happy. Last but not least, I thank my wonderful fiancée, Bryony, for always being there for me, through the highs and the lows, and for making my life an adventure.

CONTENTS

Abstract.....	i
Publications.....	iii
Acknowledgements	iv
Contents.....	v
List of Figures	x
List of Tables.....	xii
List of Abbreviations and Symbols.....	xiii
1 General Introduction.....	1
1.1 The structured environments of microorganisms	1
1.1.1 Methods for investigating microbial (micro)environments.....	4
1.2 Soil as a Structured Environment	8
1.2.1 Soil texture	8
1.2.2 Soil Aggregation	11
1.2.3 Soil Pore Space	13
1.3 Microorganisms in Soil and their Importance.....	16
1.3.1 Yeasts in Soil.....	16
1.3.2 Importance of Soil Microorganisms.....	18
1.3.3 Phenotypic heterogeneity in microorganisms.....	20
1.4 Interactions between Microorganisms and Soil Structure	24
1.4.1 The Impact of soil structure on microbial communities.....	25
1.4.2 The impact of microbial communities on soil structure	27
1.5 The Impact of Environmental Perturbation on Soil Microorganisms	29
1.6 Impacts of Soil Disturbance and Global Environmental Change.....	29
1.6.1 Perturbation in soil temperature and moisture	30
1.6.2 Perturbation in soil oxygen	31
1.6.3 Metal Pollution.....	32
1.7 Summary and Thesis Aims.....	34
1.7.1 Aims.....	36

2	The Impact of Soil Aggregation on Microbial Stress Resistance.....	37
2.1	Introduction.....	37
2.1.1	Aims.....	38
2.2	Materials and Methods	40
2.2.1	Yeast strains and culture conditions.....	40
2.2.2	Soil preparation.....	41
2.2.3	Production of manufactured soil aggregates and incorporation and recovery of microorganisms	41
2.2.4	Selective recovery of organisms from the aggregate interior and exterior	42
2.2.5	Assessing colony area variation in isolates of <i>S. podzolica</i>	44
2.2.6	Manufacturing aggregates for stress response experiments	45
2.2.7	X-ray Computed Tomography (CT)	46
2.2.8	Water evaporation analysis	47
2.2.9	Stress survival of cells located within and outside of aggregates	47
2.3	Results	49
2.3.1	Manufacture of discrete soil aggregates mimicking natural aggregates and introduction of organisms to aggregate-interior or -exterior	49
2.3.2	Phenotypic heterogeneity of <i>S. podzolica</i> in the aggregate interior or exterior	54
2.3.3	Cells within aggregates show stressor-dependent, differential survival compared with cells at aggregate surfaces	60
2.3.4	The impact of altering aggregate physical characteristics on survival of <i>S. podzolica</i> within an aggregate	63
2.4	Discussion	68
2.4.1	Manufacture of aggregates.....	68
2.4.2	Recovery of organisms from manufactured and natural aggregates..	69
2.4.3	Interaction between organism heterogeneity and position in soil aggregates.....	70
2.4.4	Survival of stress by organisms with respect to aggregate location....	73
2.4.5	Conclusions	78
3	The Impact of Inter-Particle Pore Size on Microbial Stress Resistance	79

3.1	Introduction.....	79
3.1.1	Aims.....	81
3.2	Materials and Methods	82
3.2.1	Yeasts and culture conditions	82
3.2.2	<i>S. podzolica</i> IC ₅₀ and heterogeneity measurements.....	82
3.2.3	iChip design, production, and testing	84
3.2.4	Inoculating glass beads with yeast.....	86
3.2.5	Preparation of glass bead structures	87
3.2.6	X-ray Computer Tomography (CT) and image analysis.....	87
3.2.7	Stress resistance assays	88
3.2.8	Outgrowth of organisms from glass beads	88
3.2.9	Manufacturing lattice structures	91
3.2.10	Stress survival assays in manufactured lattices	92
3.2.11	Determination of lead content of yeast cells in lattice structures	93
3.2.12	Inductively coupled plasma mass spectrometry (ICP-MS).....	93
3.2.13	Determining effect of cell concentration.....	93
3.2.14	Statistical analysis	95
3.3	Results	96
3.3.1	iChip manufacture and testing.....	96
3.3.2	Production of glass bead structures with different pore sizes	98
3.3.3	Assay of stress resistance using recovery of yeast from inoculated beads	100
3.3.4	Environmental pore size impacts lead nitrate resistance in yeast	102
3.4	Discussion	113
3.4.1	Creating three-dimensional structures that support assay of microbial stress resistance	113
3.4.2	Pore size of an organism's (micro-)environment impacts resistance to stress	115
3.4.3	Conclusions	119
4	Structures at the microscale- a microfluidics approach	120
4.1	Introduction.....	120

4.1.1	Aims.....	122
4.2	Materials and Methods	123
4.2.1	Yeast strains and culture conditions	123
4.2.2	Determination of cellular GFP.....	124
4.2.3	Soil micromodel setup	124
4.2.4	Stress experiments within soil micromodel devices.....	126
4.2.5	Stress experiments within CellASIC ONIX II microfluidic devices	127
4.2.6	Microscopy and imaging	132
4.2.7	Image analysis	133
4.3	Results	136
4.3.1	Using fluorescent protein expression as a proxy for cellular exposure to stressor	136
4.3.2	Use of defined “spatial metrics” to quantify a cell’s local environmental structure.....	138
4.3.3	Examining the relationship between environmental structure and microbial stress response	141
4.4	Discussion	155
4.4.1	Developing spatial metrics and experimental parameters.....	155
4.4.2	The impact of microscale environmental structure on stress response	157
4.4.3	Conclusion	162
5	Summary and Concluding Remarks	163
5.1	Summary of Results.....	163
5.2	Key Themes and Discussion.....	164
5.2.1	General relationships between stress resistance and environmental structure.....	164
5.2.2	Microbial heteroresistance	165
5.3	Future Work	166
	Appendix A	168
	Appendix B	170
	Appendix C	170

Appendix D.....	171
Appendix E	172
Appendix F.....	174
References.....	175

LIST OF FIGURES

Figure 1.1- Simplified schematic of structured (micro)environments, as they may be modelled in the laboratory, and emergence of heterogeneous landscapes.....	3
Figure 1.2- Illustration of general aggregate structure.....	11
Figure 1.3- An illustration of the concept of pore space and pore connectivity	15
Figure 1.4- An example of homogeneity and heterogeneity in response to lead (Pb) stress	21
Figure 2.1- Outline of procedure for producing soil aggregates	46
Figure 2.2- Optimising parameters for manufacture of soil aggregates	50
Figure 2.3- Comparison of porous structure of natural and manufactured soil aggregates.....	51
Figure 2.4- Recovery of cells from the exterior or interior of the same manufactured aggregate.....	53
Figure 2.5- Variation in recovery of CFU from aggregates	54
Figure 2.6- Colony area variation on MYP and YEPD agar of <i>S. podzolica</i> isolated from either the interior or exterior of aggregates from an agricultural soil.....	57
Figure 2.7- Location specific stress resistance of low- and high-heteroresistance yeast isolates	59
Figure 2.8- The survival (% CFU versus control) of <i>S. podzolica</i> within or on the surface of soil aggregates in response to different stresses	62
Figure 2.9- Varying vortex settings can alter aggregate pore properties.....	64
Figure 2.10- The survival (% CFU versus control) of <i>S. podzolica</i> interior and exterior of regular or compacted soil aggregates	66
Figure 2.11- Water evaporation curves of regular and compacted aggregates under conditions mimicking heat stress experiment	67
Figure 3.1- Iterations of iChip designs and assembly	85
Figure 3.2- Illustration of use of y-intercept extrapolation from exponential growth curves to estimate starting OD	91
Figure 3.3- Production of structured environments of varying pore-space ESD.....	99
Figure 3.4- The y-intercept of bead outgrowth correlates with level of stress.....	101

Figure 3.5- Impact of environmental structure heterogeneity on survival of <i>S. podzolica</i> during lead nitrate stress.....	103
Figure 3.6- The survival of lead stress by <i>S. podzolica</i> in bead structures decreases with increasing pore size.....	105
Figure 3.7- The survival of lead stress by <i>S. podzolica</i> in lattice structures decreases with increasing pore diameter.....	107
Figure 3.8- Analysis of lead recovered from lattice-stress experiments and structureless experiments.....	110
Figure 3.9- Assessing the potential impact of cell density on lead resistance	112
Figure 4.1- Overview of soil micromodel setup.....	126
Figure 4.2- Overview of the CellASIC ONIX II microfluidic system and microfluidic plates.....	128
Figure 4.3- Expression of GFP under the CUP1 promoter correlates with copper concentration after 1 hr and 2 hr exposure.....	137
Figure 4.4- Temperature-dependent Hsp104-GFP expression under the native <i>HSP104</i> promoter.....	138
Figure 4.5- Exploring spatial metrics as a method of describing the spatial relationships between objects.....	140
Figure 4.6- Representative microscopic images of soil micromodels	142
Figure 4.7- The trialled spatial metrics do not predict cellular stress response.....	144
Figure 4.8- Illustration of CellASIC trap plates and environments with added microspheres for structure	146
Figure 4.9- Examining flow rate differences in traps with and without microspheres	147
Figure 4.10- Increasing environmental structure density decreases cell stressor exposure.....	149
Figure 4.11- Comparison of single-cell spatial measures and copper responses between traps of different microsphere densities.....	150
Figure 4.12- Reducing flow rate of copper-supplemented medium into the microfluidic traps reduces the cellular copper response	152
Figure 4.13- Differences in microsphere frequency at different angles and distances from the least and most copper-responsive fluorescent cells	154

LIST OF TABLES

Table 1- Soil separates are classified by their diameter, ranging from 2 mm to below 2 μm (USDA).....	9
Table 2- IC_{50} , heterogeneity values for listed <i>S. podzolica</i> isolates.	83

LIST OF ABBREVIATIONS AND SYMBOLS

µg	Microgram
µl	Microlitre
µm	Micrometre
µM	Micromolar
3D	3-Dimensional
CAD	Computer-aided design
CCD	Charge-coupled device
CFU	Colony forming units
cm	centimetre
CO ₂	Carbon Dioxide
CT	Computed tomography
CV	Coefficient of variation
DNA	Deoxyribonucleic acid
EPS	Extracellular polymeric substances
ESD	Equivalent spherical diameter
FITC	Fluorescein-5-isothiocyanate
hr	Hour(s)
IAA	indole-3-acetic acid
IC ₅₀	Half maximal inhibitory concentration
IPCC	Intergovernmental Panel on Climate Change
ITS	Internal transcribed spacer
mg	milligrams
min	Minute(s)
mm	millimetres
mM	Millimolar
MYP	Malt, yeast extract, peptone
N ₂	Dinitrogen
NA	Sodium
NH ₃	Ammonia
NH ₄	Ammonium
nM	Nanomolar
NO ₃	Nitrate
NOH	Sodium Hydroxide
OD	Optical density
OM	Organic matter
PBS	Phosphate-buffered saline
PCR	Polymerase chain reaction
PDMS	Polydimethylsiloxane
PSI	Pound-force per square inch
R6G	Rhodamine-6-G
RAPD	Random Amplified Polymorphic DNA
RNA	Ribonucleic acid
s	Second(s)
SEM	Standard error of the mean

SLA	Stereolithography
SLIM	School of Life Science Imaging
SO ₄	Sulfate
SOC	Soil organic carbon
SOM	Soil organic matter
USDA	United States Department of Agriculture
YEPD	Yeast extract, peptone, dextrose
YNB	Yeast Nitrogen Base (Without Amino Acids)

1 GENERAL INTRODUCTION

1.1 The Structured Environments of Microorganisms

Microorganisms such as bacteria and fungi very rarely exist in isolation and are subject to conditions prevailing in their external environments. Both abiotic (nutrients, oxygen, temperature etc.) and biotic factors can shape their environment, influencing metabolic activity and proliferation. Microorganisms persist in diverse environments, including in aqueous solutions, on solid surfaces, or even suspended indefinitely within the troposphere (DeLeon-Rodriguez et al., 2013). Further to this, these environments are very rarely homogeneous, as many of the environmental factors mentioned above can fluctuate spatially and temporally. For example, nutrients typically are not equally distributed within an environment. A key factor in the heterogeneous distribution of abiotic and biotic environmental components is environmental structure.

Almost ubiquitously, the environments of microorganisms have three-dimensional structure and create heterogeneous distributions of the space in which microorganisms reside. Here, the term “structured environments” is defined as habitats where the arrangement of the solid phase (pores/surfaces/walls) impose or facilitate the formation of spatial gradients and environmental heterogeneity (**Figure 1.1**). Broadly speaking, structured environments, from the nanometre to centimetre scale, produce a spatially heterogeneous distribution of abiotic factors such as nutrients, water, and oxygen (Schlüter et al., 2018, Borer et al., 2018, Young and

Crawford, 2004) and of the microorganisms living within these environments. The extent of this heterogeneity also varies between environments. For example, nutrient concentrations may be more homogeneous when distributed in an entirely aqueous environment than one composed of both aqueous and solid or gaseous phases. This organisation of abiotic and biotic factors can be determined by structure in several ways, such as the existence of spaces or pores of small sizes that physically exclude some organisms or of oxygen gradients that are preferential to either anaerobic or aerobic organisms (Borer et al., 2018) (**Figure 1.1**). This means that an environment structured in this way naturally establishes a heterogeneous landscape in which microorganisms fall into a range of niches to which they may, over time, adapt further.

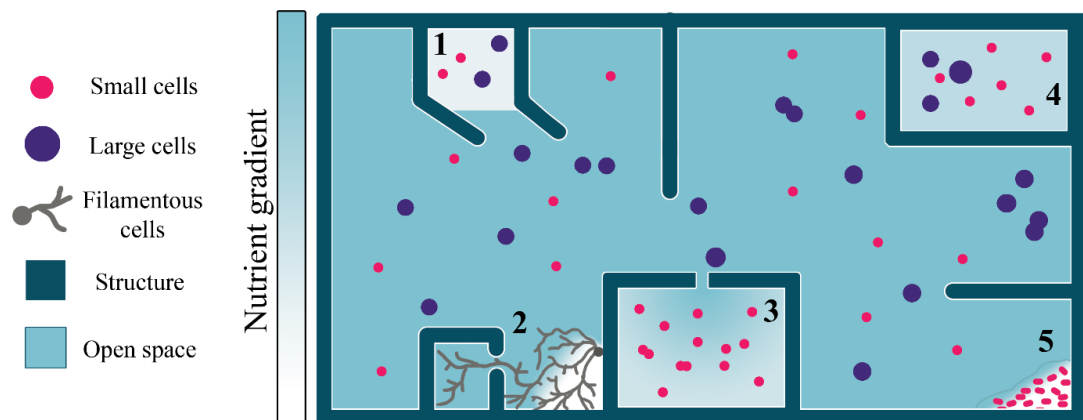


Figure 1.1- Simplified schematic of structured (micro)environments, as they may be modelled in the laboratory, and emergence of heterogeneous landscapes.

Environments are typically structured by the division of space by physical structure, creating gradients of resources needed for growth, and the physical separation of microorganisms. Physical structures can create phase boundaries (1) which limit nutrient diffusion, as well as size-selective pores (3) and the separation of space into isolated environments (4) which can isolate both organisms and nutrients, potentially leading to localised nutrient depletion and localised adaptations by the organisms. Microorganisms can also create structure within their environment, such as by filamentous exploration (2) and biofilm formation (5) which can also limit local nutrient availability.

There are many real-world examples that illustrate the impact that structured environments have on microbial life. A prime example of a structured microbial habitat, and a primary focus of this thesis, is the soil habitat which supports much of the planet's biogeochemical activity, e.g., carbon and nitrogen cycling (Ciais et al., 2013). This is possible partly because of the complex nature of the soils' constituent parts and the interaction of these to form cohesive porous structures (Kravchenko and Guber, 2017). For instance, the connectivity of pores can influence species

diversity by creating more isolated habitats when pore-connectivity is low and *vice versa* (Carson et al., 2010). The non-uniform distribution of resources mentioned above is very relevant to soils, and mathematical modelling suggests that exploration of fungal hyphae towards nutrient hotspots in turn increases the architectural complexity of that spot, as hyphae create channels while they penetrate through the soil (Young and Crawford, 2004).

Further examples of structured environments also include non-natural surfaces that are prone to biofilm formation, such as micro-scratches in surfaces used in hygienic and medical settings (Verran et al., 2010) and porous biomedical devices (e.g., catheters, voice prostheses, and porous scaffolding used to mimic bone) (Francolini and Donelli, 2010). These structures can facilitate the persistence of biofilm-forming organisms, even after physical perturbation such as mechanically cleaning a surface or when fluid flow generates shear forces (Donlan, 2002).

1.1.1 Methods for investigating microbial (micro)environments

Considering the range of microbial habitats that have structure, it is very desirable to be able to study organisms either in their native structured environments, or models thereof. The former typically poses considerable experimental challenges, many of which centre on two main concerns: (i) the difficulties of studying these environments under controlled conditions and with appropriate controls, and (ii) examining (pre-existing) environments non-destructively. In recent years, a range of new technical approaches and methodologies have been developed which help to

address these challenges, among others, enabling new understanding of important biological processes as they occur in real environments and are outlined below.

1.1.1.1 X-ray Computed Tomography

X-ray Computed Tomography (CT) is an imaging technique in which incident beams of X-rays pass through a subject as it is rotated through 360° and are subsequently collected by CCD detectors. The beam is attenuated in a manner dependent on the X-ray absorption density of the subject being examined. By computational analysis of attenuation through all angles of the subject, horizontal and vertical cross sections through the subject can be generated to form a three-dimensional computer model of the subject. X-ray CT has become a versatile tool for the non-destructive investigation of structures (Maire and Withers, 2013) and is becoming more widely applied in the material, agricultural, and biological sciences (Stock, 2013, Helliwell et al., 2014, Shearer et al., 2016), in addition to its traditional use in medical assessment and diagnosis. Recently X-ray CT has been used to study the (often reciprocal) interaction between biology and environment (Neal et al., 2020). For example, X-ray CT can be used to quantify the impact of microbial activity (respiration, hyphal exploration, etc.) on structures by imaging the same microbial-inoculated structure over time (Helliwell et al., 2014) and comparing properties such as the ratio of void (pore) space to solid, the degree of connectivity between pores, or the directionality of pores (anisotropy), as well as quantifying the spatial distribution of cells within porous environments (Bradley et al., 2017, Juyal et al., 2020).

1.1.1.2 *Microfluidic devices*

Investigating microbial populations at the single cell and microcolony levels (as opposed to the bulk population) has attracted considerable interest in recent years (Leygeber et al., 2019, Hewitt et al., 2016, Ackermann, 2015). However, this presents several challenges, including analysing and tracking organisms at the single-cell level, ideally in controlled (micro)environments. One approach to addressing these challenges is the use of microfluidic devices, here referring to devices which allow precise manipulation of fluids and fluid flow at the microlitre scale and below. This is typically achieved by introducing positive or negative pressure across confined channels. This precise manipulation of small liquid volumes allows fluid flow at defined rates, rapid transition between different fluids, and the ability to establish concentration gradients (e.g., nutrient, drug, etc.) within a chamber. These devices have been used to study single cells in isolation or within a cell community and facilitate the measurement of a plethora of microbial phenotypes, e.g., cell morphology, division dynamics, protein expression, cell-cell interactions, gene regulation etc. (Hingley-Wilson et al., 2020, Chait et al., 2017).

While there is considerable value in using microfluidics to study controlled, homogeneous environments, i.e., reducing the impact of environmental variation on microbial phenotypes of interest, structured environments can also be developed within microfluidics devices for investigating the impacts of microscale structures on microbial phenotypes and processes (Nadell et al., 2017, Hol et al., 2016, Deng et al., 2015). For example, the addition of simple pillar structures to microfluidic devices can enhance biofilm formation and disrupt the fluid flow within the device chamber.

This has been demonstrated in microfluidic devices to facilitate microbial persistence by providing physical compartmentalisation and protection from external stressors (Nadell et al., 2017, Donlan, 2002). Soil micromodels (i.e., 2D or 3D models of soil structure within a microfluidic system) provide excellent examples of integration with real-world structures (Deng et al., 2015, Rubinstein et al., 2015, Soufan et al., 2018). Unlike the pillar structure example, the structures within soil micromodels are created from computational simulations of soils, subsequently modified to remove the majority of closed pores to facilitate fluid flow through the entire model. These models have been used to examine slowing of water evaporation from porous environments by microbial extracellular polymeric secretions (EPS) (Deng et al., 2015) and the importance of protist behaviour for particle migration and soil turnover (Rubinstein et al., 2015).

1.1.1.3 Additive manufacturing

Additive manufacturing also provides an avenue for generating structured environments with high precision. Additive manufacturing is the process of printing successive layers of material on top of each other, although the methods of achieving this vary [see Ngo et al. (2018) for a broader overview]. Soil structural information acquired by X-ray CT has subsequently been used for printing three-dimensional soil-mimetic structures, in either Nylon 12 or resin with paraffin wax to preserve pore structure (Lamandé et al., 2020, Otten et al., 2012). Hyphal growth of fungi within the pores of the printed structures has also been demonstrated, showing that the structures support fungal growth and hyphal exploration (Otten et al., 2012). In principle, a wide range of environmental structures could be additively

manufactured, provided that the material used for printing is biocompatible and that the structure can be computationally modelled.

1.2 Soil as a Structured Environment

Soil supports much of the planet's biogeochemical activity, e.g., carbon and nitrogen cycling (Ciais et al., 2013). The soil environment has been described as the "most complex biomaterial on the planet" (Young and Crawford, 2004). In a purely structural sense, it comprises solid soil particles ranging in size from the nanometre to millimetre range. These particles are further organised, often by biotic and abiotic factors, into larger aggregations which themselves range in size from nanometres to centimetres. These primary particles and aggregates, along with rock material, plant roots, and any other physical debris, creates a three-dimensional porous structure, with pores existing between particles, aggregates, and even within aggregates. These pores are considered as void space and can contain air, which can be similar or dissimilar in composition to atmospheric air, and liquid water.

In summary, soil can be thought of as a porous structure composed of solid particles and void space that acts to separate gas and liquid within it from the surface atmosphere. The constituents of soil structure, and the properties they confer to the soil environment and its microbial inhabitants, are described and discussed in further detail below.

1.2.1 Soil texture

Soil texture is defined by its proportions of sand, silt, and clay particles (collectively termed "separates") (**Table 1**). Different classification systems exist to define these

components, typically by size, such as the United States Department of Agriculture (USDA) Soil Taxonomy and the Unified Soil Classification System. Together, these particles can be considered as the primary abiotic “building blocks” that constitute a soil, although not all these particles need be present.

Table 1- Soil separates are classified by their diameter, ranging from 2 mm to below 2 μm (USDA).

Soil separates	Diameter range (mm)
Sand (very coarse)	1.25-2
Sand (coarse)	0.63-1.25
Sand (medium)	0.2-0.63
Sand (fine)	0.125-0.2
Sand (very fine)	0.063-0.125
Silt	0.002-0.063
Clay	<0.002

Sand particles are generally composed of silica quartz (silicon-oxygen tetrahedra) but the sand fraction may also be composed of minerals such as feldspar and mica (Hillel, 2003). Due to the inert nature of these particles, and small surface area: volume ratios, sand largely has a physical role in soil. This may involve increasing drainage capacity by creating larger pores between particles, due to their larger size. Furthermore, it has been reported that the percentage of sand in a soil is a predictor of bacterial species richness, once other variables are accounted for (Chau et al., 2011). This may be due to the larger pores associated with coarser soils, which create

larger and more isolated water films, allowing for more discrete microbial habitats than in finer soils wherein the pores may be more connected.

Silt particles, in terms of mineral composition and physiology, resemble sand particles and are typically produced during the fracturing of quartz crystals (Moss and Green, 1975). Silt particles are often coated in smaller clay particles, meaning they can exhibit some properties of clay. High silt content in soils can be correlated with a reduction in soil bulk density (soil weight per volume) (Jones, 1983).

Clay-separates occur in sheets predominantly comprising silicon tetrahedral and aluminium octahedral molecules and are often described as 1:1 or 1:2 depending on if they are composed of alternating tetrahedral and octahedral layers or two tetrahedral sheets to one octahedral sheet. They have a large surface area to volume ratio, an overall negative charge, and possess colloidal properties due to their small size (Jackson, 2014). These properties allow clay separates to act as cation exchange surfaces to bind nutrients, water, and base-cations such as calcium, magnesium, sodium, and potassium, which can affect the pH and nutrient availability within a soil (Helling et al., 1964). Clay minerals, such as montmorillonite and kaolinite, can also facilitate microbial biofilm formation (as seen in the soil bacterium *Bacillus subtilis*), by triggering upregulated expression of key biofilm-formation genes as a stress response mechanism (Ma et al., 2017). Clay content has also been suggested to govern the occurrence of anoxic microsites within soil, as clay is thought to limit diffusion of gases in microbial respiratory hotspots (Keiluweit et al., 2018). However, whereas clay can facilitate microbial activity as described above, it is not always

essential to the stability of soil structure; sand and silt content have been suggested as more significant factors in the relationship between soil texture and structure in some soil systems (Idowu, 2011).

1.2.2 Soil Aggregation

Soil aggregation refers to the formation of a larger collection of particles from the smaller constituents of soil including clay, silt, and sand, as well as other particles such as root debris, that “adhere to each other more strongly than to surrounding particles” (Martin et al., 1955, Nimmo, 2005a). Furthermore, the aggregate shape can determine the inter-aggregate pore size and shape, as particles with irregular shapes tend to produce larger spaces between them (Nimmo, 2005b).

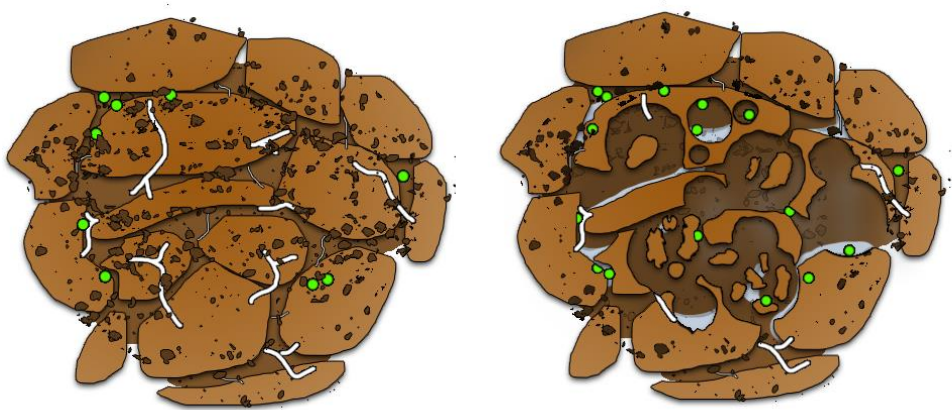


Figure 1.2- Illustration of general aggregate structure

A single aggregate is composed of primary soil particles with large root segments and smaller fungal hyphae contributing to overall structure. The cross section of an aggregate is also presented (right), illustrating both connected and isolated open pore space with the potential to contain both aqueous and gaseous phases (blue), and microbial distributions (green dots, size exaggerated for visibility) within connected and isolate pore spaces.

Soil aggregates are in a constant state of deformation, reposition, and reformation due to processes including surface weathering, wetting and drying cycles, freeze-thawing cycles, soil-root interactions, and soil-microbe interactions (Hillel, 2003), with aggregate turnover rates varying from weeks to months (De Gryze et al., 2006). These processes impact on both the overall soil structure, which varies seasonally in a manner dependent on factors as described above, and the extent to which aggregates can act as a habitat for microorganisms.

Agricultural practice also impacts on stability of soil aggregates. For example, under zero-tillage, where soils are not cultivated prior to planting, aggregates tend to be more stable and resilient. This is often due to an increase in organic matter content (Sasal et al., 2006), although aggregate stability will also depend on other factors of the agricultural regime in place. The existence and stability of soil aggregates can also influence carbon and nitrogen storage in soils as smaller aggregate fractions have been shown to protect soil organic carbon (SOC) from microbial decomposition in comparison to larger fractions (Mustafa et al., 2020).

Individual soil aggregates also contain their own interconnected pore networks, often not connected to the bulk soil pore space, and possess a range of pore sizes within them (Ananyeva et al., 2013). This intra-aggregate network can impact the soil microbiota as aggregates may contain chemical (e.g., oxygen, organic carbon) gradients (Sextstone et al., 1985) as well as physical barriers to surrounding pore space or other soil particles (Rabbi et al., 2016). These differences can contribute to the

creation of contrasting soil microenvironments, leading to heterogeneity in the microbial community composition and structure over small spatial scales (Carson et al., 2010, Blaud et al., 2014, Ebrahimi and Or, 2016, Upton et al., 2019). Taking the example of organic-carbon gradients, of which the heterogeneity has been shown to increase as the range of pore size distribution increases, suggesting that microbial spatial distributions could be more heterogeneous in more heterogeneous aggregate pore networks (Ananyeva et al., 2013). In addition, there can be local adaptation to specific microenvironments in circumstances where aggregates are more stable and aggregate breakdown and formation is relatively slow, prolonging the duration over which an aggregate may exert localised selection pressures (Almås et al., 2005; Upton et al., 2019).

1.2.3 Soil Pore Space

The pore space of a soil is the volume of a soil that is not occupied by solid material (**Figure 1.3**) and therefore contains gases or liquids. The pore volume can support soil microbiota, either in suspension or on the surface of a solid (Juyal et al., 2020). Because of this, the composition and accessibility of this space are key features of the soil habitat for microorganisms.

Fundamentally, the amount of pore space is dependent on the packing density of the soil, the variation in particle size distribution, and the shape of particles (angular, sub-angular, flat etc.) (Nimmo, 2005b). If it is assumed that all particles in a soil were spherical, the idealized void fraction (e.g., the proportion of pore space within a given soil volume) of a monodisperse (i.e. single particle size) system must fall between ~

0.48 and 0.26 depending on the packing configuration (Dullien, 1992). In polydisperse structures, the pore space and size-distribution depend on both the ratio of the diameters between particles and the relative numbers of particles of each diameter within the structure (Farr and Groot, 2009). In real soils, the void fraction can be anywhere between ~ 0.3 in a polydisperse sand to 0.8 or greater in peat soils (Nimmo, 2005b).

Pore size and shape can also impact on the attributes of a soil, such as its filtration rate, and whether a pore is air or liquid filled at “field capacity” (which relates to the water content of a soil after excess water has drained away by gravity) (de Oliveira et al., 2015). Broadly speaking, pore sizes can be categorised into macropores ($> 75 \mu\text{m}$ diameter) which are generally too large to exert a strong capillary force and are air filled at field capacity; mesopores ($30\text{-}75 \mu\text{m}$) which are water filled at field capacity and act as an accessible water store for plant roots; and micropores ($5\text{-}30 \mu\text{m}$) in which water is considered relatively immobile. Pores of the smaller size range are sometimes further subcategorised into ultramicropores ($0.1\text{-}30 \mu\text{m}$), referring to the common habitable pore range of microorganisms, and cryptopores ($<0.1 \mu\text{m}$) which remain largely water filled but inaccessible to microorganisms due to their small size (Brewer, 1964).

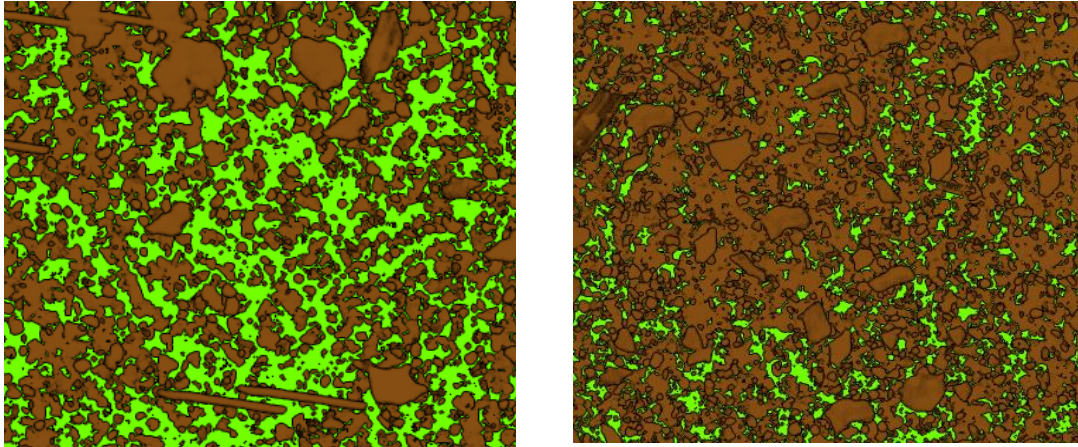


Figure 1.3- An illustration of the concept of pore space and pore connectivity

The solid soil phase is represented in brown. Highly connected pore space (green) with high porosity are illustrated (left) and contrasted with a relatively poorly connected pore space with low porosity and connectivity (right). This illustration can represent particles of any size, from nanoscale clay particles to millimetre scale sand particles. It should be noted that pore space occurs in three dimensions, and hence a two-dimensional cross section as depicted here does not display the full nature of soil pore space.

Another key parameter determined by porosity is soil permeability: the *rate* of liquid and air flow through the soil medium. Soil permeability is, theoretically, directly proportional to the square of the particle size but is also dependent on void fraction, as an increase in void fraction correlates with an increase in permeability (Metwaly et al., 2006). This implies that a greater void space facilitates a greater water potential, and a greater distribution of pore sizes would generate a greater distribution of nutrient (or other solute) flow rates within a soil. Therefore, it may be hypothesised that a broader pore-size variation may promote greater phenotypic diversity of soil microorganisms, with such diversity potentially at either the genotypic or non-genotypic levels (discussed in section 1.3.3).

1.3 Microorganisms in Soil and their Importance

Soils support broad ranges of microbial activity, diversity, and function. The composition of microbial communities within soils varies according to soil type, soil coverage, environmental perturbation, and the spatial scale over which the community is considered (Schmidt et al., 2018, Nunan, 2017, Hirsch et al., 2016, Almås et al., 2005). It is estimated that fungal and archaeal communities are generally less species-even (i.e., the difference in abundance between component species is greater) than bacterial communities, but overall are at a much lower abundance than bacterial populations (Fierer et al., 2007).

Generalisations can also be made for changing community composition with soil depth, in that fungal communities are more abundant within the upper soil horizons and bacterial communities more prominent in the lower horizons. There is a general trend of decreasing biomass at increasing soil depth, as soil becomes more compact and nutrients from root secretions and water filtration become more limited (Ekelund et al., 2001). For a data synthesis on general trends in the structure and function of the topsoil microbiome across the globe, see Bahram et al. (2018).

1.3.1 Yeasts in Soil

Often underrepresented in literature, soil yeasts are abundant. Species of *Cryptococcus*, *Filobasidium*, *Leucosporidium*, *Rhodotorula*, and *Trichosporon* make up a large proportion of soil yeasts (Botha, 2006). There is evidence to suggest that wild strains of the model organism *Saccharomyces cerevisiae* can be found in soils in

proximity to deciduous trees, in areas not associated with human activity (Fay and Benavides, 2005).

Yeasts have been suggested to play prominent roles in soil habitats, ranging from the degradation of rock to generate soil materials, to interactions with soil biota including plants, either in a competitive or synergistic manner (Botha, 2006). In many cases, distinct yeast communities have been found in the bulk soil, the plant rhizosphere and the ectomycorrhizosphere of the same soil, with fermentative yeasts more closely associated with the rhizosphere (Mestre et al., 2011). Several yeast species have been isolated from soils that are capable of biodegrading xenobiotics such as the insecticide lindane (Abdul Salam et al., 2013), indigo dye (Bankole et al., 2017), and even diesel oils (Chandran and Das, 2012).

Soil yeasts also interact with agricultural crops directly and have been shown to accelerate the development of crop seeds such as wheat, barley, and rye by stimulating seed germination (Fedotov et al., 2017). When yeasts are applied as a bio-fertiliser, it has been demonstrated that monocotyledonous sugarcane incorporates *Saccharomyces cerevisiae* yeast cells into the root tissue, which can increase nitrogen and phosphorus incorporation into roots and shoots (Lonhienne et al., 2014).

Saitozyma podzolica

Saitozyma podzolica (formerly *Cryptococcus podzolicus*) is a common yeast of well-drained soils, with a broad global distribution (Yurkov, 2018). It is thought to interact, along with many other microorganisms, with plant-root systems by secreting the widespread auxin indole-3-acetic acid (IAA), which can exert both stimulatory and

inhibitory effects on plant growth (Streletskii et al., 2016). Isolates of *S. podzolica* have been shown to have adapted to heavy metal pollutants in their environment and have been used to demonstrate the evolution of resistance mechanisms to these pollutants (Holland et al., 2014).

Many isolates have been reported to produce high levels of single-cell oil (31.8% lipid/dry biomass), predominantly composed of oleic acid (~60%) and palmitic acid (~20%), and secrete high levels of gluconic acid (30 g/L) (Schulze et al., 2014); a metal chelator and commonly used industrial compound incorporated into cleaning agents and dyes (Fischer and Bipp, 2002). Some isolates have also been described as containing a similar oil profile to cocoa butter and vegetable oil (Hoondée et al., 2019).

1.3.2 Importance of Soil Microorganisms

1.3.2.1 Biogeochemical Cycling

Microorganisms in soil play a pivotal role in processes such as carbon, nitrogen, and nutrient cycling. Carbon cycling and carbon sequestration is necessary to enable microbial activity within the soil. However, soil also act as a carbon sink, as the Earth's soil is estimated to contain more carbon than in the atmosphere, living plants, and animals combined (Lal, 2004). Nitrogen and nutrient cycling by microorganisms also play a fundamental role in agriculture, as soil microorganisms help make elements such as nitrogen, phosphorus, and sulphur bioavailable for plant uptake (Fowler et al., 2013).

Soil organic carbon plays a fundamental role in sustaining the terrestrial ecosphere (Lal, 2004). It is predominantly fungal communities that break down the carbon-rich litter layers on forest floors and grasslands (as well as root debris within the soil) into more readily available substrates for further microbial metabolism. Significant carbon input to soils also occurs from the exudate of living plant roots (Koo et al., 2005). Organic carbon within the soil matrix is converted into microbial biomass and the carbon in turn is released back into the system as organisms secrete extracellular polymeric substances (EPS), respire, become lysed through mechanical or chemical perturbations, or are consumed by other organisms including mesofauna.

Soil microorganisms are also largely responsible for the turnover and movement of soil nitrogen (Fowler et al., 2013). In brief, some soil microorganisms fix atmospheric N_2 into NH_4^+ , they nitrify NH_4^+ into NO_3^- , and undertake ammonification to release NH_3 via organic matter (OM) breakdown, with NO_3^- and NH_3 being the assimilable forms of nitrogen for plants. In addition to organic carbon and various forms of nitrogen, soil microorganisms convert recalcitrant forms of phosphorus and sulfur into plant-bioavailable molecules (Jacoby et al., 2017).

These properties also make soil microorganisms essential for agriculture, and studies continue to assess the impact of microbial abundance on diversity of crop yield and soil sustainability (Fowler et al., 2013, Lal, 2004, Jacoby et al., 2017, Jansson and Hofmockel, 2020, Gadhave et al., 2018, Wubs et al., 2016, Zhao et al., 2016, Hirsch et al., 2009, Lupatini et al., 2016, Mangalassery et al., 2015, Morrison-Whittle et al., 2017).

1.3.2.2 Source of medicinal compounds and food

Soil microorganisms are also of substantial value to humans, such as being a source of pharmaceuticals and foods. Many microbial secondary metabolites produced by soil microorganisms (produced naturally to inhibit competing microorganisms or otherwise facilitate growth) have been used as pharmaceuticals, such as the antibiotics streptomycin and tetracycline (Smith, 2000) and the cancer drug dactinomycin (Waksman and Gregory, 1954) from *Streptomyces* species. Presently, antibiotics such as teixobactin isolated from the previously uncultured *Eleftheria terrae* (Ling et al., 2015), and malacidins discovered via soil metagenomic analysis (Hover et al., 2018), continue to be discovered and developed.

Soil organisms are also used in the production of food products for human consumption. For example, production of mushrooms as fruiting bodies by many fungi of the phylum *Basidiomycota* (many of which were originally discovered in soils (Boa, 2004)). Furthermore, fungi such as *Penicillium roqueforti* and other species are used in the production of cheese, and fungi and bacteria found in soil are often used during the manufacturing process of products such as fermented drinks and breads. The food product “Quorn” is produced from the fungus *Fusarium venenatum*, which was originally discovered and isolated from soil (Whittaker et al. 2020).

1.3.3 Phenotypic heterogeneity in microorganisms

Phenotypic heterogeneity describes the phenomenon whereby individual cells within genetically-uniform cell populations exhibit different phenotypes (**Figure 1.4**) (Sumner and Avery, 2002). Phenotypic heterogeneity has been shown, both

theoretically and empirically, to provide a selective advantage to such cell populations in response to environmental stress or other perturbations (Bishop et al., 2007, Smith et al., 2007, Holland et al., 2014, Ozbudak et al., 2002). Importantly, and in contrast to adaptation by mutation and natural selection, phenotypic heterogeneity within a population is typically considered transient and non-heritable. That is, a subset of cells which may be highly sensitive or resistant to a stress, for example, can revert back to a normal distribution of phenotypes after sub-culturing (Smith et al., 2007).

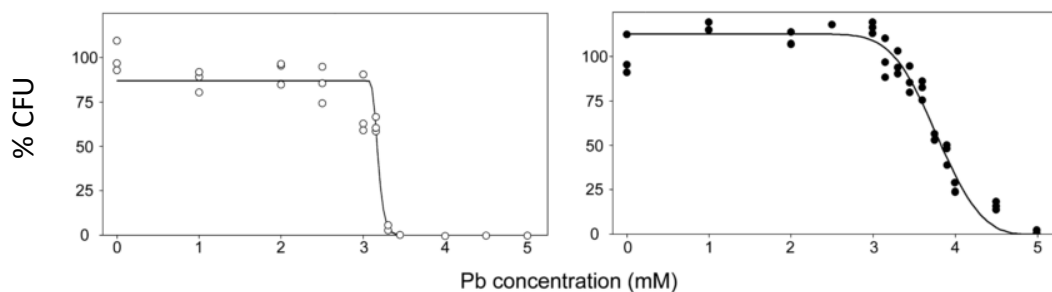


Figure 1.4- An example of homogeneity and heterogeneity in response to lead (Pb) stress

Left- In this hypothetical dose-response curve, the percentage of colony forming units (CFU) drops sharply over a narrow range of lead concentrations, indicating a relatively homogeneous response within an isogenic population. Right- The range of increasing lead doses over which CFU drops from 100% to 0% is broader than in the homogeneous dose-response curve, indicating a more heterogeneous response to lead stress among the individual cells. Adapted from Holland et al (2014).

1.3.3.1 Phenotypic heterogeneity in natural, industrial, and medical settings

Phenotypic heterogeneity has been observed almost ubiquitously in genetically-uniform cell populations, both in microbial (prokaryotes and eukaryotes) and mammalian cell populations (Holland et al., 2014, Stockholm et al., 2007, Nikolic et

al., 2017). This phenomenon is thought to provide an important survival mechanism in natural, industrial, and medical settings.

In nature, phenotypic heterogeneity has been shown to occur in wild yeast isolates and the level of heterogeneity (measured here as cell-to-cell variation in Pb resistance) was elevated in isolates from lead-polluted sites; furthermore, phenotypic heterogeneity could be evolved by long-term culture with lead in the laboratory (Holland et al., 2014). Some work has also been conducted with natural bacterial populations, including observations of metabolic heterogeneity in *Chlorobium phaeobacteroides* in its natural environment (Zimmermann et al., 2018), and single-cell variation in ammonium and carbon uptake in several species from lake water samples (Musat et al., 2008).

In laboratory strains of the yeast *Saccharomyces cerevisiae*, a number of heterogeneous phenotypes conferring resistance to stressors (heteroresistance) including metal toxicity, hydrogen peroxide resistance, heat-stress resistance, antibiotic resistance, and weak-acid preservative resistance have been observed (Stratford et al., 2014, Levy et al., 2012, Smith et al., 2007, Sumner et al., 2003, Wang et al., 2014). Numerous other general phenotypes exhibiting phenotypic heterogeneity have also been reported, such as single cell growth rate, micro-colony morphology, sugar utilisation, spore dormancy entry and exit, spore germination, division time, and lifespan (Levy et al., 2012, Nikolic et al., 2017, Graham et al., 2014, Mutlu et al., 2018, Janssens and Veenhoff, 2016). Many of these phenomena are yet

to be characterised either in wild strains or *in situ*, possibly due to the experimental difficulty involved in such observations.

Broadly speaking, the potential mechanisms underlying phenotypic heterogeneity can be divided into two categories- Intrinsic heterogeneity: originating from the stochastic nature of gene expression, which can even differ between alleles of the same gene within the same cell; and extrinsic heterogeneity: describing heterogeneity that is evident only between cells, rather than also within cells, and may arise from differences in the levels of intracellular molecules such as transcription factors or other regulatory proteins (Raser and O'Shea, 2004). Therefore, intrinsic heterogeneity tends to be gene-specific, whereas extrinsic noise can have a global influence within a cell.

1.3.3.2 Benefits of phenotypic heterogeneity

Perhaps the most commonly proposed adaptive benefit of phenotypic heterogeneity is that it can allow for the survival of small subpopulations of cells in a fluctuating environment (Levy et al., 2012, Ackermann, 2015, Wolf et al., 2005, Acar et al., 2008). This strategy could somewhat reduce the necessity for cells to sense and respond to environmental cues, which is limited by both a cell's ability to sense a cue and the time taken to generate a response. With phenotypic heterogeneity, cell subpopulations may be pre-equipped for different conditions as they may arise, rather than having to adapt in response. Survival of such sub-populations may then enable reconstitution of any population decline that may occur as a result of the environmental fluctuation, all while maintaining genetic uniformity within the population as a whole.

Hence, an organism may evolve to express variation (noise) in the abundances of protectant molecules, for example, between cells of the population. As a result, particular sub-populations may be better able to survive in an environment at the cost of a reduced fitness in another. A paradigm example of this is that of the trehalose synthase encoded by the *TSL1* gene of *S. cerevisiae*: a higher abundance of cellular Tsl1 correlated with slower cell growth, but much greater resistance to acute heat stress than in cells with lower Tsl1 expression (Levy et al., 2012).

Notably, Kussell and Leibler (2005) derive a relationship between increasing degrees of phenotypic heterogeneity and increased long-term growth rates in fluctuating environments using theoretical modelling. Further modelling by Luck et al. (2018) has suggested that both constant and rapidly-fluctuating environments would result in similar adaptations, and that expression noise is only advantageous with equal time periods of nutrient availability- suggesting that heterogeneity may only provide an adaptive advantage in very particular fluctuations of stress and nutrient levels.

1.4 Interactions between Microorganisms and Soil Structure

Because the structure of a soil can create a wide range of environments and niches for microorganisms, and microorganisms are key figures in the development of structures within a soil (Crawford et al., 2012), there is an inherent reciprocal relationship between microbial communities and their heterogeneous soil environment. The soil provides spatially and temporally compartmentalised environments favouring different organisms, and the nutrient uptake, metabolism,

and movement of these organisms in turn alters the structure of the environment around them, such as by hyphal exploration or gas evolution (Helliwell et al., 2014).

1.4.1 The Impact of soil structure on microbial communities

Relatively large spatial differences, such as the micrometre to millimetre distances between the surface and centre of a soil aggregate, can contribute to the different microenvironments within a soil (Mummey and Stahl, 2004). For example, soil aggregation can influence microbial diversity and spatial composition, as it has been found that stable aggregates of the millimetre scale tend to predominantly harbour different bacterial and fungal communities than aggregates of sub-millimetre scales; which in turn can affect parameters like respiration (CO₂ production) rates and pH within those aggregates differently (Yang et al., 2019). Soil aggregation, especially when facilitated by clay content, influences bacterial community structure by enhancing aggregate and stability and trapping bacteria within the same aggregate for a longer period (Biesgen et al., 2020). Bulk density can also impact on the distribution of microorganisms within a soil, as demonstrated in Juyal et al. (2020), where cells can accumulate to a greater extent in soils with lower bulk densities. This study also implicated soil porosity and availability of solid-pore interface at which microorganisms can reside as influencers of bacterial dispersal within the soil, reflected by higher cell densities in soils with larger pores.

Aside from large-scale spatial structure, much of the potential micro-habitat differentiation in soil occurs at smaller scales, such as within pore spaces ranging from 0.01 µm to 75 µm in diameter (Zaffar and Lu, 2015). These microenvironments can

vary greatly, such as in their moisture content, nutrient and oxygen availability and hence different microenvironments will be more, or less, favourable to some microorganisms depending on their environmental preferences. However, small scale spatial heterogeneity does not impact all soil chemistry, as soil redox potential, for example, has been shown to be impacted by differences in larger air-filled pore volume but less so by small-scale heterogeneity (Dorau et al., 2018).

The formal concept of an ecological niche has existed for over a century (Grinnell, 1917). However, more recently, the concept specifically of a microbial niche within a soil habit has become a more prominent concept within microbial ecology. Soil micropores can generate large differences in micro-scale oxygen diffusion rates within close proximity, resulting in anoxic microsites (Keiluweit et al., 2018) and creating preferential sites for either aerobic or anaerobic microorganisms at small distances from each other. In terms of the connectivity of pore space, lower connectivity can increase bacterial diversity within soil by creating more isolated pores compared to a more highly connected pore space of the same volume (Carson et al., 2010).

Furthermore, the perturbation of soil under rainfall can create seals at the soil surface, whereby impermeable layers of soil are created, reducing the porosity of the topsoil to a greater extent than soil below this (Armenise et al., 2018). This would then alter the conditions between these pore spaces, potentially creating varying selection pressure between pores within the soil seal and those further away (Keiluweit et al., 2018). In contrast to rainfall, season-long drought has been shown

to alter fungal community composition, but not the extent of diversity within the community (Schmidt et al., 2018). However, whether this is due primarily to depletion of available moisture, or the impact of soil drying on pore structure, remains unclear.

1.4.2 The impact of microbial communities on soil structure

While soil structure impacts microbial communities, microorganisms can also have a significant influence on the structure of their environment, such as by altering soil pore geometry and pore connectivity (Helliwell et al., 2014). In Helliwell et al., (2014), soil porosity was increased primarily due to microbial gaseous release and more so in coarser soils than in finer soils, due to the more cohesive nature of the finer soils. Pore circularity also significantly altered over time, either due to the development of soil cracks into irregular shapes, or gaseous release generating more regular pore shapes.

Microbial communities have been shown to influence micro-aggregation of clay in a temperature dependent manner (Watts et al., 2005), such that aggregation rates are higher at temperatures optimal for microbial growth. Furthermore, aggregate stability in ex-arable soils has been shown to be positively correlated with fungal community succession over time, with fungi and hyphal networks acting as enhancers of aggregate stability (Duchicela et al., 2013). Modelling of fungal hyphal exploration through the soil pore space also suggests that soil-fungal interactions have the potential to “self-organise”. That is, fungal exploration and growth around nutrient hotspots can increase the structural complexity of the soil in these areas by

reinforcing the structure with hyphal secretions and compaction of soil around hyphae, potentially resulting in increased soil structure complexity in nutrient-rich spaces (Crawford et al., 2012).

In addition to fungal exploration, the presence of extracellular polymeric substance (EPS) secreting bacteria within the soil may dramatically increase water retention and decrease water evaporation rate, according to predictions from studies with soil micromodels (described in 1.1.1.2) under a constant atmosphere (Deng et al., 2015). It could be speculated that the water retention properties of EPS may be beneficial for plant water uptake and root growth, with further consequences for soil structure. Inoculation of soil with microbial communities from different ecosystem types can accelerated plant community development, which can in turn alter soil structure through root growth and soil properties such as pH and nutrient availability in response to plant root exudate (Wubs et al., 2016).

A recent exploration of microbial processes in soil provided evidence that soil physical structure can be considered as an “extended composite phenotype” of the microbial metagenome (Neal et al., 2020). This relates to the impact of nutrient input and soil management on the microbial metagenome, and even on microbial allele frequency, which then alters the soil structure as this leads to changes in overall protein secretion into the soil, motility of microorganisms, and metabolic rates of the soil microbial community.

In summary, soil structure influences the position and composition of soil microorganisms, creating a broad range of environmental conditions and niches

according to soil pH, oxygen, nutrient availability, etc. between different compartments within the same soil. At the same time, soil microorganisms reciprocally alter soil structure, by their metabolism (e.g., respiratory), secretion of adhesive substances, and growth and exploration within soil. Together, this creates an inter-relationship between soil structure and its microbial inhabitants.

1.5 The Impact of Environmental Perturbation on Soil Microorganisms

Contamination and disturbance of soil can impact on microbial communities, altering the relative abundances of species and total microbial biomass within a soil (Yergeau et al., 2018, Schmidt et al., 2018, Banning and Murphy, 2008, Hirsch et al., 2009). This is often interlinked with changes in soil structure brought about by disturbance through both anthropogenic (e.g., agriculture, building, mining) and natural means (e.g., flooding, drought, earthquakes, landslides). Because of this and the awareness of microbial activity for soil health, there is growing research emphasis on the impact of these changes on microbial life in soils.

1.5.1 Impacts of Soil Disturbance and Global Environmental Change

Anthropogenic disturbance, such as through tillage or land management changes, can alter soil microbial community composition. For example, the conversion of bare-fallow land to grassland can enrich for bacterial reductase genes involved in nitrogen fixation, and vice-versa in grassland converted to bare-fallow (Hirsch et al., 2016). However, starving soil by removing crop cover and not adding any form of nutrient input to the soil over a long-term experiment (50 years) reduced microbial

abundance, but not diversity (Hirsch et al., 2009). In zero tillage soils, higher microbial biomass is reported (Mangalassery et al., 2015), possibly due to the higher structural complexity seen in zero tillage soil (e.g., increased porosity and aggregate size distribution), which protects organic matter (OM) resulting in less OM oxidation and nitrogen mineralisation (Silva et al., 2014). Soil disturbance does not only lead to short-term changes in microbial community composition, but also changes in microbial community composition and soil chemistry that persist for as long as 100 years post conversion, as seen in historically arable land converted to forest (Fichtner et al., 2014).

Global environmental change can also indirectly impact microbial activity within soils. Waldrop and Firestone (2006) reciprocally transplanted soil cores between open grassland and oak canopy soil to assess potential impacts of climate change on microbial community composition. The microbial community composition changed rapidly in the oak canopy core, but not the grassland core, emphasising that aboveground vegetation change (one anticipated effect of climate change) can have a knock-on effect on the soil microbiome in some circumstances.

1.5.2 Perturbation in soil temperature and moisture

Two abiotic factors expected to increasingly fluctuate as a result of climate change are temperature and rainfall distribution (IPCC, 2013), which can have profound consequences for soil biology. For example, it has been demonstrated that incubation of soil microcosms at 50 °C reduces total microbial biomass and fungal species abundance, but not bacterial species abundance (Riah-Anglet et al., 2015). Even in

long-term chronic warming experiments, raising the temperature to 5 °C above ambient temperature for 12 years, showed a reduction in microbial biomass and fungal biomarkers, resulting in Gram-positive bacteria and actinomycetes becoming more dominant in the soil (Frey et al., 2008). It is uncertain whether soil structure may influence the temperature stress sensed by soil microorganisms but it is known that soil can act as a thermal insulator (Slegel and Davis, 1977).

Changes in the soil water content, such as wetting and drying cycles, can impair osmotically sensitive microorganisms on wetting, while other organisms release organic solutes accumulated during the drying period. Furthermore, long term waterlogging of a soil (e.g., resulting from excessive rainfall and/or poor soil irrigation) can create anaerobic sites, as the diffusion of oxygen through water is orders of magnitude slower than through air (Yan et al., 2015). As with temperature change, the impact of soil structure on anoxic stress has not been fully explored.

1.5.3 Perturbation in soil oxygen

As mentioned earlier, spatially, soil can exhibit markedly heterogeneous oxygen concentrations due to depletion via respiration and differences in oxygen diffusion between the above ground atmosphere and either air or water-filled soil pore space. Whereas both aerobic and anaerobic microorganisms inhabit soil, the proportion of facultative anaerobes tends to increase with soil depth (Linn and Doran, 1984). Furthermore, there is a prevailing assumption that certain soil types are well aerated (Keiluweit et al., 2017) and hence favour aerobic microorganisms. However, even

when soils appear aerated overall, anoxic microsites may be distributed throughout the soil matrix and within aggregates (Keiluweit et al., 2017).

In some circumstances, the oxygen concentrations within soil can be perturbed by external influences such as by water logging, which will reduce the volume of gaseous pore space and hence total available oxygen. This can alter community composition, as some aerobic microorganisms, such as *S. podzolica*, show some loss of viability over several days of anoxia exposure (Harvey et al., 2020b).

1.5.4 Metal Pollution

Metal pollution of soils, a result of mining and smelting activities for example, can hinder agricultural soils (Toth et al., 2016) as well as natural soil ecosystems (Tiwari and Lata, 2018). Such pollutants include complexes of metals like Pb, Cu, Cd, As, Cr, Co, Zn, and Ni, which vary in toxicity depending on factors such as mode of action, specificity to biological targets, and the bioavailability of metals as either ions or in a complex (Gadd et al., 2005; Sharma and Agrawal, 2005).

Broadly speaking, fungi tend to be more resistant to perturbation by metal pollutants than bacteria (Maliszewska et al., 1985), suggesting that metal pollutants may alter microbial community composition by disproportionately impacting bacteria in a mixed-kingdom community. Whereas trace metals are essential for many core biological proteins, at higher concentrations (toxic) metals elicit a dose-dependent decline of microbial activity. This is observable in natural settings, such as the decrease in microbial biomass and enzyme activity with increasing proximity to industrial copper smelts (Wang et al., 2007) and along an increasing concentration gradient of metal in

soils contaminated by mining (Navas et al., 2020). Furthermore, the temporal aspect of metal pollution must also be considered in these systems, as gradual versus acute addition of copper has been shown to alter microbial community abundance and respiratory activity in soils differentially, even if the copper concentration eventually attained is similar (McTee et al., 2019). In addition, metal exposure can co-select for antimicrobial-resistance genes in bacteria (Cao et al., 2020), providing another rationale for understanding the impact of soil structure on microbial exposure to metal pollutants.

Different metal chemistries may also produce different interactions with soil structure and texture. For example, metals such as chromium, copper, and cadmium can tend to be bound by the charged clay portion of a soil whereas lead is more commonly associated with the silt fraction (Orroño and Lavado, 2015). Furthermore, metal distribution is spatially heterogeneous within soils, although evidence of this in the context of pore space is often conflicting. Previous work has suggested that microorganisms located within aggregate micropores are less exposed to metals (Almås et al., 2005), whereas other evidence suggests that some metals tend to concentrate in the smaller pores at the interior of soil aggregates (Ilg et al., 2004). This conflict also emphasises the difficulties in studying soil contaminant distribution and microbial response in relation to soil structure.

1.5.4.1 Lead in soils and surrounding environments

Of specific interest in this thesis, lead is one of the most common and persistent heavy metal pollutants in the environment, with little to no biological function (Kushwaha et al., 2018). In soils, lead can be found as a free metal ion, as a complex

with inorganic components such as sulfate and chloride, or adsorbed onto the surface of particles such as clays in various forms (Pourrut et al., 2011). The mobility and bioavailability of lead species depends on environmental variables such as pH and the presence of chelators such as humic acid (Ahmed et al., 2019), as well as the presence of charged clay minerals (Helios Rybicka et al., 1995). When the soil pH is low (approximately pH 3 or below), lead is more likely to exist in more soluble forms as either ionic or as simple ionic pairs such as $PbSO_4$, and increasing pH tends to increase lead insolubility as it forms organic Pb complexes (Sauvé et al., 1998).

The toxicity of lead to microorganisms is multifactorial and may include binding to cell membrane functional groups, intracellular proteins, and hydroxyl groups of nucleic acid (Kushwaha et al., 2018). This binding activity can therefore cause widespread cellular disruption. Additionally, environmental lead has been shown to inhibit extracellular enzymes secreted by microorganisms, which may then reduce the quantity of the nutrient components that these enzymes normally make accessible (Jaroslawiecka and Piotrowska-Seget, 2014).

1.6 Summary and Thesis Aims

In summary, the nature of soil and its composition is dynamic and multifactorial, forming a complex biomaterial. Soil can exhibit a high degree of structure and is composed of soil separates and other particles such as root debris, some of which aggregate, resulting in both intra-aggregate pore space and pore space between aggregates and particles, in the presence also of other solids such as rock and root material. This structural skeleton then possesses an array of chemical properties such

as gradients in gases and liquids, salinity, and pH, and heterogeneity in the spatial distribution of chemicals such as in nutrients and trace metals. Such heterogeneous soil structures are typically inhabited by an enormous diversity and quantity of life, with microorganisms (specifically yeasts) being the focus of this thesis. Soil microorganisms are both influenced by and exert influence on, the soil structure. Soil composition and structure may alter the nutrient and stressor flux to microorganisms, affecting microbial metabolism and exploration, which in turn can alter soil structure by changing pore shape, configuration, connectivity, stability and so on. However, it is poorly understood how the soil structure may influence microbial exposure and response to stressors. In addition to environmental heterogeneity, there is microbial phenotypic heterogeneity to consider, evident in diverse traits. Potential interaction between soil spatial heterogeneity and microbial heterogeneity has yet to be explored.

1.6.1 Aims

This thesis aims to assess how the structural features of soil can impact on environmental perturbation of microorganisms – primarily in relation to stress response – as well as develop methods to enable this. Specifically, the aims of this thesis are:

1. Test the hypothesis that organisms residing in the intra-aggregate pore space of soil may be more protected from stress than those on the aggregate surface (or surrounding bulk pore space).
2. Determine whether variation in pore size can impact stress resistance of soil yeasts.
3. Examine whether a microorganism's position in a micrometre-scale structure impacts its stress response phenotype.
4. Overarching aims 1-3, examine the relationship between an organism's phenotypic heterogeneity (regarding stress-response phenotype) and the structural heterogeneity in which the organism resides. It is hypothesised that a more structurally heterogeneous environment will distribute externally applied stressors more heterogeneously, favouring organisms with a more heterogeneous stress response.

2 THE IMPACT OF SOIL AGGREGATION ON MICROBIAL STRESS RESISTANCE

2.1 Introduction

Soil aggregation has been described in chapter 1, General Introduction. Briefly, soil aggregates are formed when particles such as sand, silt, and clay and other debris such as root and rock materials stick to each other more strongly than to surrounding particles (Nimmo, 2005) forming 'discrete units' of soil. These aggregates can be stable for weeks to months (De Gryze et al., 2006) depending on environmental factors such as weathering and land use (Hillel, 2003; Sasal et al., 2006) and can often be associated with organic matter such as plant roots and debris, and other living and dead (micro)organisms.

Recent theoretical work in which water-stable soil aggregates are considered as "evolutionary incubators" has suggested that microorganisms within aggregates can be isolated from much of the environmental fluctuation around them, such as from pollution, moisture variation or predation by other organisms (Rillig et al., 2017). This may result in different environmental pressures on microorganisms located on the aggregate interior and exterior and between cells in different aggregates, resulting in local adaptation within species over small distances (Rillig et al., 2017). In addition, the soil microbiome is affected by aggregate size, as microaggregates (<250µm) are reported to harbour relatively dynamic and diverse microbial communities, whereas microbial communities of macroaggregates (>250µm) are more stable (Upton et al.,

2019). Furthermore, the extent of this incubatory period and whether it does indeed provide discrete microbial environments has yet be fully explored. In particular, there is very little experimental evidence that soil aggregation can confer a protective effect to the microorganisms within them, such as protection from exogenous stress events.

Previous work describing the microbiota of the interior versus exterior soil-aggregate environment has relied on isolating organisms from either location retrospectively, using soil samples taken from natural environments (Mummey and Stahl, 2004, Blaud et al., 2014, Garbuz et al., 2016). Whereas this approach offers a snapshot of the microorganisms present from the particular soils examined, it does not allow researchers to ask other questions concerning aggregate associated microorganisms, under the robust control of an *in vitro* approach where the exact history and composition of an individual aggregate could be recorded over time.

2.1.1 Aims

This chapter sets out to explore the development of a new method for producing field-representative soil aggregates in a laboratory environment, while enabling the incorporation of know quantities of selected microorganisms to the interior or exterior of the aggregates.

The survival of environmental stress by a common soil yeast localised to the surface or within the aggregate's interior was examined to test the hypothesis that the aggregate interior confers a protective effect and also whether heteroresistance (see General introduction) may impact this interaction.

Additionally, a method was developed to recover organisms independently from the aggregate interior or exterior to confirm that organisms were spatially separate in manufactured aggregates. This method was further applied to natural aggregates to assess whether either aggregate fraction conferred a variable adaptation in colony growth.

2.2 Materials and Methods

2.2.1 Yeast strains and culture conditions

The haploid *Saccharomyces cerevisiae* strains W303 (*MAT α ura3-1 ade2-1 trp1-1 his3-11,15 leu2-3,112*) and BY4741 (*MAT α his3-1 leu2-0 met15-0 ura3-0*) were maintained and grown in YEPD medium [2% peptone (Oxoid), 1% yeast extract (Oxoid), 2% D-glucose] or YNB medium [0.69% yeast nitrogen base without amino acids, (Formedium)] supplemented with 2% (w/v) D-glucose and amino acids or nucleobases as appropriate for strain auxotrophies (Moreno-Martinez et al., 2015). *Saitomyza podzolica* used to inoculate aggregates were wild isolates recovered by other researchers in the Avery laboratory from soil near a disused metal smelting works in the north-east of the UK (<http://www.twsitelines.info/SMR/4192>). These isolates were identified by laboratory colleagues using ITS sequencing and RAPD PCR as described in Holland et al. (2014). Further *S. podzolica* isolates were obtained from either the interior or exterior of aggregates of the soil samples as described in section 2.2.3.1. *S. podzolica* was maintained and grown in MYP medium [7% malt extract (Sigma), 0.5% yeast extract (Oxoid), 2.5% soytone (BD Bacto)]. Where required, media were solidified with 2% (w/v) agar. For experiments, single colonies were used to inoculate 10 ml of medium in 50 ml Erlenmeyer flasks and incubated with orbital shaking (New Brunswick Scientific) at 120 rev min⁻¹, either at 30°C for *S. cerevisiae* or 24°C for *S. podzolica*.

2.2.2 Soil preparation

A sandy silt loam soil (1% clay, 39% sand, 60% silt) classified as a luvisol (FAO) was collected from agricultural land in Rutland, UK (52.6448051°, -000.6071415°) and used for manufacturing soil aggregates. To prepare the soil, large debris such as plant roots were removed before splitting the soil into 10 g samples per 12 cm² petri dish (Greiner Bio-One) and drying at 50 °C for one hour to aid subsequent grinding steps. Soil was sieved to <2 mm to remove remaining debris, then ground using a ceramic mortar and pestle to disaggregate the soil before autoclaving (121 °C, 1.15 bar, 15 min). Before commencing experiments, sterile soil was gently ground again using a mortar and pestle, under sterile conditions, to disrupt any minor aggregation that occurred during the autoclave process.

2.2.3 Production of manufactured soil aggregates and incorporation and recovery of microorganisms

For demonstrating aggregate production, 7 µl of sterile water was mixed with ~20 mg of sterile ground soil. The moist soil was vortexed (Vortex Genie 2, Scientific Industries Inc) at speed setting 3 (unless otherwise stated) for 15 s in a sterile 15 ml centrifuge tube (Scientific Laboratory Supplies) causing the loose soil to bind into a single cohesive aggregate. A large tube of this shape was used because it allowed the aggregate to “roll” around the inner circumference of the tube when vortexed, collecting soil particles and collating them into a single aggregate. The aggregate was then transferred to a clean tube, vortexed with a further ~10 mg of sterile soil, to create a barrier between interior and exterior layers, and transferred to a clean tube again. For the outer layer of the aggregate, ~10 mg of sterile soil mixed with 7 µl of

sterile water was added to the tube and vortexed for 15 s (unless otherwise specified) together with the existing aggregate to produce a single aggregate.

To incorporate different organisms into the interior and exterior of single aggregates, the procedure was performed exactly as described above except sterile water was replaced with the same volume of water containing a suspension of exponential phase cells ($OD_{600} \sim 1$ in water) of either *S. cerevisiae* W303 (first water addition) or *S. cerevisiae* BY4741 (final water addition).

2.2.4 Selective recovery of organisms from the aggregate interior and exterior

For determining independent recovery of organisms from the exterior or interior of aggregates, aggregates were transferred to a FisherBrand X50 cell strainer (mesh size 40 μm) and submerged in 1 ml sterile water with manual agitation for one minute to recover surface organisms in the water fraction. Aggregates were then bathed for 1 min in 1 ml of 20% (v/v, diluted in sterile water) electrolysed water (Ozo Innovations) (Wohlgemuth et al., 2020) to sterilise the aggregate surfaces. Aggregates were then disrupted by vigorous vortexing for 1 min in sterile water to release organisms from the aggregate interior. The two isolated fractions were subsequently streak-plated to selective YNB agar, supplemented as appropriate to select for the different auxotrophies of the two introduced *S. cerevisiae* strains (see above).

2.2.4.1 Isolation of wild yeast from natural aggregates

The interior-exterior isolation method described above was also used to isolate organisms from aggregates of natural, non-sterile soils, except that both isolated

fractions were plated separately onto MYP agar supplemented with 100 µg/ml ampicillin and 200 µg/ml streptomycin to reduce bacterial growth. Eighteen hours after incubation at 24 °C, single yeast colonies were picked and streaked onto MYP agar and incubated at 24 °C until single colonies formed. Single colonies were picked, mixed with 20% glycerol and frozen at -80°C to create isolate stocks.

2.2.4.2 *Internal Transcribed Spacer (ITS) sequencing*

Genomic DNA was extracted from overnight cultures of each isolate (see above) using a Wizard Genomic DNA Purification Kit (Promega) as per manufacturer's instructions. Briefly, the kit method involved a lysis step to digest the cell wall and release cytoplasmic content followed by a nuclei lysis step to release genomic content. Protein was then precipitated using a precipitation solution before the supernatant containing DNA was transferred to a tube containing isopropanol for DNA precipitation. The Internal Transcribed Spacer (ITS) region of genomic DNA was amplified via PCR using primers ITS1 (5'-TCCGTAGGTGAACCTGCGG-3') and ITS4 (5'-TCCTCCGCTTATTGATATGC-3') (White et al., 1990). ITS amplicons were sequenced by Eurofins Scientific, and the sequence used to identify the isolate genus and species where possible.

PCR reactions were carried out using a PrimeG Thermocycler (Techne) with a 1 minute 98 °C denaturing step, followed by cycling of 98 °C (1 minute), 55 °C (1 minute), 72 °C (1minute/KB), before a final elongation step of 72 °C (5 minutes). Unless stated otherwise, 30 cycles were conducted. PCR reactions were carried out in 50 µl reactions, unless stated otherwise, using NEB Phusion (M0530L) as follows- Phusion HF Buffer (1X concentration), 1.5mM MgCl, 25µM forward and reverse

primer, 200ng DNA template, up to a total volume of 50 μ l with deionised water. PCR products were purified by gel electrophoresis (1% w/v agarose) in TE buffer, cut out of the gel and extracted using a QIAquick Gel Extraction Kit (QIAGEN) as per manufacturer's instructions. Briefly, this involved dissolving the gel containing DNA in a DNA solubilising and binding buffer at 50 °C, before binding the DNA to a column by passing the DNA-buffer sample through the column via centrifugation. After two washing steps to remove salts and impurities, the DNA was then eluted from the column using 20 μ l sterile water.

2.2.5 Assessing colony area variation in isolates of *S. podzolica*

To compare variation in colony area of yeast isolates from the interior and exterior of natural soil aggregates, single colonies from seven-day old MYP plates of wild *S. podzolica* (taken from -80°C glycerol stocks), isolated as above (2.2.4.1) were used to inoculate 1 ml sterile deionised water. Cell suspensions were subsequently diluted to ~ 0.3 cells/ μ L and 100 μ L spread onto 9 cm MYP agar plates (or 9 cm YEPD plates supplemented with specified glucose concentrations for glucose starvation experiments) resulting in ~ 30 colonies per plate. After 3 days incubation at 24 °C, plates were imaged using a Protos 3 Colony Counter. Colony size was measured in ImageJ-win64 using a custom macro (see **Appendix A**). Briefly, the macro first specified the plate area (with manual correction where this area was misaligned with the plate) before enhancing the contrast between the agar background and colonies. Then, images were binarized using the built-in auto-threshold function, to produce binary images where colonies were white and the background black. Then, touching colonies were separated using the built-in watershed function. Colonies showing low

circularity (i.e., overlapping colonies) were excluded from analysis as these tended to be two overlapping colonies that could be separated by the watershed function. The areas of the selected colonies were then measured using the built-in analyse particles function. The coefficient of variation (CV) in colony area for each isolate was calculated as below:

$$\text{Coefficient of Variation (CV)} = \frac{\sigma}{\bar{x}} * 100\%$$

Where σ is the standard deviation of colony area and \bar{x} is the mean colony area.

2.2.6 Manufacturing aggregates for stress response experiments

To assess the relative stress resistance of organisms located to the surface or interior of aggregates, aggregates were manufactured with defined quantities of yeast cells introduced at the relevant process steps (**Figure 2.1**). In this case, each aggregate was manufactured to contain organisms (*S. podzolica*) either on the interior or exterior, not both, to enable quantitative recovery of all cells of each aggregate. To achieve this, the same procedure was used as in section 2.2.3 except that a ~ 700 cells μl^{-1} suspension ($\text{OD}_{600} \sim 0.03$) was used as inoculum for the interior-aggregation step ($\sim 4,900$ cells). These aggregates were then processed exactly as above except that the second yeast inoculum was omitted at the exterior-aggregation stage. To generate aggregates with sterile interiors and organisms in the exterior layer, the same process was used but the inoculum was omitted for the interior-aggregation stage but included (7 μl of 700 cells μl^{-1} suspension) for the exterior-aggregation stage. In experiments where aggregate properties were altered to produce more compacted

aggregates, the same process as above was repeated, except that vortexing was for 30 seconds at speed 3 instead of the original 15 seconds for one compacted aggregate type, or speed setting 3 for 10 seconds followed by speed setting 6 for 20 seconds for the second compacted aggregate type.

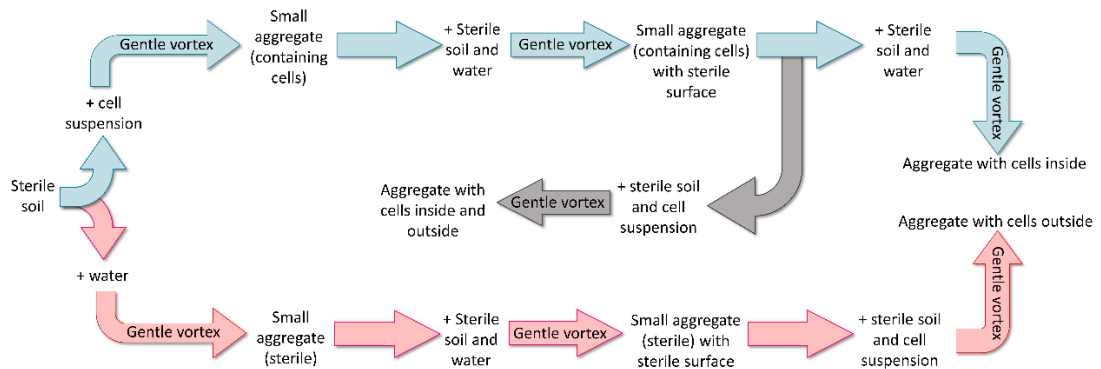


Figure 2.1- Outline of procedure for producing soil aggregates

Microbial cells either contained within the aggregates (green-blue), near the surface of aggregates (red), or both inside and outside of each aggregate (black).

2.2.7 X-ray Computed Tomography (CT)

The pore structures of natural and manufactured soil aggregates were imaged using a Phoenix Nanotom S X-ray CT scanner at the Hounsfield Facility at the University of Nottingham. Each projection image was an integration of 3 images with a skip setting of 2 discarded images. Voxel resolution was set at 2 μm , potential energy at 90 kV and current at 65 μA . The total scan time was 63 min per aggregate and a total of 1440 projections were captured for each aggregate. VGStudio MAX was used to generate and calculate the 3D pore volumes of CT imaged aggregates as well as pore-surface connectivity. The images were then exported as image stacks to ImageJ-

Win64 where the images were binarised using the Li threshold algorithm (Li and Tam, 1998) and the total porosity and pore equivalent spherical diameter (a measure of pore size) subsequently determined using the BoneJ plugin (Doube et al., 2010).

2.2.8 Water evaporation analysis

Sterile regular- and more compact-aggregates were manufactured as described previously and transferred in 15 ml centrifuge tubes to the Advanced Manufacturing Building, University of Nottingham for thermogravimetric analysis. Thermogravimetric analysis was then conducted on each aggregate individually at 50°C for 1 hr using a PerkinElmer TGA 4000 with the chamber pre-heated to 50°C. Weight measurements of individual aggregates, taken every second, were converted to percentage of starting weight to obtain percentage weight loss over time. A sigmoidal curve was fitted to each replicate dataset (GraphPad Prism 9), and the derived Hill slope of each curve was used to compare water evaporation rates between samples.

2.2.9 Stress survival of cells located within and outside of aggregates

Approximately 400 mg sterilised, ground soil was transferred to each well of a 24-well microtiter plate (Greiner Bio-One) and a single aggregate, prepared as described above, was then placed on the centre of each soil sample, before covering with a further 400 mg sterilised, ground soil. For lead (Pb) stress treatments, each well was then treated for 1 h with 1.2 ml of 2% (w/v) D-glucose supplemented or not with 12 mM $\text{Pb}(\text{NO}_3)_2$. For anoxia stress, the 24-well plates were incubated for 220 h at 24°C either under anaerobicity [Whitley DG250 anaerobic workstation; Don Whitley

Scientific (10% CO₂, 10% H₂, 80% N₂) or in ambient air. For heat stress, 24-well plates were incubated for either 30 min at 50°C or 3h at 40°C, or 24°C for either duration for control treatments. After treatment, each aggregate was recovered using a sterile metal spatula, deposited into 3 ml sterile water and vortexed vigorously for 1 min to break up the aggregate and release cells. After allowing soil to settle for ~20 s, 1 ml of supernatant was taken and centrifuged at 4500 g, 7 min. The supernatant was removed, and the cell pellet re-suspended in 500 µl sterile water before spread plating 100 µl aliquots to Petri plates containing MYP agar. Colony forming units were counted after incubation at 24 °C for 7 d. Percentage survival was determined from counts obtained for stressed versus control treatments.

2.3 Results

2.3.1 Manufacture of discrete soil aggregates mimicking natural aggregates and introduction of organisms to aggregate-interior or -exterior

To enable the study of soil microbes both within and on the surface of soil aggregates under controlled conditions, a method to manufacture artificial soil aggregates in the laboratory was developed. Gentle vortexing of ground samples of the soil collected from a zero-tillage farm site in Rutland, UK (which naturally showed a strong propensity to aggregate before grinding) with sterile water was sufficient to produce aggregation of soil particles. A single cohesive aggregate per assay, approximately 1.5 mm in diameter, was achieved at an intermediate vortexing vigour, whereas low or high vortex speeds tended to produce smaller aggregates of varying number and size (**Figure 2.2A**). The volume of water added to the sample was a strong determining factor in how well the soil aggregated. At 5 μl water, not all soil particles aggregated (producing a smaller aggregate), whereas at 9 or 11 μl water, the soil tended to smear on the tube wall and single, cohesive aggregates did not form reproducibly (**Figure 2.2B**). Single aggregates were readily formed at 7 μl water. The aggregates were approximately 1.5 mm in diameter. It is likely that soils of a different particle size composition would react differently than described above, as particle size is known to affect granulation processes (Iveson et al., 2001).

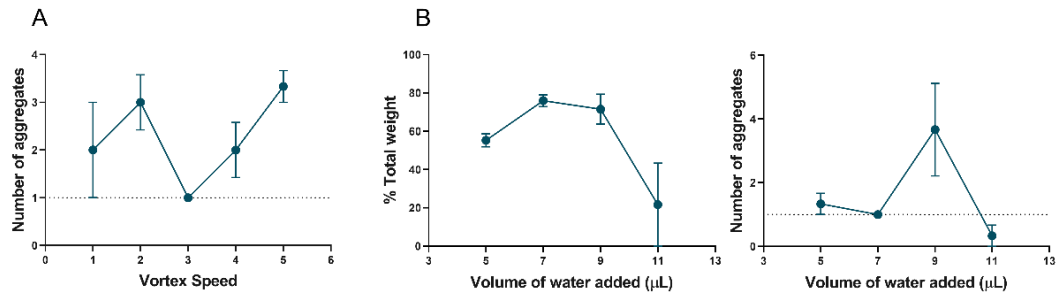


Figure 2.2- Optimising parameters for manufacture of soil aggregates

For 20 mg of soil, the vortex speed and amount of water added before vortexing influences the number of aggregates and the percentage of total mass (soil and water) accumulated into the aggregate. A) Effect of vortex speed (setting number on vortex machine) on number of aggregates produced per sample (20 mg soil + 7 μL water). B) Effect of volume of water added on percentage of total sample mass (20 mg soil + water) that accumulated in aggregate (left panel), or on number of aggregates formed (right panel); vortex speed 3. When soil slurried and did not produce any discernible aggregates, a value of zero was recorded. Values shown are mean ± SEM from 3 technical replicates.

2.3.1.1 Manufactured aggregates Properties

To compare the properties of the aggregates manufactured in the laboratory with natural aggregates, examples of both, from the same batch of soil, were scanned using X-ray Computed Tomography (CT) (Figure 2.3A). X-ray Computed Tomography is an imaging technique that combined multiple X-ray images of a subject, acquired from multiples angles, to produce a three-dimensional tomographic image. The manufactured aggregates exhibited very similar % pore space and % pore-surface connectivity compared to natural aggregates (Figure 2.3B). The pores of manufactured aggregates had a slightly smaller (c. 10 μm difference) average equivalent spherical diameter than the natural aggregates, but this was not

significant (two-sample t-test, $p = 0.084$). The mean pore space and equivalent spherical diameter were also very similar between the inner and outer halves of the manufactured aggregate ($p = 0.840$, $p = 0.371$ respectively) suggesting that the two-step manufacturing process did not produce different physical micro-environments in these fractions.

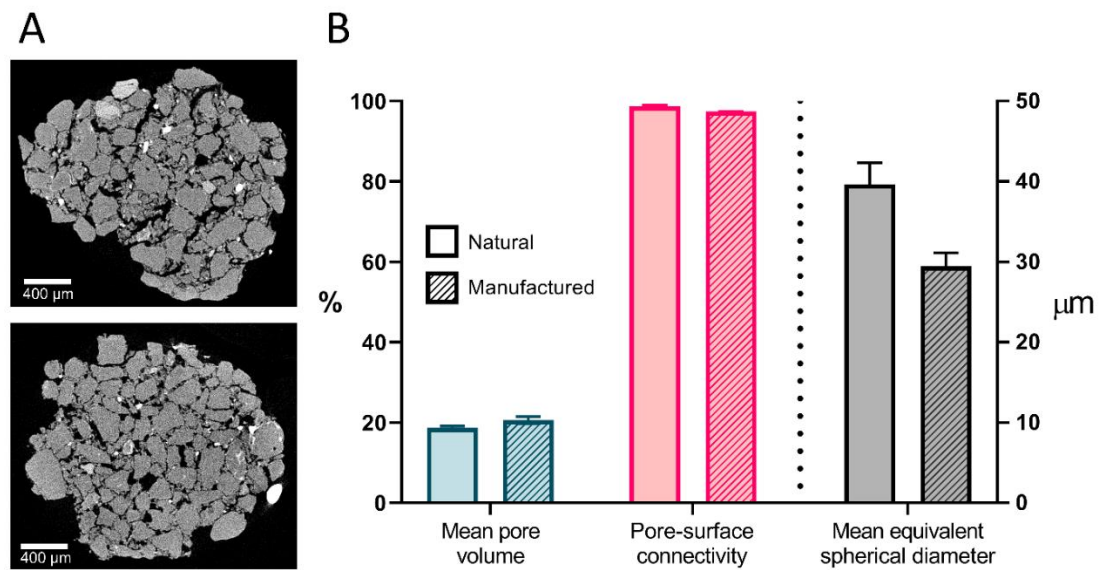


Figure 2.3- Comparison of porous structure of natural and manufactured soil aggregates

(A) Representative CT- X-ray images of natural (top) and manufactured (bottom) soil aggregate interiors where particles are grey and pore space is black. Scale bar represents 400 μm . (B) Values for mean pore volume (percentage of whole aggregate volume) in single aggregates and the percentage of internal pores connected to an aggregate's surface (left axis) and the average three-dimensional mean equivalent spherical diameter (ESD) within an aggregate (right axis) were determined by CT X-Ray analysis. $n=2$ aggregates, error bars represent SEM.

2.3.1.2 *Organisms can be independently recovered from the aggregate interior and exterior*

To study aggregate-associated microorganisms, aggregates were produced containing *S. cerevisiae* W303 cells within the aggregate interior, and *S. cerevisiae* BY4741 on the aggregate exterior. These strains were chosen as they could be distinguished by cultivation (after recovery from aggregates) on media selective for respective auxotrophies, as only the W303 strain can grow without methionine supplementation and only the BY4741 strain can grow without tryptophan supplementation. Bathing the aggregate with gentle agitation in water was sufficient to recover BY4741 cells from the aggregate surface but not the W303 cells from the aggregate interior (**Figure 2.4A**). After subsequent sterilisation of the aggregate surface with diluted electrolysed water solution (Wohlgemuth et al., 2020) and then aggregate disruption by vortexing in sterile water followed by plating, it was apparent that this second fraction comprised W303 cells that had been introduced to the interior (**Figure 2.4B**). There appeared to be negligible mixing of cells from the aggregate exterior and interior when isolated with this method: only one yeast strain was recovered from each of the two fractions, as anticipated from the manufacturing process. This showed that organisms could be selectively introduced to and/or recovered from the exterior or interior of aggregates.

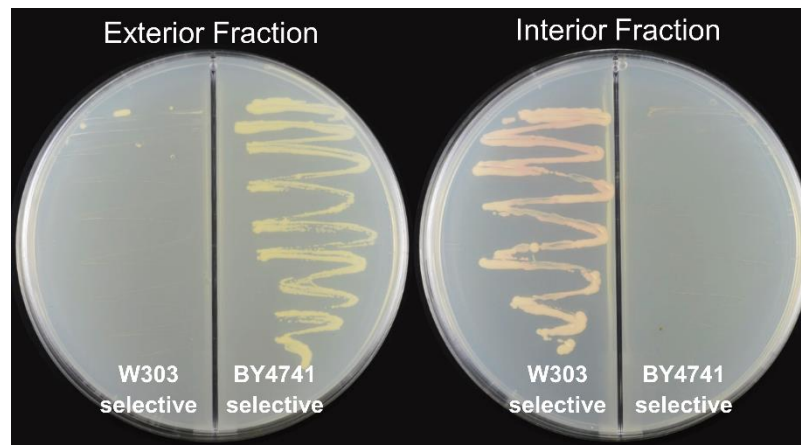


Figure 2.4- Recovery of cells from the exterior or interior of the same manufactured aggregate

Aggregates were produced which incorporated red-pigmented *S. cerevisiae* W303 cells in the aggregate interior and non-pigmented *S. cerevisiae* BY4741 cells at the aggregate exterior. Cells were recovered in fractions from the aggregate exterior (left) then the aggregate interior (right) (see Materials and Methods) for streak plating to two-compartment agar plates containing W303 selective medium in the left half and BY4741 selective medium in the right half of each plate.

The procedure was adapted to study a single soil organism, *S. podzolica*, in the aggregate; that is, the same organism at both exterior and interior locations. As the use of the single organism did not enable routine verification of purity of the interior or exterior fractions, as done above with the *S. cerevisiae* strains, the manufacture protocol was amended to incorporate *S. podzolica* into either the interior or exterior of different aggregate preparations. This was undertaken by introducing cell-free sterile water instead of inoculum at the appropriate stage of manufacture (see Materials and Methods 2.2.6). Similar numbers of cells could be reproducibly recovered from aggregates where *S. podzolica*, at equivalent inoculum size, had been introduced either to the interior (4164 \pm 767 colony forming units (CFU) recovered) or exterior (4116 \pm 605) of the aggregate (**Figure 2.5**).

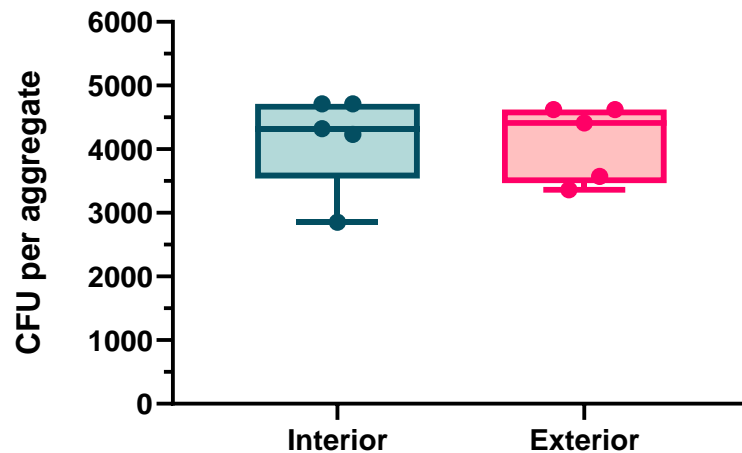


Figure 2.5- Variation in recovery of CFU from aggregates

CFU recovery from aggregates produced with ~4,900 cells of *S. podzolica* incorporated either in the aggregate-interior or -exterior. Data are shown for 5 replicate aggregates of each type. Bars show median, minimum, and maximum values.

2.3.2 Phenotypic heterogeneity of *S. podzolica* in the aggregate interior or exterior

2.3.2.1 *S. podzolica* isolated from natural aggregates showed no difference in colony size heterogeneity

Previous research had suggested that the aggregate interior possessed a more heterogeneous spatial distribution of carbon and nutrient within the pore network, relative to the aggregate exterior (Ananyeva et al., 2013). Because of this, it was hypothesised in the present study that microorganisms from the aggregate interior or exterior of natural aggregates may have been subject to different fluctuations in nutrients access as cells on the exterior would be more homogeneously exposed to

nutrients moving through the soil matrix compared to those within the heterogeneous aggregate interior.

Experiments were conducted to determine whether organisms isolated from the aggregate interior or exterior had adapted heterogeneity or homogeneity in their single-cell growth rates (a possible response to heterogeneous or homogeneous nutrient distributions), using variation in colony growth area as an indicator of growth rate of spread-plated cells. Whilst there are other measurements of phenotypic heterogeneity, colony variation was selected for study as it relates variation in growth, a broad measure of fitness.

S. podzolica isolates were prepared from the interior or exterior of aggregates of an agricultural soil (Rutland, UK) using the developed exterior-interior isolation method. Briefly, this involved washing the aggregate with water to collect exterior organisms before washing with electrolysed water solution to sterilise the aggregate surface. The surface-sterilised aggregate was then disrupted by vigorous vortexing in water to release cells from the aggregate interior. After plating these supernatants onto agar containing bacterial antibiotics to select for fungi and isolating individual colonies, ITS sequencing was used to confirm that these isolates were *S. podzolica*. Isolates were cultivated in MYP broth before spread plating onto either MYP agar, or YEPD agar with varying glucose concentrations and assessing subsequent variation in size of single colonies of each isolate. A range of glucose concentrations were used to determine whether the degree of colony size heterogeneity was influenced by nutrient limitation, as this limitation was expected to occur in natural soils. Across

four isolates from each aggregate fraction, no significant difference in colony area variation (measured as the colony area coefficient of variation (CV), calculated for each isolates as standard deviation in colony area divided by the mean colony area) was apparent between isolates from the aggregate interior and exterior when grown on MYP agar (**Figure 2.6A**) (two-sample *t*-test, $p = 0.4211$). This was also the case for cells grown on YEPD agar across a range of glucose concentrations (**Figure 2.6B**) (two-sample *t*-test with Holm-Sidak multiple test corrections, $p > 0.05$ for all tests).

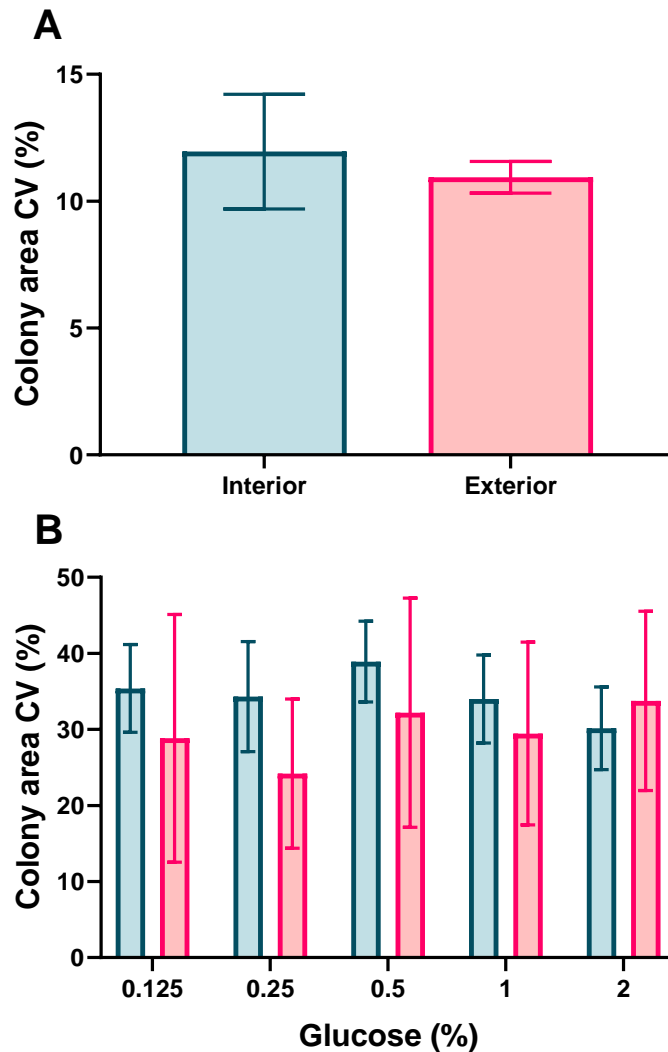


Figure 2.6- Colony area variation on MYP and YEPD agar of *S. podzolica* isolated from either the interior or exterior of aggregates from an agricultural soil

Colony area of isogenic populations isolated from the interior (blue bars) or exterior (red bars) of aggregates from an agricultural soil (Rutland, UK) were measured on either MYP agar (A) or YEPD supplemented with a range of glucose concentrations (B) and coefficient of variation (CV) in colony area was calculated for each isolate. There was no significant difference in colony area CV on MYP agar (two-sample t-test, $p = 0.4211$) or on YEPD agar in any glucose concentration (two-sample t-test with Holm-Sidak multiple test corrections, $p > 0.05$ for all tests). For each of the two aggregate fractions, four independent *S. podzolica* isolates were measured, each from a different aggregate. A total of at least 100 colonies was used to calculate the CV for each isolate in each condition. Error bars represent SEM ($n = 4$ isolates).

2.3.2.2 *Survival of lead exposure in soil aggregates by S. podzolica with different levels of lead heteroresistance*

Phenotypic heterogeneity in response stressors, here termed heteroresistance, refers to the phenotype whereby individual cells from an isogenic population display differences in resistance to a stressor, such that not all cells lose viability simultaneously (Hewitt et al., 2016). Experiments were conducted to determine if yeast heteroresistance affected survival of stress in different soil-aggregate fractions. It was hypothesised that lead introduced to the aggregates would differentially distribute within the aggregate interior or exterior, as the aggregate exterior may be more uniformly exposed to lead in these experiments, whereas lead may propagate through the interior pore network less homogeneously.

Previous research conducted at the University of Nottingham by Dr. Sarah Hewitt involved isolating *S. podzolica* from lead polluted soils and assaying their IC₅₀ and heteroresistance to lead nitrate by generating dose-response curves and measuring the angle (calculated as the “Hill slope”) of those curves, with a shallower curve representing a more heterogeneous stress response. This resulted in the isolation of several non-clonal isolates with similar IC₅₀ but different degrees of heteroresistance. Aggregates were produced as described in section 2.2.6, incorporating characterised *S. podzolica* isolates with either a relatively low or high heteroresistance in response to lead into either the aggregate interior or exterior. Aggregates were then mixed in with a larger amount of the soil (twice-autoclaved) of the same type (sandy silt loam) as that from which the aggregates had been produced. After 12 mM lead nitrate challenge (sufficient to elicit a partial reduction in CFU) introduced to the soil in water

solution for 1 hr, cells were recovered from the aggregate and spread-plated to assay survival by comparing the number of colony forming units (CFU) relative to control aggregates. There was no significant difference in survival between cells in either aggregate location for both low- ($p = 0.1387$) and high- ($p = 0.7442$) heteroresistance strains, determined by two-sample t -test (**Figure 2.7**).

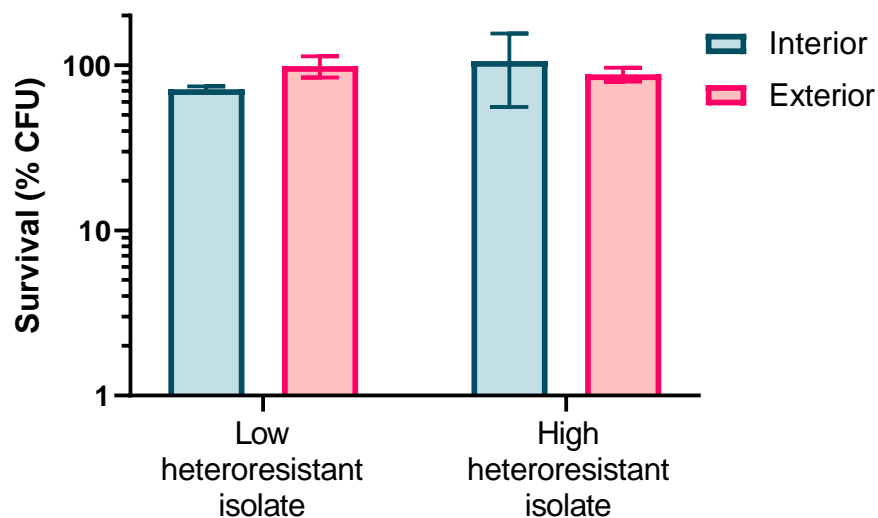


Figure 2.7- Location specific stress resistance of low- and high-heteroresistance yeast isolates

Comparison of resistance in response to 12 mM lead nitrate exposure for 1h between *S. podzolica* isolates with relatively low (left) or high (right) heteroresistance, incorporated to either the interior (blue) or exterior (pink) of manufactured aggregates. For both isolates, there was no significant difference in survival between cells located in the aggregate interior or exterior ($p = 0.1387$, $p = 0.7442$, two-sample t -test). The data are averaged from three biological replicates, error bars represent SEM.

2.3.3 Cells within aggregates show stressor-dependent, differential survival compared with cells at aggregate surfaces

After seeing no obvious location specific effects of heteroresistance between relatively low and high heteroresistant isolates, artificial aggregates were generated to test the hypothesis that soil aggregation may buffer organisms from environmental stress independently of heteroresistance. Aggregates were manufactured as above with the low heteroresistant *S. podzolica* (isolate C3-11) isolate localised either to the aggregate-interior or -exterior. These aggregates were then mixed in with a larger amount of the soil (twice-autoclaved) from which the aggregates had been derived before testing a small panel of soil-relevant environmental stresses. Treatment with 12 mM lead nitrate (using the approach described above) caused ~30-40% loss of viability of aggregate-associated yeasts within 1 h, according to counts of CFUs recovered from aggregates. However, there was no significant difference in survival of this Pb stress by cells at the interior or exterior of aggregates (**Figure 2.8A**).

Soil samples were also incubated under anaerobicity, as anoxia is a common issue in soils prone to seasonal or permanent waterlogging because water displaces air in the pore spaces of these soils. This caused some loss of *S. podzolica* viability over time as this yeast is an obligate aerobe (**Figure 2.8B**).

Moreover, similar to the acute Pb-stress, there was no evidence that the aggregate interior buffered cells from anoxic stress compared to the cells from the aggregate exterior. High temperature, as an alternative physical stress (e.g., associated with

forest fires, soil solarisation, etc.), caused some loss of yeast viability within 30 min at 50°C and also within 3 hours at 40°C. In this case, and in contrast to the other stresses, relative survival of heat stress at the aggregate exterior was <50% of that by cells in the aggregate interior (**Figure 2.8C**).

This difference was reproducible over three independent replicate experiments. However, despite both treatments eliciting a loss of viability, the difference in survival between cells in the aggregate interior or exterior was lost after incubation for a longer period of 3 h at the higher temperature (40°C) (**Figure 2.8C**). Collectively the data indicate that soil aggregates may buffer microbial communities from environmental stress only in particular circumstances.

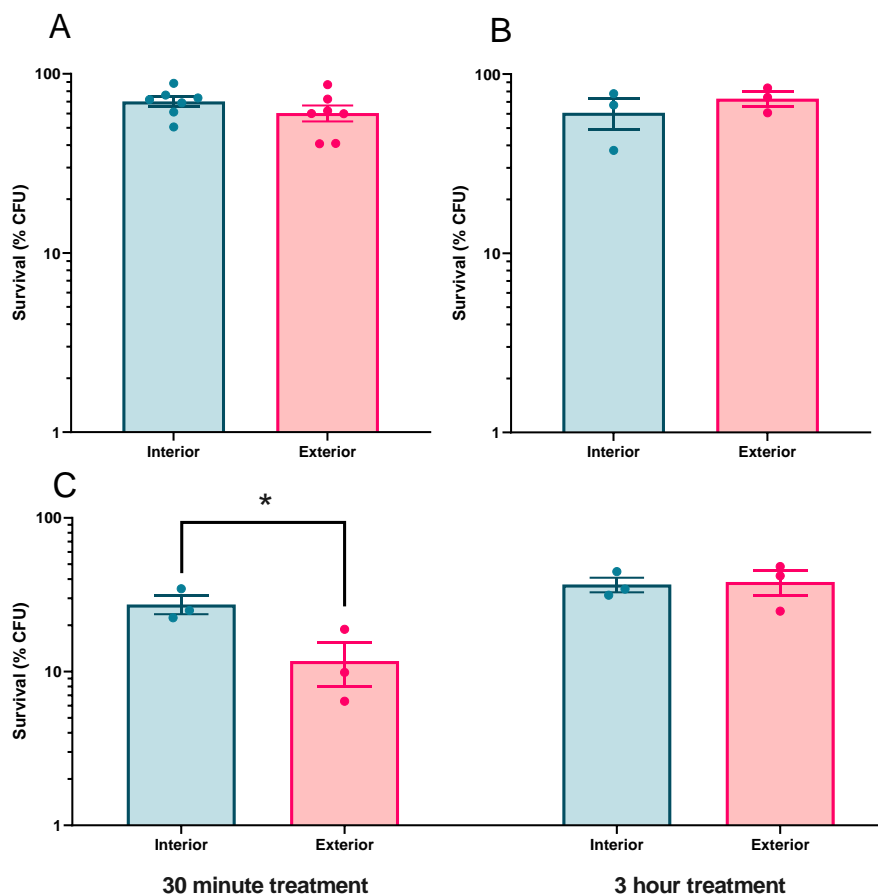


Figure 2.8- The survival (% CFU versus control) of *S. podzolica* within or on the surface of soil aggregates in response to different stresses

The survival of *S. podzolica*, within the interior and exterior of manufactured aggregates, in response to acute (60 min) exposure to 12 mM lead nitrate (A) ($p = 0.2335$, two-sample t-test), incubation in anoxic conditions (B) for 216 h ($p = 0.4630$), and in response to acute heat stress (C) at 50 °C for 30 min (*, $p = 0.0408$), or 40 °C for 3 h ($p = 0.4903$). Post treatment, aggregates were disrupted, and the cells pelleted and washed before spread plating onto MYP agar to assess survival according to colony forming ability. Error bars represent SEM. Individual points represent biological replicates.

2.3.4 The impact of altering aggregate physical characteristics on survival of *S. podzolica* within an aggregate

For most purposes it would probably be desirable that manufactured aggregates resemble natural counterparts (from the parent soil), but production of aggregates with alternative properties does allow investigation of the impact of changing aggregate structure, e.g., on microbial activities. The feasibility of this was explored here by altering either the vortex duration, speed, or both when manufacturing soil aggregates in order to produce more-compacted aggregates. Here, the term “compaction” refers to the pressing together of soil particles, reducing pore space between them, and is common in soil systems as a result of heavy machinery usage in agricultural practice. The proportion of aggregates occupied by pore volume (percentage pore volume) and pore-surface connectivity could be significantly reduced by increasing the vortexing speed, but not by increasing vortexing duration (**Figure 2.9**). Although equivalent spherical diameter (ESD) appeared somewhat reduced in both cases, this was not statistically significant (there was relatively large error in the short duration, low speed condition). When increasing vortex speed, it was necessary to first establish a “proto-aggregate” by vortexing for 10 seconds at speed 3, before increasing the vortex speed to speed 6 for 20 seconds, otherwise many smaller aggregates would form and not combine to produce a single, stable aggregate.

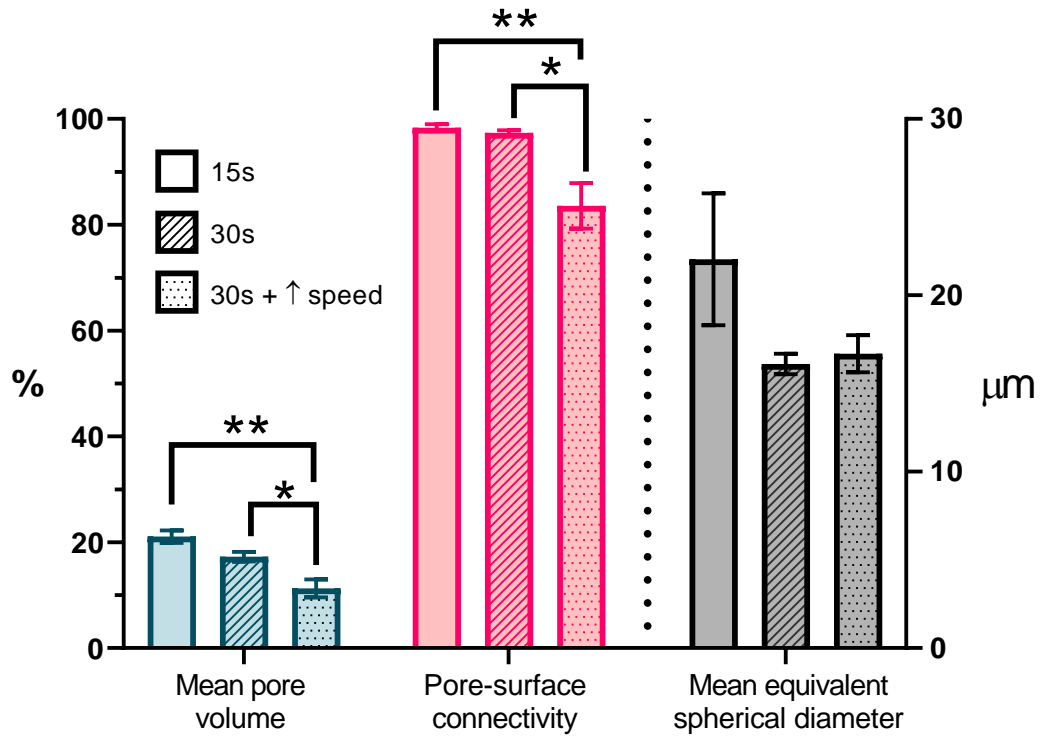


Figure 2.9- Varying vortex settings can alter aggregate pore properties

Values for mean pore volume (as a percentage of whole aggregate volume) in single aggregates and the percentage of internal pores connected to an aggregates surface (left axis), and the average three-dimensional mean equivalent spherical diameter (ESD) within an aggregate (right axis) were determined for aggregates manufactured with different vortex settings. Aggregates were produced with 15 seconds vortexing at speed 3 (open bars, n=3), 30 seconds at speed 3 (dashed bars, N=4), or 10 seconds at speed 3 followed by 20 seconds at speed 6 (dotted bars, n=4). Error bars represent SEM. *, p < 0.05; **, p < 0.01.

After establishing a method for producing higher density aggregates to mimic aggregate compaction (i.e., longer duration, higher speed vortexing), *S. podzolica* was incorporated either interior or exterior of aggregates produced in this way. These were subsequently exposed to lead nitrate (12 mM for 1hr) or heat stress (30 min at 50°C) as in previous experiments. Aggregate compaction did not significantly affect

survival of lead nitrate exposure for cells in either aggregate location (**Figure 2.10A**). In contrast, cells within compacted aggregates showed a significantly greater resistance to heat stress in comparison to regular aggregates, which was not the case for cells on the aggregate exterior (**Figure 2.10B**). In contrast to previous data (**Figure 2.8C**), here there was no significant difference in heat stress resistance between cells in the interior or exterior of regular aggregates. This may possibly have been related to the overall higher percentage survival seen in this experiment in comparison to the original aggregate experiments (the experiments were performed several months apart and day to day consistency of absolute killing rates by stressors are very difficult to control, even with the culture history of test organisms is the same; being potentially affected by minor changes in ambient laboratory conditions, water quality, batches of media etc).

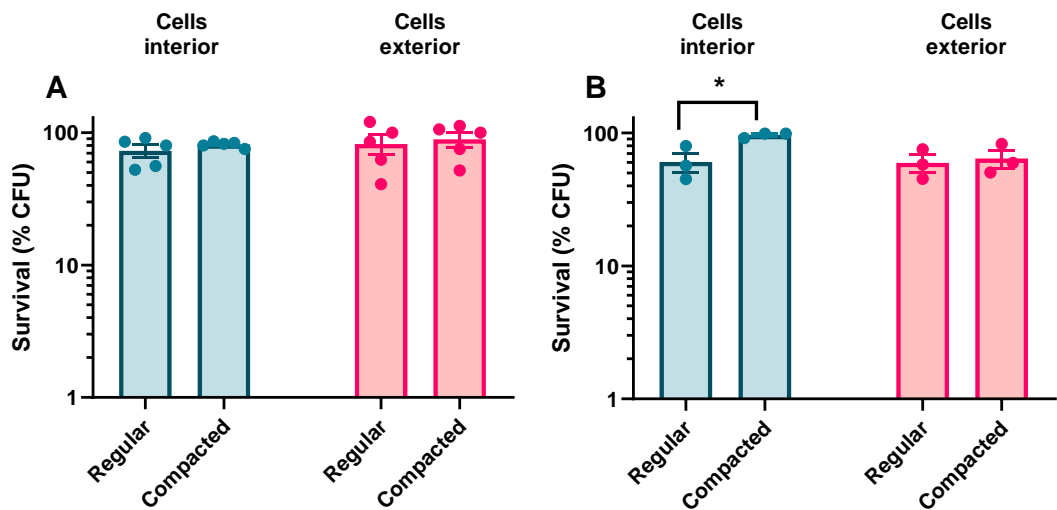


Figure 2.10- The survival (% CFU versus control) of *S. podzolica* interior and exterior of regular or compacted soil aggregates

The survival of *S. podzolica* in the interior (blue, $p = 0.326$, two-sample t-test) or exterior (red, $p = 0.699$, two-sample t-test) of regular or compacted manufactured aggregates in response to 12mM lead nitrate exposure (60 min) (A) was compared to examine the impact of compaction on microbial stress resistance. This comparison was also considered after 50°C heat stress for 30 min (B) for cells in the interior (blue, $p = 0.027$, two-sample t-test) or exterior of (red, $p = 0.738$, two-sample t-test) regular and compacted manufactured aggregates. Error bars represent SEM, individual points represent independent biological replicates.

It was hypothesised that differences in water evaporation rates between compacted and regular aggregates could explain the survival differences seen during heat stress treatments (**Figure 2.10**) as water has a higher heat capacity than air (4200 Jkg⁻¹K⁻¹ vs 993 Jkg⁻¹K⁻¹, respectively) and can reduce heating by evaporation. To test this hypothesis, sterile compacted and regular aggregates were produced and their water

evaporation rates at 50°C were measured over the course of 1 hr by heating individual aggregates to 50°C and measuring their weight loss over time. There was no significant difference between evaporation rates (measured as the Hill slope of the evaporation curve) between regular and compacted aggregates (two-sample *t*-test, $p = 0.4211$) (**Figure 2.11**). It was noted that there was some variation in water evaporation between samples. This may be because all aggregates were manufactured at once, but only one aggregate could be weighed and measured at a time, meaning evaporation may have occurred between manufacturing and weighing to produce evaporation curves (regular and compacted aggregates were weighted alternately, accounting for the apparent “pairing” between curves of each aggregate type). The results are discussed further in section 2.4.4 below.

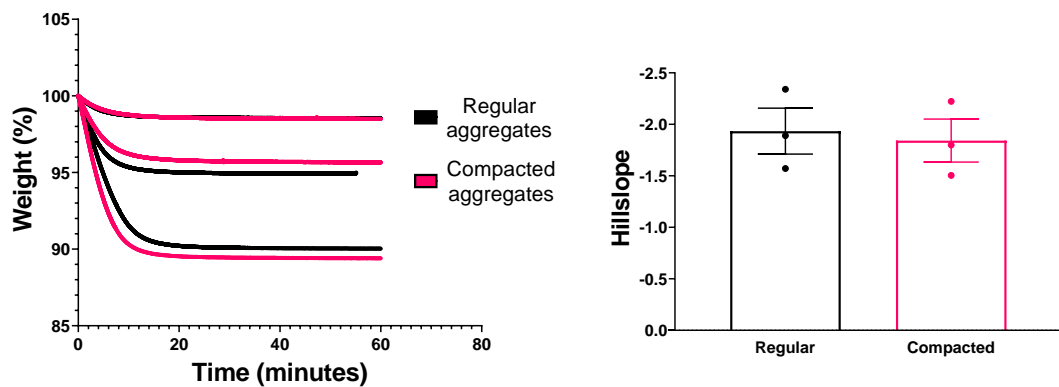


Figure 2.11- Water evaporation curves of regular and compacted aggregates under conditions mimicking heat stress experiment

Water evaporation curves of individual regular (black) and compacted (pink) aggregates were measured and presented as a percentage of aggregate starting weight (left) ($n=3$ of each aggregate). The gradient (Hill slope) derived from each aggregate replicate evaporation curve

to indicate evaporation rate was also compared between regular and compacted manufactured aggregates (right) (n=3).

2.4 Discussion

This chapter describes a simple and reproducible method for manufacturing realistic soil aggregates that could be readily adopted by other laboratories. Aggregates could be manufactured with a microbial composition that is defined qualitatively (i.e., choice of organisms), quantitatively, and spatially (i.e., localisation to aggregate-interior or -exterior), with organisms also being selectively recoverable from aggregate interior and exterior. These features enable the study of the impact of soil aggregation on microbial activities in soils, previously limited by retrospectively analysing aggregates from natural soils. This was exploited here to demonstrate selective buffering by aggregates of some environmental stresses and to examine interaction between microbial phenotypic-heterogeneity and the structured aggregate environment. Furthermore, manufactured aggregates could be compacted, altering their pore properties, to assess the impact of aggregate compaction on microbial stress resistance.

2.4.1 Manufacture of aggregates

Analysis by X-ray CT showed that there was close morphological similarity between the manufactured and naturally formed macroaggregates from the same parent soil material. This was reflected quantitatively by similar measurements of pore space and connectivity. These pore properties are important determinants of gas and liquid accessibility into aggregates and of the available space for microorganisms to occupy and modify (Sexstone et al., 1985; Carson et al., 2010).

Additionally, aggregates could be produced with differences in physical characteristics, such as the internal porosity and pore-surface connectivity, by varying the vortex speed and duration during production (here used to produce compacted aggregates, relative to the original manufactured aggregates). This facilitated assessing the impact of changing aggregate structure on microbial stress response. Unfortunately, it was not possible to alter individual characteristics separately, e.g., changing % porosity while maintaining the same pore-surface connectivity.

Cells were recovered reproducibly from aggregates that had been manufactured with incorporation of yeast cells. The technical variation in recovery was low and similar for cells recovered from either the interior or surface of aggregates. This suggested that similar numbers of cells are incorporated to each aggregate and that their recovery rates post-experiment are relatively reproducible.

2.4.2 Recovery of organisms from manufactured and natural aggregates

Selective recovery of yeast cells from either the interior or exterior of aggregates only required a simple wash to collect exterior organisms then aggregate-disruption to release yeast from the aggregate interior, with an intervening surface sterilisation step. This also corroborates that the aggregate manufacturing process does generate spatially discrete environments for organisms, with only one of the two environments readily accessible (to a sterilising solution) from the aggregate surface. Whereas the procedure for recovering organisms from the interior and exterior of the same aggregate lacks the quantitative recovery from aggregates carrying cells only either

internally or externally (as performed here in experiments involving stress exposure of *S. podzolica*), it does allow assay of both microhabitats in the same aggregate. This could be valuable for experimental evolution applications, for example, where absolute recovery rates can be less important. Where quantitative recovery was necessary, such as in the stress experiments, aggregates could easily be produced with organisms in just one fraction and recovered by disrupting the aggregate as before.

2.4.3 Interaction between organism heterogeneity and position in soil aggregates

2.4.3.1 Colony area variation

In addition to validating the aggregate manufacturing method, isolation of organisms from an aggregate exterior and interior was also applied to natural aggregates. The intra-aggregate pore network is likely to be more heterogeneous than the inter-aggregate network, and there is evidence that a more heterogeneous pore network results in a more heterogeneous distribution of carbon available to microorganisms (Ananyeva et al., 2013). This is also more likely to be the case in soils where aggregates tend to be more stable (Sasal et al., 2006) and aggregate turnover is expected to be slower (Six et al., 2000), reducing the likelihood of aggregate breakage and reformation.

Because of this, it was reasoned in this study that organisms from the aggregate interior would possess a more heterogeneous growth phenotype to match their more heterogeneous environment, relative to exterior counterparts. This was measured

using variation in colony area (Chacon et al., 2018, Bar et al., 2020, Altamirano et al., 2018), with the underlying assumption that differences in single cell growth rate are reflected subsequently in the macroscopic colony area that they produce. In contrast to the hypothesis, there was no apparent difference in colony size variation between *S. podzolica* isolated from the aggregate exterior or interior when plated either on MYP agar plates, or on YEPD plates with lower (~ 0.1 %) glucose concentrations to mimic reduced carbon availability. However, this does eliminate the possibility that growth variation may adapt to variable carbon availability. For example, it may have been the case that the aggregates used in this experiment were recently formed and hence sufficient time for adaptation was lacking, or that any adaptive growth difference may not be expressed in the agar-based growth conditions tested here. These issues could be partly addressed by making aggregates with organisms inside, conducting long-term evolution experiments, and assaying colony size and variation before and after inoculation. However, it would be difficult to ensure that any additional nutrients supplied to the soil would distribute in the same manner as in natural systems. Furthermore, the relatively slow growth in soil substrates would drastically increase the doubling time of any introduced organism, and many hundreds of doublings are typically required in evolution experiments (Van den Bergh et al., 2018).

A future experiment to assess colony area variation, although beyond the scope of this thesis, could be to isolate and examine organisms from the interiors of aggregates of a conventional agricultural system and soils from a natural, successive vegetation system. It has been demonstrated that aggregates of a natural successive

system have greater intra-aggregate variation in pore size and carbon localisation than those of a comparable agricultural system (Ananyeva et al., 2013). In that case, it might be hypothesised that interior organisms of the natural successive system would show a more variable phenotype (e.g., in colony area) than those adapted to the more homogeneous internal aggregates of the agricultural system.

2.4.3.2 *Lead nitrate heteroresistance*

In addition to differences in nutrient distribution between the aggregate interior and exterior, it was also hypothesised that there would be variation in stressor exposure between organisms in the interior and exterior aggregate fractions. In the present experiments lead nitrate was introduced to each aggregate, externally, as an aqueous solution. Therefore, it was expected that the aggregate exterior would be more completely exposed to the stressor, whereas it would differentially propagate through the aggregate interior depending on the pore architecture of each aggregate; consequently producing a more heterogeneous exposure to lead within the aggregate interior, relative to the aggregate exterior. Therefore, it was hypothesised that *S. podzolica* isolates expressing relatively homogeneous or heterogeneous resistance to lead nitrate would favour the aggregate exterior or interior, respectively. However, no relationship between heteroresistance and position within aggregate was apparent from these experiments. This could suggest that either there was no substantial difference in stressor distribution and microbial exposure to the stressor between aggregate interior and exterior, or that heteroresistance did not significantly impact survival in these conditions.

It would be challenging to determine accurately the variation of lead nitrate concentration across a single manufactured aggregate (measuring only 1.5 mm in diameter) during a stress response experiment. Therefore, an alternative future approach for assessing the adaptation of heteroresistance in response to stressors would be to isolate wild yeast from a recently polluted soil site (such that the stressor has not become homogeneously distributed within the soil over time) with a slow aggregate turnover rate (to allow sufficient time for microbial adaptation of different isolates within the same aggregate). Then, the heteroresistance of organisms from the interior and exterior of single aggregates could be determined in response to pollutants present at the site. However, such conditions are not very common in nature and hence it may be more widely applicable to consider average stressor resistance in relation to position within a soil aggregate when, as discussed in greater detail below.

2.4.4 Survival of stress by organisms with respect to aggregate location

Regarding metal stress and microbial metal resistance, previous work has suggested that strongly attached organisms located within pores of the aggregate interior are less exposed to toxic metals in the soil matrix (Almås et al., 2005). In contrast, other work suggests some metals tend to concentrate in the aggregate interior (Ilg et al., 2004). These examples highlight the difficulty of disentangling the relationship between microbial positioning within an aggregate and stress exposure. Pb stress was examined using manufactured aggregates, relevant to soils polluted with lead as a result of mining and smelting activity among other possible activities (Toth et al., 2016). No evidence was found for the protection from Pb by cell localisation within

the aggregate interior, suggesting that the dissolved metal equilibrates at a similar available concentration within the aggregate pore space as near the aggregate surface. Furthermore, even when manufacturing higher density aggregates to reduce both available pore space and connectivity between pores, similar levels of survival were observed between cells in both aggregate fractions. This would suggest that reducing pore-surface connectivity was not sufficient in these aggregates to reduce the penetration of the metal solution. It may be that the solution was able to penetrate through the aggregates via pores of diameter below the X-ray CT scanning resolution of 2 μm , as it has been noted that these smaller pores are less prone to compaction than larger pores (Sumner, 2000).

Soils are also known to present marked, spatially heterogeneous oxygen gradients, even within single aggregates (Sexstone et al., 1985; Schlüter et al., 2018). *S. podzolica* is unable to grow in anaerobic conditions, but some (not all) cells may survive and resume growth, after a short delay, if restored to an oxygenated environment. Using this phenotype, it was shown that the encapsulation of the yeast cells within aggregates did not reduce the impact of external anoxic stress on cell viability. This evidence suggests oxygen gradients which may arise over the spatial scales of soil-aggregate microenvironments are not sufficient to impact oxygen-sensitive viability, or that the aggregate interior is sufficiently connected to the external environment.

Heat stress was also examined, as soils are naturally exposed to a wide range of temperatures; across different locations, between varying depths at the same

location, and over time (Fick and Hijmans, 2017). Furthermore, events such as wildfires can transiently raise the soil temperature to 60-80 °C (Grant et al., 1997) and even greater (Mataix-Solera et al., 2011), while soil solarisation (used to control plant pathogens in agricultural soils) often produces soil temperatures exceeding 40 °C at 10 cm depth for several days (McLean et al., 2001). Previous literature has reported that some soil physiochemical properties, such as texture and soil organic carbon (SOC), can impact upon microbial heat stress response (Griffiths et al., 2007). Here, aggregation appeared to insulate yeast cells at the aggregate interior from heat stress but only in the short term (30 min), showing a decreased protective effect when treatment was prolonged to 3 hours. This reveals a potentially important role for soil aggregation in buffering microorganisms within the aggregate microenvironment from heat stress in soils. As soil can act as a thermal insulator (Slegel et al., 1977), it stands to reason that the temperature difference between the aggregate exterior and interior may differ initially but will eventually equilibrate over time (within 30 minutes under the experimental conditions used here), in a manner dependent on the thermal conductivity of the soil. In the context of these experiments, it is suggested that the aggregate surface confers some thermal resistance, insulating organisms in the aggregate interior over shorter timescales (e.g., ≤ 30 min) but with thermal equilibration between the aggregate interior and exterior as time progresses.

Conventional agriculture management often leads to soil aggregates and the intra-aggregate pore space becoming compacted, such as by heavy machinery (de Moura et al., 2021). Because of this, the ability to manufacture aggregates from parent soils

and alter their bulk density and subsequent porosity (to mimic compaction) is valuable. Manufacturing aggregates at higher densities to mimic compaction was easily achieved here by increasing the vortex speed and duration during the manufacturing process. However, it was not possible to alter pore parameters independently using this approach, e.g., decreasing pore size while maintaining the same pore-surface connectivity.

It was hypothesised that reducing the pore-connectivity of aggregates would reduce the accessibility of lead into the aggregate interior pore space, hence protecting cells in those pore spaces and increasing survival. However, this was not apparent in lead-survival experiments. As suggested in the discussion above, it is very likely that pores in compacted aggregates could be connected by channels below 2 μm in size, below the X-ray CT resolution used here. If so, these could potentially facilitate lead transport between pores and hence microbial exposure, even though these pores appear disconnected in imaging data.

Regarding heat stress, it was expected that cells within the aggregate interior of compacted aggregates would show reduced survival in comparison to cells within regular aggregates, as compaction reduced the air and water filled spaces within the aggregate. This would be expected to facilitate greater heat conductivity through the aggregate. However, cells in the interior of compacted aggregates showed a greater survival of heat stress than exterior cells. Assuming it is the aggregate physical properties that influence microbial stress exposure, this outcome may seem counter-intuitive, as thermal conductivity is typically greater in solid materials in comparison

to liquids and gases, and a reduced porosity and pore-surface connectivity would suggest a greater solid phase within compacted aggregates by which to transfer heat. This increase in thermal conductivity with increasing density is typical of previous observations in soil materials (Beziat, 1988, Ekwue et al., 2006, Mahdavi et al., 2016). In the present study, as there were no apparent differences in water content or evaporation rate between regular and compacted aggregates, it does not appear that differences in evaporative cooling or latent heat capacity was responsible for the difference in heat stress survival between cells in the interior of regular and compacted aggregates. However, if water content between compacted and regular aggregates is similar, but total pore space is reduced, then compacted aggregates should contain more water filled pore space. If this were the case, it may be that heat is more easily transferred to the water in pore spaces in compacted aggregates, meaning that more heat can be absorbed without increasing the overall temperature within the aggregate.

Regardless of mechanism, it can be suggested that reducing the porosity and pore-surface connectivity of aggregates, at least at the site where this soil was sampled, may increase microbial resistance to some stressors. This is the type of result which should be considered when implementing future changes to land practice, considering the essentiality of microbial vigour for sustaining the health of soil ecosystems.

2.4.5 Conclusions

Soil aggregates can provide other benefits to microorganisms beyond the scope of this chapter, such as protection from predation (e.g., by soil nematodes) (Vargas, 1986), isolation from environmental fluctuation (e.g., nutrient and toxin fluxes) of the bulk soil (Rillig et al., 2017) and compartmentalisation to support discrete micro-communities and associated species resilience (Mummey and Stahl, 2004). Although poorly explored, there are also likely advantages of localisation at the aggregate exterior, such as greater access to carbon and nutrient flow from the bulk soil.

Soil aggregation is an important parameter governing distribution and activity of soil microbiota. The method for manufacturing soil aggregates developed in this study now enables key questions to be tackled in a controlled manner, not available previously. The rationale that aggregate-associated microbial communities can be differentially affected by environmental perturbation according to their relative localisation in or on the aggregates, in a time dependent manner was explored. Consequently, it was demonstrated that certain environmental stress scenarios produce no such effect of localisation, except potentially in a time-dependent manner as observed for thermal stress. Furthermore, altering aggregate physical architecture showed that compaction can further enhance the protective effect of an internal localisation from heat stress. These new insights into interactions at the soil structure / biology interface opens the door to addressing further related questions such as how soil aggregation may influence microbial community composition and longer-term adaptations in response to environmental pressures.

3 THE IMPACT OF INTER-PARTICLE PORE SIZE ON MICROBIAL STRESS RESISTANCE

3.1 Introduction

The previous chapter aimed to assess the impact of soil aggregation, and the intra-aggregate pore space, on microbial stress response. A significant proportion of the pore space in soils is also made up by the spaces between aggregates and other debris, often forming larger pore spaces than those seen within aggregates (Nimmo, 2005b). Furthermore, the size of these pore spaces can vary greatly within a soil, creating a pore-size distribution (Nimmo, 2005b). This pore-size distribution contributes to establishing a heterogeneous environment, with pore sizes ranging from micrometres to the millimetre scale, creating distinct micro-habitats which can impact microbial diversity within the soil (Carson et al., 2010). For example, this pore network can generate nutrient and microbial “hotspots” (Crawford et al., 2012), creating variations in gaseous composition (Ebrahimi and Or, 2016) and altering fluid flow within the structure.

There is also evidence that stressors and pollutants are heterogeneously distributed between these inter-aggregate pores, generating a distribution of stressor concentrations within a soil (Ilg et al., 2004). However, standard measurements of bulk-soil parameters, such as nutrient or pollutant concentrations, typically reflect an average. These do not provide the spatial resolution necessary to understand the micro-habitats that individual, resident microbial cells experience.

To date, studies that have explored relationships between soil heterogeneity and microbial processes have focused on a few particular aspects. For example, metagenomic analysis has demonstrated that soil texture heterogeneity can differentially impact bacterial diversity (Seaton et al., 2020) and environmental modelling has highlighted microscale spatial heterogeneity as an important parameter in governing soil organic matter (SOM) mineralisation (Falconer et al., 2015). However, whilst some studies have cultivated cells in structured environments to examine parameters such as microbial differentiation (Nguyen et al., 2005), migration through porous substrates (Bhattacharjee and Datta, 2019), and competition between microbial genotypes (Coyte et al., 2017), there has been little work dissecting the impact of physical porous structure on microbial stress resistance in a controlled laboratory setup.

Because pore size can affect the rate of movement and diffusion of fluids through a porous medium (often termed hydraulic conductivity) (Whitaker, 1986), it could be hypothesised that environmental structure, and pore-size specifically, would influence the exposure of microorganisms to an imposed stressor within the liquid phase. Furthermore, whereas some attention has been given to the importance of microbial phenotypic heterogeneity (see “General Introduction 1.3.3”) in responding to exogenous stressors, so far, the interaction between phenotypic heterogeneity and environmental structural heterogeneity (such as in pore size variation) has yet to be explored.

3.1.1 Aims

The aims of the work described in this chapter are: (i) to test the hypothesis that phenotypic heterogeneity in stress response interacts with environmental structural heterogeneity, such that more heterogeneous organisms will show greater survival of stress in heterogeneous environments; (ii) to examine the impact of mean pore size and microbial stress response more broadly, developing the use of glass bead- and 3D printed lattice-structures to produce structured environments with distinct mean pore sizes and distinct pore size distributions.

3.2 Materials and Methods

3.2.1 Yeasts and culture conditions

The haploid *Saccharomyces cerevisiae* strain BY4741 (*MATa* *his3-1 leu2-0 met15-0 ura3-0*) was maintained and grown in YEPD medium [2% peptone (Oxoid), 1% yeast extract (Oxoid), 2% D-glucose]. *Saitozyma podzolica*, identified by ITS sequencing and RAPD PCR as described in Holland et al. (2014), are wild isolates recovered from soil near a disused metal smelting works in the north-east of the UK (<http://www.twsitelines.info/SMR/4192>). *S. podzolica* was maintained and grown in MYP medium [7% malt extract (Sigma), 0.5% yeast extract (Oxoid), 2.5% soytone (BD Bacto)]. For experiments, single colonies were used to inoculate 10 ml of medium in 50 ml Erlenmeyer flasks and incubated with orbital shaking (New Brunswick Scientific) at 120 rev min⁻¹, either at 30°C for *S. cerevisiae* or 24°C for *S. podzolica*.

3.2.2 *S. podzolica* IC₅₀ and heterogeneity measurements

The heterogeneity of stress resistance (degree of variation in resistance between individual cells) and IC₅₀ values of *S. podzolica* isolates used for subsequent experiments were determined by Dr. Sarah Hewitt, University of Nottingham (unpublished data) (**Table 2**). Briefly, values were calculated by plating cells on agar supplemented with a range of lead nitrate concentrations and recording colony forming units (CFU) relative to control plates to generate a dose-response curve (Holland et al., 2014). The IC₅₀ (midpoint of curve) and heterogeneity (gradient) values were calculated using these dose-response data by generating a sigmoidal plot, fitted using GraphPad Prism software using the following equation:

$$Y = \frac{\text{Bottom} + (\text{Top} - \text{Bottom})}{1 + 10^{(\log_{10}IC_{50} - X)\text{Hillslope}}}$$

Where X is $\log_{10}[\text{stressor} + 0.01]$, Y is percentage viability, Top is maximum percentage viability, Bottom represents minimum percentage viability, and Hillslope represents the gradient of the sigmoidal slope at the point of inflection.

IC₅₀ was calculated as the stressor concentration that elicited a 50% survival. The arctan of the hillslope was taken to reflect the gradient of the slope, which was used as the measure of heteroresistance.

Table 2- IC₅₀, heterogeneity values for listed *S. podzolica* isolates.

Isolate ID	IC ₅₀ (mM)	Heteroresistance value ^a
C4-3	6.37	-1.42
C3-11	6.62	-1.40
C4-5	6.77	-1.38
C4-2	6.16	-1.31
C4-18	8.22	-1.29
C4-17	6.62	-1.26

^athe values decrease (become more negative) with increasing heteroresistance, reflecting degree of variation between cells

3.2.3 iChip design, production, and testing

Initially, iChip devices were produced in order to incubate yeast cells in soil structures, to which a stressor would be applied, for subsequent recovery of cells to determine survival post-experiment. iChip designs were drawn using Autodesk 123D V2.2 computer aided design (CAD) software, based on the original design presented in Nichols et al. (2010). The design measures 73 mm width(W) x 20 mm depth(D) x 7 mm height(H) when fully assembled, with a smaller version measuring 38Wx20Dx7H mm also produced. A modified version of the iChip inspired by the designs in Berdy et al. (2017) was also produced, measuring 35Wx20Dx3H mm (**Figure 3.1**). Designs were produced by additive manufacturing (3D printing) at the Advanced Manufacturing Facility, University of Nottingham, using Autodesk Standard Clear Resin PR48 Formulation printed with a DLP SLA Ember 3D Printer (AutoDesk Inc.).

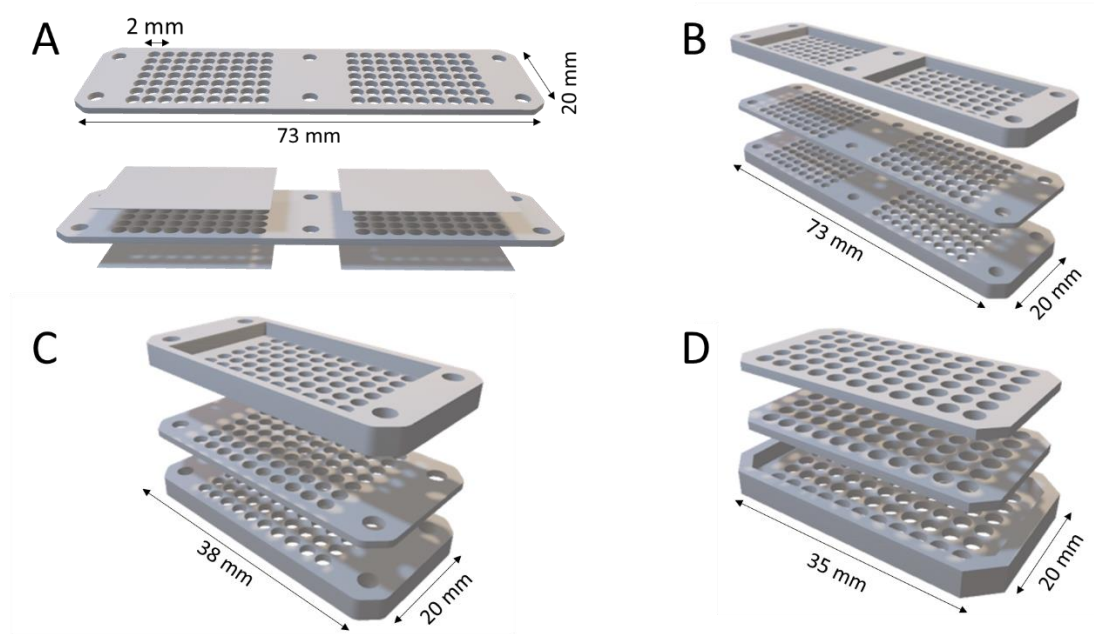


Figure 3.1- Iterations of iChip designs and assembly

The iChip consists of a middle plate with wells (measuring 2 mm in diameter) to fill with agar and microbial culture (A, top), which are then covered with a polycarbonate membrane with pores to allow fluid diffusion but prevent microbial contamination from the external environment (A, bottom). The middle plate and membranes are then clamped together by two outer plates, illustrated in (B), with nuts and bolts around the plate perimeter in the original iChip design (measuring 73Wx20Dx7H mm). A smaller version of the original iChip was also produced here (C) which measured 38Wx20Dx7H mm, as well as an alternative smaller version based on designs by Berdy et al. (2017) (D) measuring 35Wx20Dx3H mm. The latter relies on a silicone glue to secure polycarbonate membranes and outer plates to the middle plate instead of nuts and bolts.

These iChips comprised of a middle panel with a series of small wells, each measuring 2 mm in diameter (**Figure 3.1A**). These wells are filled with either sterile agar or agar inoculated with microorganism at a density adjusted to approximately one microbial cell per well equivalent volume. Nuclepore 47mm (0.2 μ m pore size) track-etched

polycarbonate membranes (Whatman) were used to cover both sides of the iChip middle panel (this was to allow nutrient diffusion into the agar but prevent contamination in experiments). Outer panel(s) were also designed, in order to secure the polycarbonate membrane and produce a watertight seal around each well. For the model based on Berdy et al. (2017), silicone sealant (Qualtex) was used to adhere the polycarbonate membranes to the chip as well as seal the exterior of the chip.

To test whether iChip devices were watertight (such that fluid could only reach the middle plate by passing through the polycarbonate membrane), the wells of the middle panel were filled with sterile agar and the complete iChips assembled. Then, assembled iChips were submerged in 20 ml of *S. cerevisiae* culture at OD₆₀₀ 0.5 and statically incubated for 48 hours. Post incubation, iChips were washed in sterile water, dried, and disassembled. Agar plugs in wells of the middle panel were visually examined under 20x magnification to check for yeast contamination from the external culture.

3.2.4 Inoculating glass beads with yeast

Autoclaved glass beads measuring 5 mm in diameter (Dixon Science) were submerged in 2 mg/ml concanavalin A (ConA, Sigma) dissolved in sterile deionised water, and subsequently dried at room temperature. Following this, ConA coated beads were submerged for 10 min in a culture (OD₆₀₀ ~ 1.0) of exponential phase yeast cells, with gentle agitation every 2 min. For experiments, beads were briefly rinsed in fresh medium to remove excess culture medium before use.

3.2.5 Preparation of glass bead structures

To produce structured environments, glass beads of different sizes (Dixon Science) were used. For monodisperse structures (structures composed of one particle size) McCartney bottles were filled with either 2-, 4-, or 6-mm diameter beads up to a volume of 5 cm³. For bidisperse structures, beads of 2- and 4-mm diameter were mixed to give either 1:3, 1:1, or 3:1 ratios by volume of the two bead types, to a total volume of 5 cm³. After autoclaving, bottles were vigorously shaken to evenly mix the beads and three 5 mm beads inoculated with cells (described above) were placed on the sterile glass beads within the bottle, before a further 5 cm³ volume of the same type of bead mix was decanted on top from a separate bottle. This produced a ~10 cm³ structure, with cell-inoculated beads positioned in the middle of the structure and an even mix of beads above and below these. This method prevented the cells on the inoculated beads from being dislodged by the vigorous shaking used to mix the bead structures.

3.2.6 X-ray Computer Tomography (CT) and image analysis

The pore structure of glass bead structures was imaged using a Phoenix Nanotom S X-ray CT scanner at the Hounsfield Facility, University of Nottingham. Voxel resolution was set at 12.5 μm, potential energy at 90 kV and current at 75 μA. The total scan time was 15 min per structure and a total of 1,200 projections were captured for each structure. VGStudio MAX was used to determine 3D pore volumes of CT imaged structures. Images were exported as image stacks to ImageJ-Win64, where they were binarised using the Li threshold algorithm. Total porosity and

equivalent spherical diameter (ESD) were determined using the BoneJ plugin (Doube et al., 2010).

3.2.7 Stress resistance assays

To determine whether cells of inoculated beads could be stressed then recovered, three 5 mm beads inoculated with *S. cerevisiae* cells were submerged in a 2 ml Eppendorf tube containing 1.5 ml YEPD culture medium supplemented with a range of lead nitrate concentrations for 1 hour at 24 °C, or submerged in YEPD and heat stressed at a range of temperatures for 10 min. Beads were rinsed in fresh medium before assessing cell survival as described in the next section.

To assess the impact of environmental structure on yeast survival, 10 ml MYP medium supplemented with 30mM succinic acid and 9 mM lead nitrate (the latter being omitted in controls) was added to glass bead structures, prepared as described above. After one hour of static incubation at 24 °C, the cell-coated beads were recovered by decanting the medium, pouring beads onto a flat sterile surface and picking out the 5 mm beads (which were visually distinguishable from other bead sizes) with sterile tweezers. The three inoculated beads from each structure were briefly rinsed in fresh MYP medium to remove traces of the lead-supplemented medium before assessing cell survival as described in the next section.

3.2.8 Outgrowth of organisms from glass beads

To assess the relative survival of organisms post-experiment, glass beads recovered from experiments (above) were transferred to a single well of a 24-well microtiter plate (Greiner Bio-One), with each well containing 350 µl of fresh medium. These

beads were incubated for five hours at 24°C, 120 rev. min⁻¹ to allow adhered cells to shed and divide in the medium. To measure growth post-treatment, 300 µl of the bead supernatant, now containing cells, was transferred to a 48-well microtiter plate. Plates were incubated at 24 °C with shaking in a BioTek Powerwave XS microplate spectrophotometer and optical density (OD₆₀₀) measured every 30 min. Resulting growth curves were used to infer back to a theoretical starting OD using multiple regression.

Since the growth of a yeast culture in exponential phase follows an exponential curve, this curve can be back-extrapolated to determine a theoretical culture OD₆₀₀ at time zero (after the five hour bead outgrowth), where the OD₆₀₀ at early time points is too low to be detectable. After a stress event which kills a proportion of the cell population, surviving cells can be grown in this manner and an exponential regression used to estimate the number of viable cells post-stress, which can then be used to calculate % cell survival [method adapted from Wohlgemuth et al. (2020)]. However, it should be noted that growth delay of stressed cells (i.e., an increased lag phase) may result in a lower survival estimate compared to survival determined by colony forming unit (CFU) enumeration (Wohlgemuth et al., 2020).

After plotting growth curves for bead-outgrowths, an exponential regression equation was determined, in the form:

$$y = ae^{bx}$$

Where Y is culture OD_{600} , X is time (hours), b is the gradient of the curve, and a is the y-intercept of the curve. Regressions were calculated using the OD values at which the greatest OD change occurred within a 3-hour period (reflecting the greatest value of b in the regression equation)- see **Figure 3.2**. The y-intercept of this equation was determined and used as a theoretical starting OD following each stressor treatment, with lower OD values reflecting a lower survival of stressor (Wohlgemuth et al., 2020).

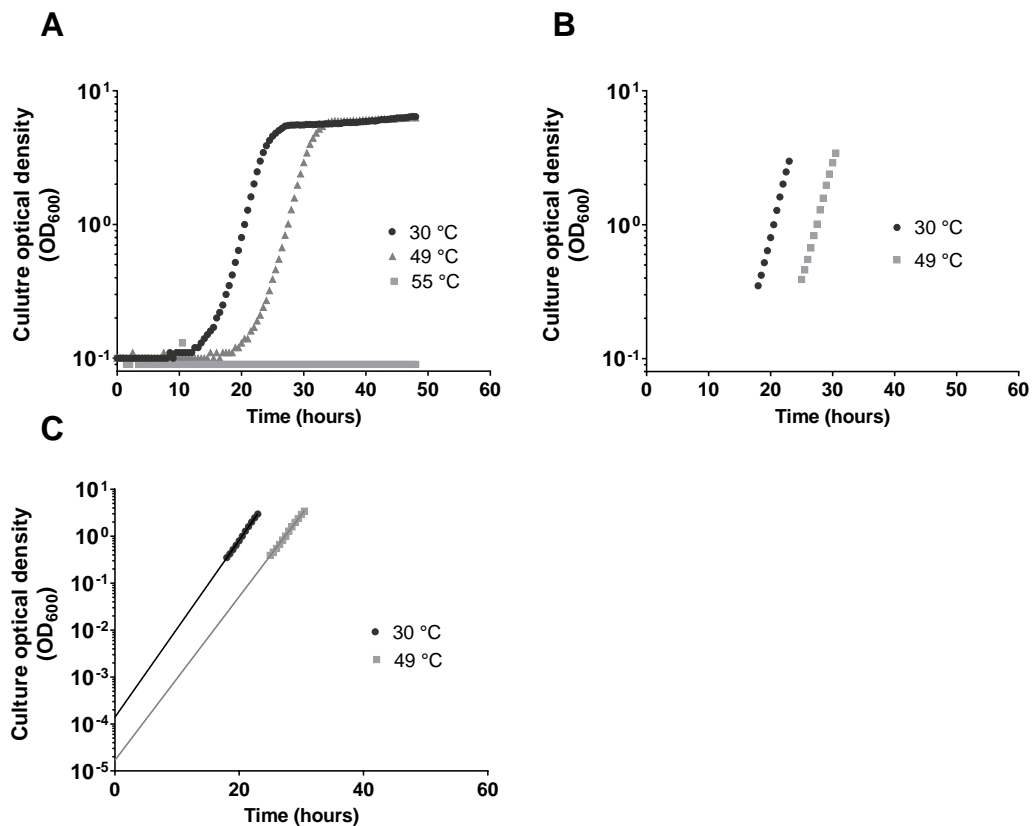


Figure 3.2- Illustration of use of y-intercept extrapolation from exponential growth curves to estimate starting OD

(A) Example growth curves for intercept analysis. (B) Datapoints encompassing the apparent exponential growth-phase, from which the 3-hour window encompassing the largest change in OD is determined. (C) Exponential regression equations are derived for points over 3 hours selected as in (B) and the y-intercept ($x=0$) calculated.

3.2.9 Manufacturing lattice structures

FLatt Pack V 1.3, a software that generates 3D lattice structures for additive manufacturing applications, was used to produce lattice structure with similar pore diameters to bead structures (Maskery et al., 2018). The lattice was designed using the “cuboid” geometry within the software, and the “primitive” cell type (under the

“network” phase selection) was used as the repeating cell of the lattice. The lattice was composed of 12 repeating cells in the Y plane and 6 repeating cells in the X and Z planes. The overall lattice dimensions were set to 30 mm width by 30 mm length by 15 mm height. Different pore diameters were produced by altering the width (thickness) of the lattice walls, such that increasing the wall thickness reduced pore size, while maintain the same total number of pores within each lattice. Lattices were printed at the Advanced Manufacturing Facility, University of Nottingham, on a Formlabs Form 2 SLA 3D printer, using Formlabs Clear Resin (product code RS-F2-GPCL-04).

3.2.10 Stress survival assays in manufactured lattices

Lattices were sterilised with isopropanol (70% v/v), then coated with ConA (2 mg/ml) by submerging each lattice individually within the solution and drying at room temperature. ConA-treated lattices were submersed for 10 min in a culture ($OD_{600} \sim 1.0$) of exponential phase yeast cells, with agitation every 2 min, before washing in MYP medium to remove non-adherent cells. Subsequently, lattices were submersed in MYP medium supplemented with 30 mM succinic acid and 9 mM lead nitrate (the latter being omitted in controls) was added to inoculated lattices. After one hour, lattices were washed with MYP medium and transferred to 40 ml fresh MYP, then incubated for five hours at 24°C with shaking 120 rev min⁻¹. Subsequently, and immediately after agitation, 300 µl of supernatant was transferred to a 48-well microtiter plate and outgrowth measured as in the bead outgrowth experiments described above.

3.2.11 Determination of lead content of yeast cells in lattice structures

Cells were exposed to lead within lattice structures as described above, but at 2 mM lead nitrate concentration to reduce cell death. Lattices containing cells were thoroughly washed, then placed into 50 ml of 27% (v/v) nitric acid at 70 °C for 1 hour to digest cells in the lattices and solubilise cell-associated lead. The resultant digest was subsequently diluted to a final nitric acid concentration of 2% (v/v) and filtered through a 0.2 µm filter for analysis by ICP-MS.

3.2.12 Inductively coupled plasma mass spectrometry (ICP-MS)

ICP-MS was conducted in the School of Biosciences, University of Nottingham, using a Thermo-Fisher Scientific iCAP-Q instrument equipped with CCTED (collision cell technology with energy discrimination). Readings were analysed using Qtegra software (Thermo-Fisher Scientific).

3.2.13 Determining effect of cell concentration

To test for potential effects of different cell concentrations on lead depletion from the medium, first the cell concentration in each structure was calculated as the estimated number of cells per volume of pore space. This involved calculating the estimated number of cells per lattice from outgrowth OD_{600} , and then dividing this number by the volume of pore space for each lattice type. These cell concentrations were then reproduced in assays conducted in 15 ml Falcon tubes containing 10 ml MYP medium supplemented with 30 mM succinic acid and 9 mM lead nitrate (or without lead nitrate in controls) and inoculated with exponential phase *S. podzolica*

cells at the desired cell concentrations. After incubation for 1 hr, cell suspensions were syringe filtered through a 0.2 μm filter to separate cells from the medium. Filtered medium was subsequently diluted using 2% nitric acid (v/v) to the appropriate analytical range for multi element analysis ICP-MS (see above).

To examine the effect of cell concentration on survival of lead exposure, cell concentrations and stress conditions were used as above, but the assays were conducted in 1 ml volumes within wells of 12-well microplates (Greiner Bio-One). After one hour, cell suspensions were diluted to decrease Pb to sub-inhibitory concentrations and 300 μl of diluted cell suspension was transferred to wells of a 48-well plate to conduct outgrowth experiments and determine Y-intercepts from resulting growth curves, as outlined above (section 3.2.8).

To examine the effect of lattice surface-bound cell density on survival of lead exposure, the number of cells per lattice was calculated as above then divided by the total pore surface area to estimate the number of cells per unit surface area. Then, wells of a 48-well plate were coated with ConA (2mg/ml) and allowed to dry in a sterile environment. These wells were then inoculated with 500 μl of cell suspension containing a total number of cells sufficient to coat the bottom of the well at the desired cell/surface area. Plates were then centrifuged at 3000g for 3 minutes to force cells to the bottom of well, before aspirating the medium and replacing with MYP medium supplemented with 30 mM succinic acid and 9 mM lead nitrate (or without lead nitrate in controls). After static incubation for 1 hr at 24 $^{\circ}\text{C}$, plates were centrifuged as above, and wells washed twice with sterile water to remove excess

lead. Aliquots (350 μ l) of fresh MYP medium were added and cells grown for 5 hr at 24 °C, shaken at 120 rev min⁻¹, before transferring 300 μ l to a new 48-well plate for outgrowth and Y-intercept analysis as described previously (section 3.2.8).

3.2.14 Statistical analysis

Simple linear regression was with GraphPad Prism version 8.2.1, accounting for sample size and variation between replicates, with a significance threshold of $p = 0.05$. A two-way ANOVA was used to analyse the interaction between yeast heteroresistance, structure heterogeneity, and stressor survival, with a significance threshold of $p = 0.05$. Comparison between treatments for experiments on the effect of cell concentration were performed using an unpaired *t*-test, or one-way ANOVA for multiple comparisons, with a significance threshold of $p = 0.05$.

3.3 Results

3.3.1 iChip manufacture and testing

The iChip is a device that allows microorganisms to be incubated in and recovered from the soil environment, among other potential applications (Nichols et al., 2010). The iChip is composed of a middle plate containing a series of wells (with each well measuring 2 mm in diameter) that allows single cells to be incorporated into agar plugs (**Figure 3.1A**) within the wells. These are then sealed with a semipermeable polycarbonate membrane on either side of the plate to allow nutrient diffusion from the external environment while protecting from non-specific microbial contamination (membrane pore size 0.2 μm). In the original design based on the iChip used by Nichols et al. (2010), two exterior plates tightly clamped the membranes to the middle plate (via nuts and bolts), in order to create a seal to prevent liquids from bypassing the membrane and contaminating the agar plugs (**Figure 3.1B**)

Initially, several iterations of iChip devices were produced (**Figure 3.1B, C, D**) by additive manufacturing (3D printing). These were intended for introducing microorganisms to soil samples with different pore-size characteristics, with subsequent introduction of stressor, then recovery of the microorganisms in chips to compare survival in the different soil types. These iterations were smaller than the original device presented in Nichols et al. (2010), to help minimize disruption of the soil structure during introduction and removal of the chips.

However, a design modelled after the original iChip design (**Figure 3.1B**) was prone to contamination in preliminary trials, observed when submerging the intact device

in 50 ml of OD₆₀₀ *S. cerevisiae* culture in YEPD medium for 48 hours, and later inspecting the agar plugs within the plate perforations. It was speculated that the seal was inadequate because: (i) the nut and bolt configuration did not apply pressure uniformly over the device; (ii) the 3D printing method created a raised surface around each perforation on the middle plate, precluding a flush contact between the middle and outer plate required to form a seal. Therefore, two additional devices were produced – one smaller device to reduce the amount of contact area that needed to be sealed (**Figure 3.1C**) and a second device that was dependent on silicone glue as a sealant, based on designs presented in Berdy et al. (2017) (**Figure 3.1D**).

Similar to the original design, contamination occurred in the smaller revised device. For the glue-based device, silicone glue was applied to the middle plate around each perforation in order to stick and seal the polycarbonate membrane to the plate, with the outer plates acting as additional protection from liquid permeation, which were also sealed around the plate perimeter with silicone glue. However, as with the other iterations tested, a water-tight seal was not successfully achieved. There were problems with reproducible application of glue around every well of the middle plate, and the silicone glue tended to tear and damage the fragile polycarbonate membrane. Subsequent communications with the original author, Professor Slava Epstein (Northeastern University, USA), revealed that they had also found similar issues with additively manufactured devices, and suggested that this printing method did not afford sufficient precision for creating sealable devices.

3.3.2 Production of glass bead structures with different pore sizes

After unsuccessful attempts to produce iChip devices, an alternative experimental setup was designed to investigate the impact of environmental pore size on microbial resistance to applied stress. In this system, structured environments were created by mixing different ratios of glass beads of different sizes. The use of glass beads instead of soil samples gave more precise control over the structure and meant that glass beads could be directly inoculated with microorganisms (described in section 3.2.4), minimally disrupting the overall structure of the environment (unlike the larger iChip device). The total volume occupied by beads (10 cm^3) was adjusted to be constant across different structures. The structures comprised either 6 mm, 4 mm, or 2 mm-diameter glass beads, or different ratios of 4 mm and 2 mm beads (**Figure 3.3A**). These different bead compositions proved sufficient to alter the average pore-space “equivalent spherical diameter” (ESD) within the different structures, as determined by X-ray computed tomography. The ESD decreased with decreasing average bead diameter (**Figure 3.3B,C**).

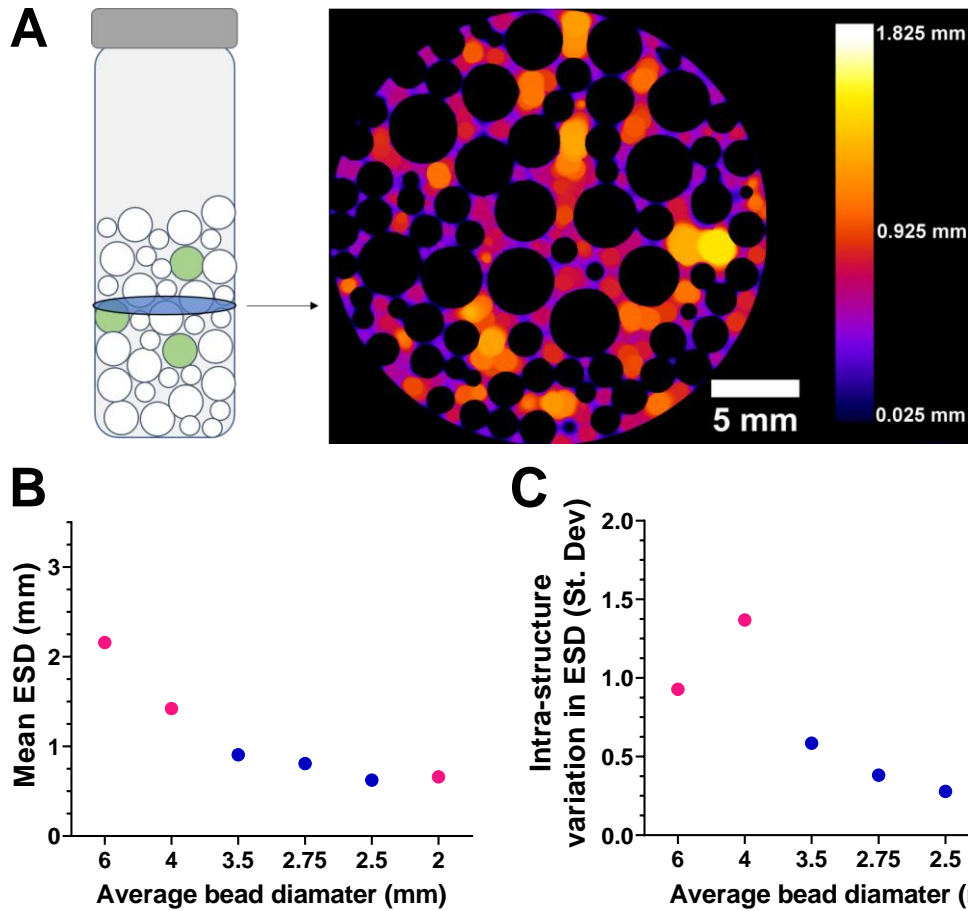


Figure 3.3- Production of structured environments of varying pore-space ESD

Different sizes and ratios of glass beads were mixed in McCartney bottles to create structured environments (A, left). In this schematic, white circles indicate sterile glass beads, green circles indicate beads surface-inoculated with microbial cells (the yeast *S. podzolica*); bead/bottle dimensions are not to scale. Structures were scanned using X-ray CT to determine pore-space equivalent spherical diameter (ESD) (right). The example shown is a single X-ray slice of a structure comprising a mixture of 2 mm and 4 mm beads. Colour scale represents the ESD, and black indicates solid (bead) volume. The mean pore-space ESD across structures with varying bead diameters was calculated (B), as well as the standard deviation of ESD within a single structure (C), demonstrating that the distribution of ESD differs between structures. In B and C, pink squares represent monodisperse structures (i.e., structures composed of one particle size) blue circles represent bidisperse structures of varying proportions of 2- and 4-mm beads. Data shown is of one representative structure of each type.

3.3.3 Assay of stress resistance using recovery of yeast from inoculated beads

Next, a method of introducing microorganisms into the glass bead structures was devised by coating sterile 5 mm glass beads with concanavalin A (a lectin carbohydrate-binding protein), then inoculating these coated beads with cells and incorporating the inoculated beads within the structures (see section 3.2.4). First, to demonstrate that microorganisms treated with stressor could be recovered from coated glass beads, beads inoculated with yeast cells were either submersed in medium either supplemented or not with lead nitrate at different concentrations or incubated at different elevated temperatures. The beads were then transferred to fresh medium to allow surviving cells to grow into the medium; this growth was required as the cell inoculum per bead was too low to allow reliable OD measurement initially. Resultant growth curves were analysed by exponential regression to estimate the y-intercepts (after outgrowth from beads) by extrapolation from the exponential phase of growth (**Figure 3.4A,B**). These values were compared between treatments to estimate retrospectively the relative viable cell numbers after this outgrowth step. The extrapolated y-intercept OD₆₀₀ determinations progressively decreased with increasing lead concentration (**Figure 3.4**). This observation of these anticipated relationships with the level of stress applied corroborated the approach used with cell-inoculated glass beads as a tool for assaying growth and survival. Next, this was scaled up to the bead structures.

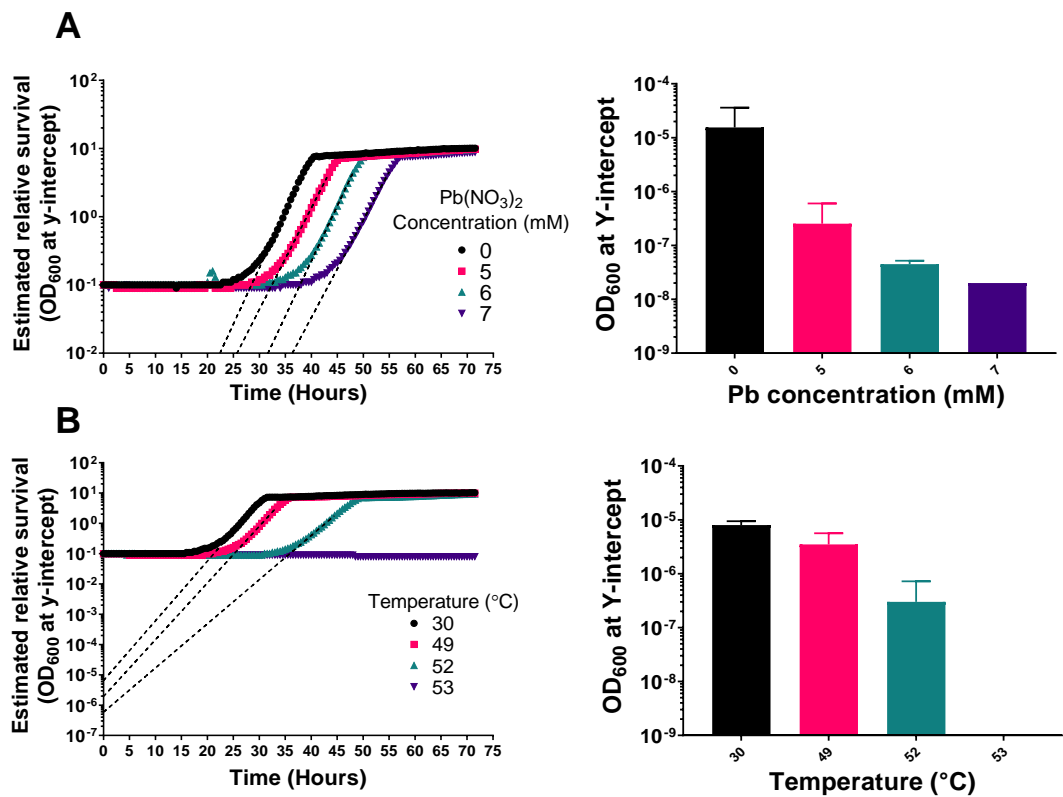


Figure 3.4- The y-intercept of bead outgrowth correlates with level of stress

Glass beads were coated with exponential phase *S. cerevisiae* cells and exposed to a range of lead nitrate concentrations or temperatures. After 1 h, beads were washed, incubated in fresh medium at 30 °C for five hours before transfer (time 0) to 48-well plates and growth curves generated. (A) Growth curves of bead outgrowth experiments after lead nitrate treatment (left) and corresponding Y-intercepts derived from exponential regression of the exponential-phase growth slopes (right). (B) Growth curves from bead outgrowth experiments after heat shock treatment (left) and corresponding Y-intercepts derived from linear regression of the exponential-phase growth slopes (right). In growth curves, dashed lines are examples of the exponential regression slopes used to determine y-intercept values. Growth curves are representative of two independent experiments, error bars in y-intercept graphs represent SEM of two biological replicates.

3.3.4 Environmental pore size impacts lead nitrate resistance in yeast

3.3.4.1 *Interactions between isolate heteroresistance and environmental pore-size variation*

Because the size of pores within a porous structure can alter the movement and diffusion of fluids through it, it was hypothesised that microorganisms within structures carrying broader distributions of pore sizes could be subject to a broader range of stressor intensities, reflected in differences in survival. To compare stress resistances of cells in the structured glass-bead environments, stress-survival experiments were conducted using inoculated beads introduced to six types of structure and across six isolates of the soil yeast *S. podzolica*. Cells on beads were exposed to MYP medium supplemented with succinic acid and either 9 mM lead nitrate (treatment) or an equivalent volume of water (control) (**Figure 3.5**).

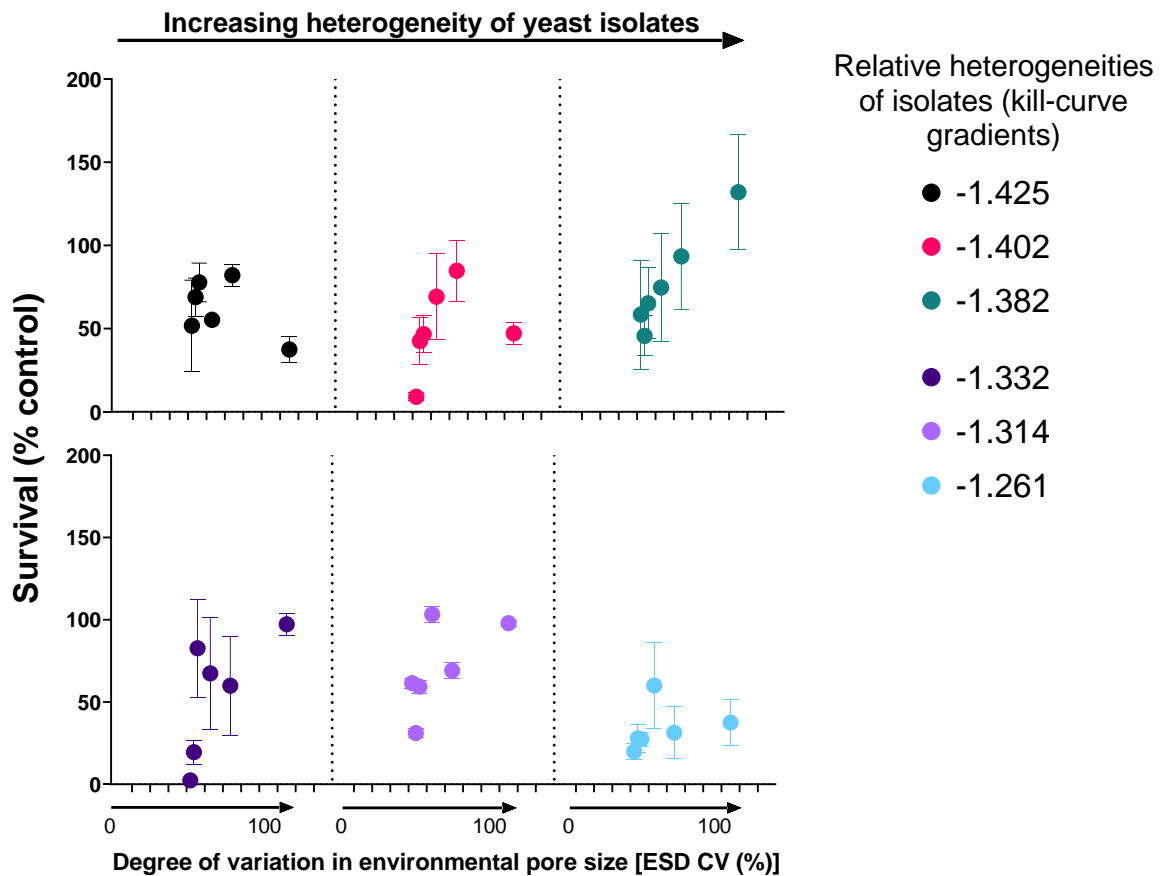


Figure 3.5- Impact of environmental structure heterogeneity on survival of *S. podzolica* during lead nitrate stress

Isolates of the yeast (*S. podzolica*) were exposed to 9 mM lead nitrate for 1hr in glass bead structures. Survival relative to minus-lead controls was plotted against the coefficient of variation (CV) in the equivalent spherical diameter (ESD) of pore spaces within each structure. Each isolate is separated by a dotted vertical line and are plotted from top-left to bottom-right with increasing phenotypic heterogeneity of Pb resistance (values pre-determined for each isolate). Error bars represent SEM, n=3 biological replicates, each in technical triplicate.

Environmental heterogeneity (variation in ESD within structures) and isolate heterogeneity significantly accounted for 22.8% ($p = 0.0007$) and 14.4% ($p = 0.0024$) of variation in survival between isolates, respectively. Nevertheless, there was no significant interaction effect between these parameters ($p = 0.1846$). This indicated that the influence of isolate heterogeneity on survival was not dependent on

structure variation (determined by two-way ANOVA with Tukey's multiple comparisons test)

3.3.4.2 Interactions between mean stress resistance and environmental pore size

In contrast to influence of phenotypic heterogeneity on resistance trends, there was a significant negative relationship between mean pore-space ESD of the structures and survival across the six yeast isolates when averaging the survival of all isolates in each structure ($Y = -30.08 * X + 94.2$, $R^2 = 0.277$, $p < 0.001$). That is, the survival of *S. podzolica* under lead stress was decreased with increasing pore-space ESD (**Figure 3.6**).

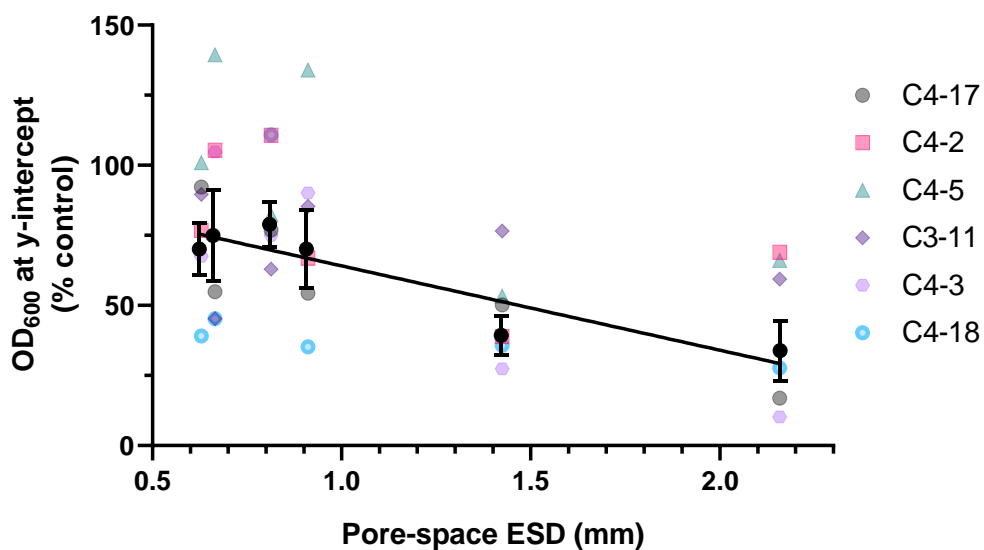


Figure 3.6- The survival of *S. podzolica* in response to lead nitrate in bead structures decreases with increasing pore size

Beads inoculated with exponential phase cells *S. podzolica* were introduced to a series of structures (three inoculated beads per structure) comprising glass beads of different sizes and varying pore space diameters, before challenge for 1 hr with 9 mM lead nitrate in MYP medium (supplemented with 30mM succinic acid, pH 4.5). The percentage survival (OD₆₀₀ y-intercept) of *S. podzolica* in each structure was determined against corresponding controls where water was added instead of lead nitrate. Data points for individual yeast isolates (mean of three biological replicates) are shown, with symbols of different colour and shape for each isolate; black symbols represent mean values across all isolates. Error bars represent SEM. The slope was fitted by linear regression ($R^2 = 0.277$, $p = 0.001$).

Earlier, a general positive relationship was observed between mean pore size and pore-size variation in glass bead structures (**Figure 3.3B, C**). This suggested that either of these variables could be at least partly responsible for the change in survival across structures observed in **Figure 3.6**. To distinguish these two variables with respect to

effects on microbial survival, and to improve reproducibility of “replicate” structures (by their nature, each glass-bead structure was unique), it was decided to use additive manufacturing to produce uniform lattice structures. With this approach, manufactured lattices (dimensions 60Wx60Dx30H mm) were composed of repeating units of the same size, producing a consistent pore diameter across each structure. The sizes of repeating units were different for different lattices manufactured, giving different pore diameters between lattices but a single pore diameter within a lattice (**Figure 3.7A**). These structures were inoculated by submersing them in *S. podzolica* broth culture before substitution of the medium with lead nitrate-supplemented broth. Similar to the results from the bead experiments, simple linear regression indicated that there was a significant negative relationship between lattice pore diameter and *S. podzolica* survival post-treatment ($Y = -25.20 * X + 91.65$, $R^2 = 0.485$, $p = 0.008$) (**Figure 3.7B**). As the pore size was uniform within each lattice, unlike for the glass bead structures, this suggested that a relationship with yeast survival could be attributed specifically to mean pore diameter of the different types of structure.

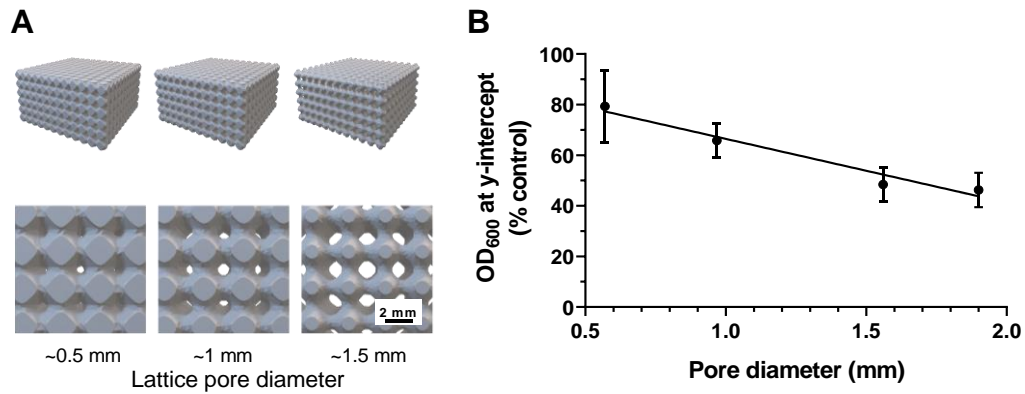


Figure 3.7- The survival of *S. podzolica* in response to lead nitrate in lattice structures decreases with increasing pore diameter

Additively-manufactured lattices structures with four different pore diameters (0.5 mm, 1 mm, 1.5 mm, 1.9 mm) (computer models shown in A) were inoculated with exponential phase *S. podzolica* cells (isolate C4-17), which were subsequently challenged with 9 mM lead nitrate in MYP medium including 30mM succinic acid, pH 4.5. (B) The percentage survival (OD₆₀₀ y-intercept) of *S. podzolica* in each structure was determined against corresponding controls where water was added instead of lead nitrate. Mean results are shown from three biological replicates; error bars represent SEM. The slope was fitted by linear regression ($R^2 = 0.485$, $p = 0.008$).

A series of experiments were conducted to investigate the basis for the interaction between pore-size and stress survival. Initially, a lattice experiment was conducted with a reduced lead nitrate concentration (to reduce cell killing) to determine whether cells in lattices with larger pores showed a greater lead uptake than those in lattices with smaller pores, hence potentially accounting for the differences in survival between cells in different structures. Post experiment, lattices with attached cells were washed and partially digested in nitric acid and the supernatant Pb content analysed by ICP-MS. ICP-MS analysis showed no significant difference in the amount

of lead recovered from each lattice type (**Figure 3.8A**) (one-way ANOVA with Tukey's multiple comparisons test, $p = 0.660$). However, further examination determined that lead has adsorbed onto the lattice surface, as similar levels of lead were recovered from lattices treated with lead in the absence of cells (see Appendix B) which could not be removed by washing. This meant that any difference in intracellular lead could be masked by much greater differences in lattice-bound lead. To circumvent this issue, further experiments were conducted outside of lattice structures using estimates of cell density to reflect the properties of the structured environments, detailed below.

Because each lattice had the same overall dimensions and the same total number of pores, but differed in pore diameter, the proportion of lattice occupied by pore space increases with increasing pore diameter in the different designs. Given also that the starting inoculum per lattice (i.e., numbers of cells retained on lattice surfaces after washing out the broth inoculum) was similar across lattices – as indicated by similar levels of outgrowth in control tests with lattices of different designs (see Appendix C) – it follows that the number of yeast cells per unit-volume of pore space decreases with increasing pore diameter in the different lattices. Accordingly, cell concentrations were calculated as 95, 12, and 3.2 cells per μl pore space for lattices with pore diameters of 500, 1000, and 1500 μm , respectively.

Complementary to measuring intracellular lead concentrations, it was hypothesized that cells at these varying concentrations may differentially deplete available lead in the different structures, with any resultant differences in lead concentration

potentially exerting different levels of stress. To test this, the estimated cell concentrations in the different lattice designs (above) were reproduced by appropriate dilution of broth cultures in 15 ml Falcon tubes, omitting the structured environments. Lead nitrate was supplied at 9 mM as in the lattice experiments. The differences in cell concentration did not result in detectable differential depletion of lead from the culture supernatant (**Figure 3.8B**), suggesting that cell mediated lead depletion was not responsible for the survival differences of cells in different lattices.

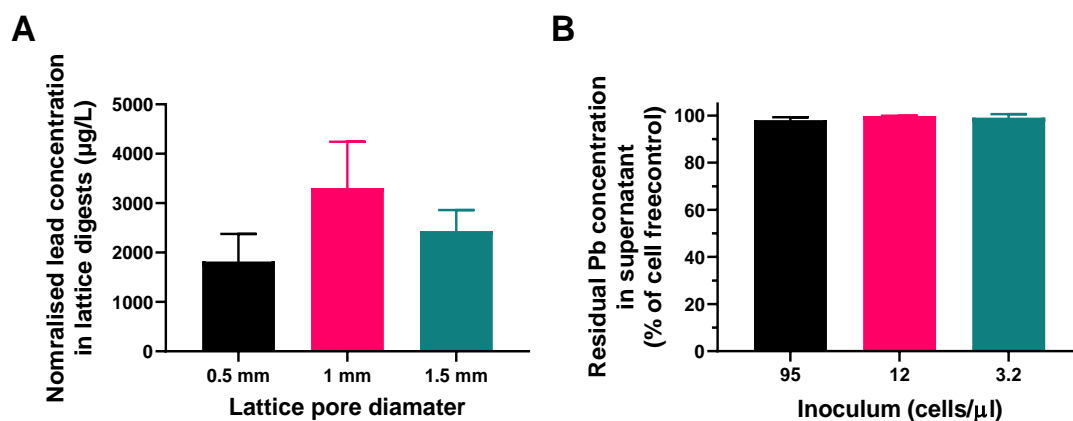


Figure 3.8- Analysis of lead recovered from lattice-stress experiments and structureless experiments

(A) Cells within lattices were exposed to 2 mM lead nitrate for 1hr. Lattices were subsequently washed in deionised water and submerged in nitric acid at 70 °C for 1 hr to digest cells and release intracellular contents. Supernatant was analysed by ICP-MS to determine elemental concentrations in the digests (volume 40 ml). Determinations for Pb were normalised against the average of sodium, potassium, and phosphate concentrations for each lattice to account for potential differences in cell concentrations between lattices. Mean results are shown from three biological replicates, error bars represent SEM. (B) Cells in 24-well plates were exposed to 9mM lead nitrate and the lead level in the supernatant determined after 1 hr incubation with *S. podzolica*, supplied at cell densities equivalent to those calculated for lattice structures with pore diameters of 500 µm (black), 1000 µm (pink) and 1500 µm (teal). Pb concentrations after 1 hour are expressed as percentages of no-cell controls.

Consistent with the lead-depletion experiment (**Figure 3.8B**), there were no significant differences in % survival at the different cell densities when cells were stressed in suspension in 24-well plates (one-way ANOVA with Tukey's multiple comparisons test, $p = 0.166$). (**Figure 3.9A**). There was an apparent dip in survival at

the intermediate cell concentration, but there was no trend similar to that seen in the structured-environment experiments. Finally, since many or most cells would be adhered to (lattice pore-) surfaces in the structured environments, the possibility of an effect of surface-density of cells on lead resistance was assayed. A similar experiment as above was conducted, but here with cells adhered to the bottom of microplates and at densities calculated by considering pore surface-area in the lattice structures rather than volume (this calculation gave densities of 15.9, 4.0 and 1.8 x 10³ cells/cm² for the lattices with pore diameter 500, 1000, and 1500 μm, respectively). Similar to the observations with cells in suspension, there was no significant effect of surface-adhered cell density on lead nitrate resistance (p =0.243, one-way ANOVA with Tukey's multiple comparisons test) (**Figure 3.9B**). The results collectively indicate that cell-density effects do not contribute to the difference in survival seen in bead and lattice structures. This reinforces the inference that it is differences in pore size, specifically, which determined microbial survival of the lead stress.

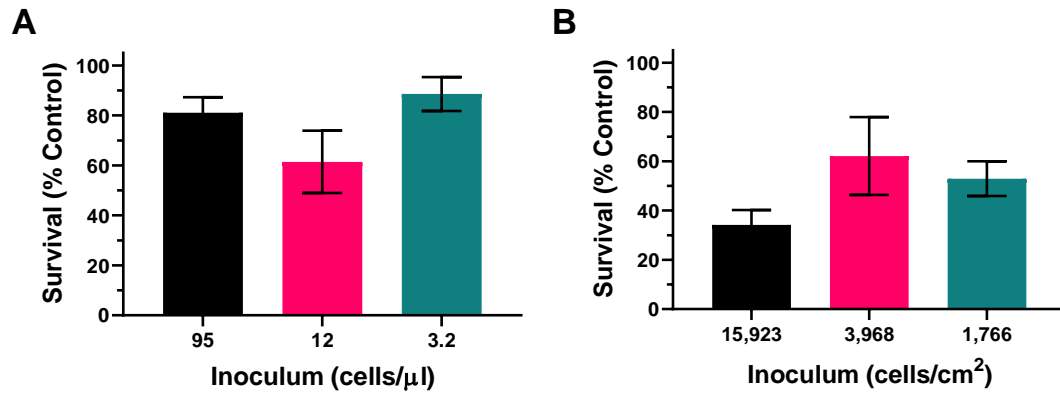


Figure 3.9- Assessing the potential impact of cell density on lead resistance

The survival of *S. podzolica* in response to a 9mM lead nitrate challenge for 1hr at cell densities equivalent to those calculated for lattice structures with pore diameters of 500 μm (black), 1000 μm (pink) and 1500 μm (teal). Cell densities were calculated and reproduced to represent either the number of cells per unit pore volume (A) or per unit surface area (B) for each lattice. Cells at these densities were then stressed either in suspension in, or adhered to the bottom of, 48-well plates. Mean results are shown from three biological replicates, error bars represent SEM.

3.4 Discussion

The study described in this chapter examined the stress resistance of a natural soil yeast incorporated into porous environments of varying pore diameters. The results showed that increases in the average equivalent spherical diameters (ESD) of a structure's pore architecture are associated with decreased survival of cells to a toxic-metal challenge. This was evident in both glass bead, and additively manufactured, model structures developed in this work. The findings highlight the importance of the physical architecture of an organism's immediate environment for its response to environmental perturbation.

3.4.1 Creating three-dimensional structures that support assay of microbial stress resistance

Initially, iChip devices were additively manufactured and used to introduce microorganisms to soils with different pore size and distributions. The intention was to apply an external stressor to the soil, and subsequently recover the microorganisms to assess survival in relation to soil structure. However, after several device iterations proved to be prone to contamination from the external environment, and correspondence with the authors who originally produced this device (Nichols et al., 2010) which suggested that additive manufacturing was not an appropriate production method, the iChip approach was abandoned. Instead, a new experimental setup using glass beads was designed to examine the impact of environmental pore size on microbial stress resistance. Importantly, this new design

allowed more precise control of the configuration of the structure in comparison to using soil. In addition, it was minimally impacted by the introduction of microorganisms (as opposed to the disruption to soil structure caused by the large iChip), and isolated structural properties of the environment without simultaneous change to other spatially variable factors such as pH, salinity, organic carbon distribution, etc.

The new system developed here used glass beads of different diameters (and mixed at different ratios) to produce structures with different mean pore equivalent spherical diameters (ESDs) – a measure of pore size. Furthermore, it was demonstrated that individual glass beads could be inoculated with yeast, exposed to a stressor, with subsequent recovery of cells by growth to determine relative survival. Glass beads have previously been inoculated to study bacterial denitrification in porous environments (Schlüter et al., 2018), and used as a solid interface to cultivate and study bacterial differentiation on solid surfaces (Nguyen et al., 2005). In this study, this system demonstrated a simple method for making and incorporating organisms into three-dimensional structures, so enabling investigation of interrelationships between microbial function (e.g., stress resistance) and environmental structure. Following this, it was demonstrated that additively manufactured lattices with uniform pore diameter could be produced which, similar to the glass bead structures, supported inoculation and subsequent recovery of microbial cells. This alternative approach gave control of technical variation in structures between experiments, while offering uniform structures with defined pore sizes. In this study, each lattice was designed with a uniform pore size, but designs

with variable pore size within a lattice could also be manufactured if desired. Future experiments could aim to re-introduce additional environmental elements into the structures, such as by pre-treating glass beads with Piranha solution (a mixture of sulfuric acid, hydrogen peroxide, and water) to alter structure hydrophobicity (Seu et al., 2007), or by using sintered glass beads to add additional micrometre scale porosity to structures (Gueven et al., 2017).

Across the structures produced here with either method, pore diameters ranged from ~0.5 mm to ~2.1 mm, which are relatable to those found typically in soils (Anovitz and Cole, 2015, Beven and Germann, 1982), as well as building materials (Zhang et al., 2020, Takahashi and Fuji, 2002) and biomedical materials such as tissue scaffolding (Vagaska et al., 2010). It should be possible to produce smaller (or larger) pore sizes by using smaller beads or with higher-precision 3D-printing technology. Therefore, whereas these structures were developed to ask questions relevant to microorganisms in soil habitats, it is anticipated that this methodology can be adapted to investigate other types of porous environment.

3.4.2 Pore size of an organism's (micro-)environment impacts resistance to stress

Glass bead and lattice structures of various pore size distributions were used to explore the impact of pore size on microbial stress resistance. It was expected that a broader distribution of pore sizes (i.e., a more heterogeneously structured environment) would create a broader, more heterogeneous distribution of stressor across the structure. Accordingly, some cells might be exposed to the stressor in

smaller or larger pore spaces, or even partly shielded from stressor by close physical presence of glass beads, and the degree of variation in this exposure would be related to the degree of pore-space variation within a structure. In these structures, it was hypothesised that *S. podzolica* isolates expressing relatively heterogeneous resistances (termed heteroresistance) to lead nitrate would exhibit greater survival in structures with a heterogeneous distribution of stressor (relative to more homogeneous isolates). However, when exposing *S. podzolica* isolates of various heteroresistances to lead nitrate within structures with a range of pore size variations, no interaction between heteroresistance and structure heterogeneity was observed. This indicated that any survival differences between yeast isolates across different structures were not dependent on the isolates' heteroresistances.

In addition to examining the interaction between structure heterogeneity and isolate heteroresistance, it was hypothesised that structures with larger pores overall would facilitate an overall increase in total stressor exposure of cells within those pores (relative to structures with smaller pores). As there is no turbulent fluid flow in the structured environments used here, lead depleted from a cell's immediate environment by cellular uptake is predominantly replaced by diffusion (Rhodes, 2008), and diffusivity in porous media increases dependent on porosity (Matyka et al., 2008) (the proportion of the environment occupied by pore space). As the present lattice structures retained the same total volume over different average ESD (or pore diameter), porosity within these structures will increase as pore ESD/diameter increases. Therefore, it is inferred that lead depleted by local cellular uptake is subsequently replenished at different rates depending on structure porosity; with

greater diffusivity in structures with larger pores elevating the mean (over time) stressor exposure of a cell. This would reduce overall yeast survival in structures with larger pore sizes, regardless of isolate heteroresistance.

Indeed, in bead structures and lattices, yeast in structures with larger pores showed a reduced survival in response to lead nitrate exposure. Whilst it was noted that the distribution of pore size (measured as pore equivalent spherical diameter (ESD)) within bead structures tended to broaden with increasing mean pore size, survival trends in bead experiments could be reproduced in the lattice experiments, which had a uniform pore size within each lattice. This indicated that the survival trend seen in bead and lattice structures was related to mean pore size, and not degree of variation in pore-sizes of a structure.

It was noted that cell densities within pores of different sizes would differ in our structure designs, a variable that required dissecting from pore size-specific effects. Cell density is reported to influence stress resistance in other systems, such as by increasing extracellular protective molecule secretion at higher cell densities (Laman Trip and Youk, 2020) or by increasing the frequency of rare persister cells (Scheler et al., 2020, Steels et al., 2000). However, the survival difference between structures could not be explained by differences in cell densities, as survival experiments replicating cell densities in the pore volume or on the surface of different structures showed no significant differences in survival. Nor was available stressor in the medium depleted by cells to different extents in the different structures. This

provided further evidence to indicate that it is the physical structure specifically that impacts resilience to the stress.

To further examine the hypothesis that cells in structures with larger pores are exposed to a greater amount of stressor, the level of exposure of cells to stressor could be assayed dynamically. As a proxy, an attempt was made to compare net lead accumulation by cells within the different lattice structures, as this may reflect net exposure over time. However, the lattice material itself adsorbed significant amounts of lead, confounding distinction from lead uptake by cells within the lattices. In future, experiments using lattice structures should consider additive manufacturing with a low-adsorption material, such as printing lattices with metal instead of resin, although the instruments needed for printing these materials are more costly and the adherence of cells to these materials would also require assessment. Alternatively, lattices could be manufactured from a material with a refractive index similar to water, meaning that lattices submerged in water would appear transparent — such materials have been used previously in biomedical applications (Ho et al., 2020). Then, lattice experiments could be conducted as before, followed by submersion of the lattices in water where the transparency of the structure would facilitate imaging of cells within lattices. In that case, staining of cells with a fluorescent lead probe, for example, would enable measurement of lead levels in cells. This would eliminate the need to recover cells from lattices and should minimize interference from lattice-bound lead. Similar approaches have been employed by Downie et al. (2014) to observe fluorescently tagged *E. coli* associated with lettuce roots grown within a transparent substrate. However, the imaging of large three-dimensional structures

at single cell resolution would prove challenging and require a built-for-purpose imaging setup, not available at this time.

3.4.3 Conclusions

The physical environments in which microorganisms naturally reside are rarely unstructured and the impacts of microbial environmental structure are often not captured in laboratory experiments (Harvey et al., 2020a). Soil structure in particular is highly variable between different locations, with additional effects of factors such as management practice in agricultural soils (Pagliai et al., 2004, Palmer and Smith, 2013) and changing climate (Chan, 2011). Pore size is a key variable across different structures like soils. The results of this study suggest that changes in the pore size of a microorganism's (micro-) environment can influence stress resistance, as demonstrated here with lead nitrate as a soil-polluting metal stressor. Hence, when assessing the impact of environmental stressors on microorganisms, the environmental architecture in which such organisms naturally reside should be considered and even incorporated to experimental design where appropriate, as evidently physical structure alone can impact microbial stress resistance.

4 STRUCTURES AT THE MICROSCALE- A MICROFLUIDICS APPROACH

4.1 Introduction

Studies in the previous chapter examined how structured environments analogous to soils with millimetre-scale pores could impact microbial stress resistance. However, depending on the soil type, many of the pores within a soil can be below this pore size range. For example, it was demonstrated in Chapter 2 that the average pore diameter within a single aggregate of soil can be 30-40 μm in diameter. Indeed, in denser clay soils it has been suggested that as many as 70% of pores are smaller than 75 μm in diameter, with many below even 5 μm (Zaffar and Lu, 2015). Hypothetically, a pore that is a perfect sphere of 10 μm diameter would contain a volume of 523.6 μm^3 . Considering a single yeast cell, for example, within that pore would occupy ~ 42 μm^3 (Jorgensen et al., 2002), it seems likely that cell activity within such small environments may impact the local nutrient and stressor concentrations, such as by uptake of these substrates from the pore space into the cell. This may in turn influence the availability of these substrates to other nearby cells.

The rate of depletion and replenishment of diffusible substrates in such small volumes can also differ from that in larger pores. For small fluid volumes and mass, the influence of inertia (resistance of any physical object to any change in its velocity) becomes smaller relative to that of viscous forces (the resistance of a liquid body to deformation). This means that fluid mixing by turbulence does not readily occur in

such small spaces as flow becomes “laminar” and mixing occurs predominantly by diffusion (Novotny and Foret, 2017). This relationship between inertia and viscosity can be summarised by the Reynolds number (see Appendix F for the equation defining the Reynolds number). In small fluid volumes, the mixing of nutrients and stressors are reliant on diffusion, external pressure changes to generate fluid flow, and sometimes turbulence generated by flow through irregular pore shapes, even at small volumes (He et al., 2001).

Some previous research has focused on microbial migration (Rubinstein et al., 2015, Aleklett et al., 2021) and metabolic activity (Nadell et al., 2017, Dal Co et al., 2019) within micrometre-scale structures. However, there are currently few, if any, studies that have examined how micrometre-scale environmental structure impacts the exposure and response of microorganisms to environmental stressors. Such data could deepen our understanding of microbial response to perturbation as it occurs in structured environments, such as those that reflect the natural soil habitat.

Examining the interaction between microorganism and abiotic factors in structured environments of small scales is challenging (Baveye et al., 2018, Harvey et al., 2020a). However, microfluidics devices with incorporated structured elements offer potential in examining this interaction as they enable the precise control of a cells microenvironment and facilitate single cell imaging and tracking (Deng et al., 2015, Dal Co et al., 2019, Nadell et al., 2017) (see General Introduction section 1.1.1.2 for an overview of microfluidics devices). Of focus in this chapter, soil micromodels are microfluidics devices with incorporated soil-relevant structures (Deng et al., 2015)

and may offer a suitable environment to examine microbial-structure interaction. Furthermore, inert particles can be introduced into otherwise homogeneous microfluidics chambers to create simple structures to further examine these interactions.

4.1.1 Aims

This chapter aimed to assess whether microscale environmental structure can impact microbial stress response, by altering the flow and distribution of an applied stressor.

This was assessed by developing and validating suitable spatial metrics to describe the physical structure and space around single microbial cells. This was followed by experimental assay of yeast cell responses to a metal stressor in microfluidic devices containing soil-like structures, so enabling correlation with the developed spatial metrics. In a separate experimental setup, simplified structured environments with different numbers of structures were produced using microspheres in chambers within microfluidic devices. This approach was further used to assess the impact of environmental structure and structure density on microbial stress response using the spatial metrics developed previously.

4.2 Materials and Methods

4.2.1 Yeast strains and culture conditions

The haploid *Saccharomyces cerevisiae* strain BY4741-*HSP104*-GFP (MATa *his3Δ1 leu2Δ0 met15Δ0 ura3Δ0*) (Invitrogen) contains a *HSP104*-GFP translational fusion under the native *HSP104* promoter. Hsp104 is a key stress response protein, upregulated in response to heat stress (among other stressors). The haploid *S. cerevisiae* strain SVY14 *HO::pCUP1-yEGFP* (MATa *leu2-3, 112 ura3-52 trp1-289*) contains a green fluorescent protein (GFP) transcriptional fusion under control of the *pCUP1* promoter integrated at the *HO* locus (Mateus and Avery, 2000). *pCUP1* usually regulates the expression of the metallothionein Cup1p and is induced in response to exogenous copper exposure.

Both strains were maintained and grown in YNB medium [0.69% yeast-nitrogen base without amino acids (Formedium), 2% (w/v) D-glucose], supplemented as required with amino acids or nucleobases to complement auxotrophies (as listed above). Where necessary, media were solidified with 2% (w/v) agar (Sigma-Aldrich, St. Louis, MO). For experiments, single colonies were used to inoculate 10 ml of medium in 50 ml Erlenmeyer flasks and incubated with orbital shaking (New Brunswick Scientific) at 120 rev min⁻¹ at 30°C overnight. To produce exponential phase cells for experimental purposes, overnight cultures were diluted to OD₆₀₀ ~ 0.5 and incubated as above until cells reach an OD₆₀₀ ~ 1.5.

4.2.2 Determination of cellular GFP

Single-cell GFP fluorescence was determined for samples (500 μ L) of exponential phase cells in YNB medium at $OD_{600} \sim 0.5$ following treatment either with specified temperatures for *S. cerevisiae* BY4741-*HSP104*-GFP or specified copper sulphate concentrations for *S. cerevisiae* SVY14. Post stress, cells were harvested by centrifugation at 4500 g for 5 min, the supernatant removed, and cells washed twice in phosphate buffered saline (PBS) (137mM sodium chloride, 2.7mM potassium chloride, 11.9mM phosphate buffer) at room temperature. Flow cytometric analysis was performed with a FACSCanto A (BD Biosciences) collecting 10^6 events per sample. Cells were excited at 488 nm and emission was collected through a FITC 530/330 nm filter. Events were gated by median forward scatter and side scatter to exclude doublet cells and minimise interference from debris. Median fluorescence of gated cells was then calculated in Flowing Software V2.5.

4.2.3 Soil micromodel setup

4.2.3.1 Soil micromodel preparation

The soil micromodels described here are microfluidic devices consisting of a simulated soil structure moulded in polydimethylsiloxane (PDMS) polymer and plasma bonded onto a glass substrate (**Figure 4.1**) (Rubinstein et al., 2015). Holes punched in either end of the device allow fluid flow to be introduced through the open spaces within the model, while the simulated structure within it provides the structured environment. Each model contained three identical structures in parallel, supplied by the same flow inlet. Soil micromodels were produced and kindly provided by Yi-Syuan Guo, University of Connecticut, as described in Rubinstein et al., 2015.

Micromodels were sterilised before experiments by exposure to ultraviolet (UV) light for 20 min in a class II biosafety cabinet using a 30W ultraviolet lamp (Philips), with the micromodels 60 cm from the light source.

Sterile micromodels were treated overnight with 2 mg ml⁻¹ concanavalin A (ConA) (Sigma-Aldrich) by flowing ConA solution through the model until saturated. This was to promote subsequent cell adhesion to the glass floor of the device. Micromodels were then flushed with filtered (filter size 0.22 µm) YNB medium to remove excess conA solution and then inoculated with cells suspended in YNB at 750 cells µl⁻¹ by flowing the suspension into the model at a rate of 10 µl h⁻¹, resulting in ~100 cells per micromodel channel. Devices were then mounted onto an inverted microscope stage within an environmental chamber and heating system which maintained the environmental temperature at 30°C unless otherwise stated.

Cells were allowed to settle to the glass floor of the device for 20 minutes before a flow of YNB medium was introduced at 2 µl hr⁻¹ for 20 minutes to flush out non-adherent cells. Medium flow was introduced using a 20 ml syringe connected to the opening of the microfluidics device, with the syringe mounted onto a NE-500 syringe pump (New Era Pump Systems, Inc.). The syringe pump applied a constant force to the syringe plunger flange to expel the desired volume of fluid over time. The syringe pump was controlled using SyringePump Pro software, which contained pre-configured settings to account for the specific size and brand of syringe being used to ensure accurate expulsion volumes.

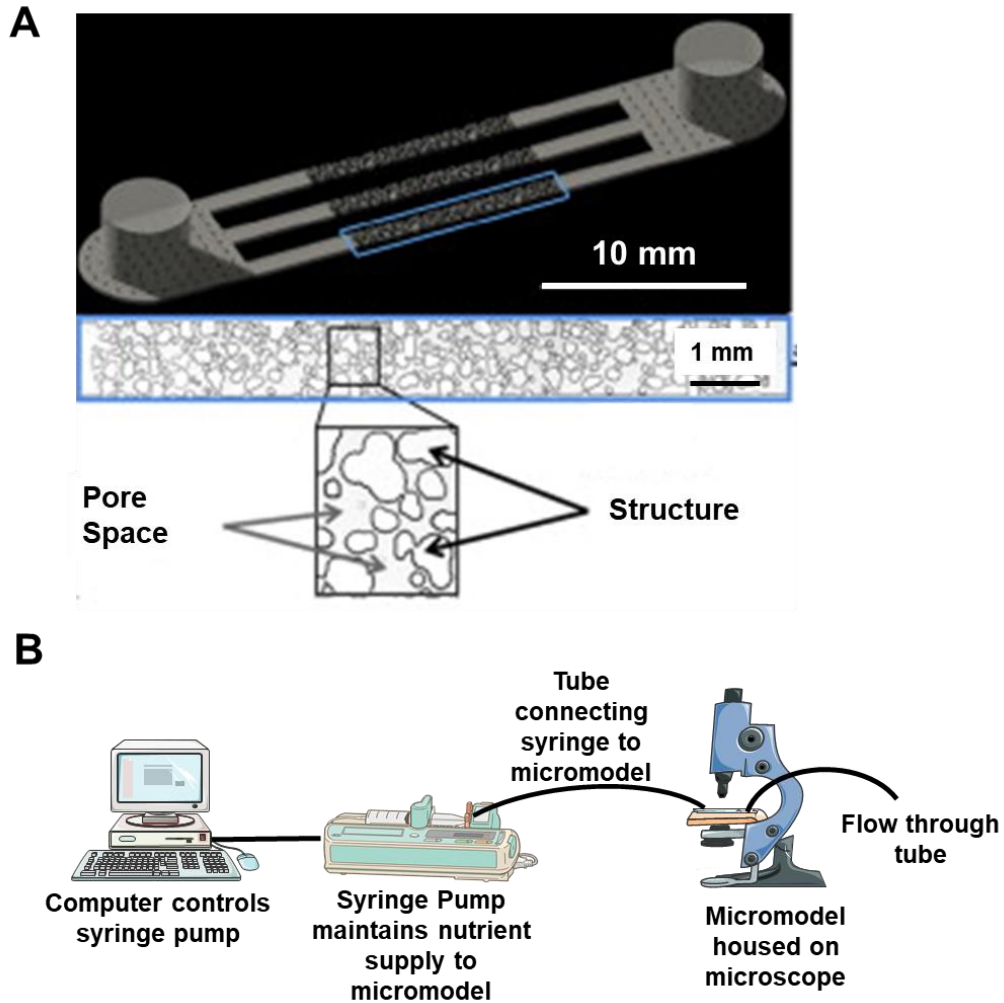


Figure 4.1- Overview of soil micromodel setup

(A) Soil micromodels are microfluidic devices containing PDSM polymer structures that resemble soil particles, which are illustrated schematically in the lower part of the figure. Figure (A) is adapted from Deng et al. (2015). Flow can be introduced to these devices by a tube connected to a syringe pump, with fluid flow-through collected in another tube at the other end. A schematic of this experimental setup can be seen in (B).

4.2.4 Stress experiments within soil micromodel devices

Before a stressor (either heat or copper) was applied, all three micromodel chambers were imaged in brightfield transmitted light and GFP emission wavelengths, to record

the micromodel structure and baseline fluorescence values for individual cells (image acquisition parameters are detailed in section 4.2.6). For heat stress experiments, flow of medium was continued at $2 \mu\text{l hr}^{-1}$ and the temperature of the environmental chamber was raised to 38°C for 1 hr, after which time cells within micromodels were imaged as before to capture post-stressor fluorescence. For copper stress experiments, the syringe and tubing were replaced with a syringe and tubing containing YNB as before but supplemented with $200 \mu\text{M}$ copper sulfate. This copper supplemented medium was then introduced to the model at the same flow rate as before, for 1 hr, before imaging again.

4.2.5 Stress experiments within CellASIC ONIX II microfluidic devices

In addition to soil micromodels, a commercial microfluidics system was used to determine whether creating structured environments in otherwise constant conditions would impact microbial stress response. Unlike the flow-driven soil micromodels described above, the CellASIC system is a pressure driven system. In this system, fluids to be introduced to the micromodel chambers are held within $500 \mu\text{l}$ solution inlets (**Figure 4.2A**). These are housed within the microfluidic plate and each solution inlet is connected to its respective chamber by a small channel within the plate (**Figure 4.2B**). A manifold is then sealed to the plate (**Figure 4.2C**), which is attached to a valve system to regulate pressure and temperature within the microfluidics plate.

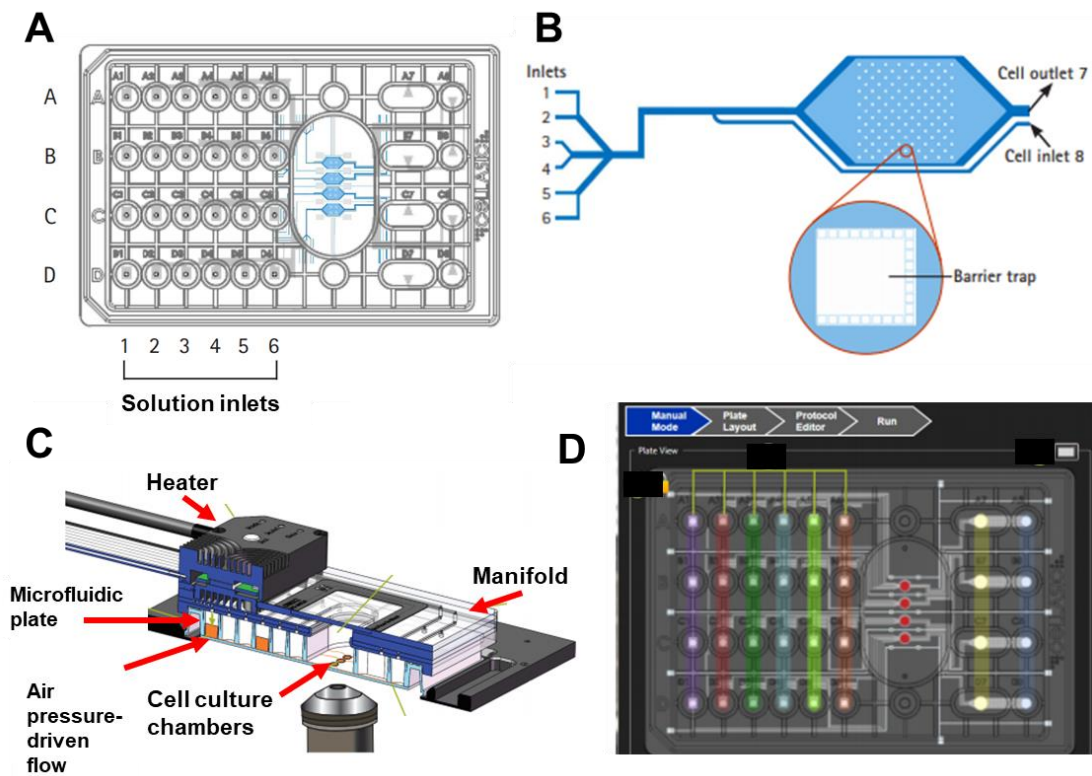


Figure 4.2- Overview of the CellASIC ONIX II microfluidic system and microfluidic plates

Microfluidic plates (85.48 mm Wide x 127.76 mm Long x 14.35 mm Height) (A) contain a series of solution inlets that can be filled with solutions to be introduced into one of four microfluidics chambers (blue, with one chamber illustrated in (B)). Note that in (A) letters A-D refer each to one chamber, allowing for up to 6 solution inlets per chambers. Each chamber contains 104 traps measuring 100x100 μm (B), designed to trap cells in place while still permitting fluid flow into the traps. Fluid flow is introduced by pressure applied to each solution inlet via the manifold system (C), which seals the device and also regulates the temperature of the microfluidics plate. The ONIX II software is used to control the pressure applied to each solution inlet by the manifold — A screenshot showing control of each solution inlet is presented in (D) (the plate layout is analogous to that shown in (A)), colours indicate groups of inlets that can be pressurised simultaneously). Illustrations are adapted from the CellASIC ONIX II Microfluidics System User Guide (EMD Millipore).

To introduce flow of a particular fluid into the microfluidics chamber, pressure is applied to each solution inlet individually through the manifold (by mechanical airflow), forcing the fluid into the chambers of the microfluidics plate. The pressure of each reservoir was controlled via ONIX II software (CellASIC) installed on a windows PC (**Figure 4.2D**). The temperature of the microfluidics plate was also measured and controlled by this software, as the manifold contained a heating element to regulate the temperature within the microfluidic device. For these experiments, the plate temperature was maintained at 30 °C.

To create micrometre scale structures for stress response experiments, commercially available CellASIC ONIX pad trap plates (Sigma-Aldrich) were used. These comprise four chambers, with each chamber containing 104 trap pads (each measuring 100 x 100 µm) and consisting of a perimeter of pillars to help trap cells while facilitating fluid flow in and around the traps (**Figure 4.2D**). The ceiling height within each trap is 4 µm, which effectively traps yeast cells (approximately 4-5 µm diameter) and prevents them from moving, whereas the ceiling height surrounding traps is ~ 20 µm, allowing cells not within traps to be removed by fluid flow.

4.2.5.1 Using microspheres to create physically structured microenvironments

Chambers of CellASIC ONIX pad trap plates (Sigma-Aldrich) were inoculated either with SVY14 cells at OD₆₀₀ ~0.1, or cells at the same concentration mixed with 4 µm TetraSpeck microspheres (Invitrogen) at either 1.26 x 10⁷ or 6.3 x 10⁶ particles ml⁻¹, suspended in YNB medium. Cells and/or microspheres were introduced to the chambers by flowing these mixtures into the model at 8 psi in three 10 s bursts. This resulted in chambers containing ~1 yeast cell per trap and an average of either 0, 16,

or 39 microspheres per trap, depending on the microsphere inoculum, to create structured chambers with different structure densities. Because the cell traps have a ceiling height of 4 μm and the ceiling outside of traps is 20 μm from the chamber floor, cells and microspheres are forced into traps by the fluid flow and are held in place between the floor and ceiling of the trap pads, while debris outside of the trap pads is removed by further fluid flow. Then, to further distribute microspheres within each trap pad and reduce their aggregation around the trap perimeter, the flow direction was alternated at 5 psi in short bursts (3-4 s). This “shuffled” microspheres away from the trap perimeter, reducing the number of microspheres might impede fluid flow into or out of the traps.

Once cells and microspheres had been introduced and distributed within individual traps, flow of YNB medium was introduced across all three chambers being used in a plate at 2 psi for 20 min, to ensure cell nourishment and removal of any cells/microspheres outside of traps. After incubation, each chamber was imaged in brightfield and at GFP excitation/emission wavelengths, as described in section 4.2.6, before flushing with YNB supplemented with 200 μM CuSO_4 (copper sulfate) at 8 psi for 10 s. The initial 8 psi flushing step ensured that the copper supplemented medium completely displaced the regular medium (the manufacturer recommends a 5 s flushing duration for this purpose). Then, fluid flow of copper supplemented medium was reduced to 2 psi and continued for 1 hr. After 1 hr stressor exposure, cells within chambers were then imaged again as before to capture post-stress cell fluorescence values.

4.2.5.2 Assay of flow-rate effect on stress response

To measure the impact of different stressor flow rates on *CUP1*-GFP expression levels, trap plates were inoculated with SVY14 cells at $OD_{600} \sim 0.3$ by flowing the suspension once at 8 psi for 10 s, resulting in ~ 1 yeast cell per trap. Then, YNB medium flow was introduced at 2 psi for 20 min to support metabolic activity of cells within traps and to remove cells not confined to traps, before imaging in brightfield and at GFP excitation/emission wavelengths (section 2.6). After baseline imaging, YNB supplemented with 200 μ M $CuSO_4$ was introduced at 8 psi for 10 s before reducing the pressure to either 1 or 2 psi (as specified) for 1 hr. Cells were then imaged again as before to capture post-stress cell fluorescence values.

4.2.5.3 Quantifying spatial relationships between cells and microspheres

To help assess the impact of microsphere proximity on cell stress response, the angle and distance of every microsphere from yeast cells within each trap were calculated. This was according to the coordinates for cells and beads in relation to the trap area, with the top left of the trap area defined as the point of origin ($X=0, Y=0$). An angle of zero degrees represented a microsphere being located directly between the trap opening and cell and exactly perpendicular to the trap opening. An angle of 90° and -90° represented beads exactly parallel to the cell relative to the trap opening. Distance was determined as linear distance between the centre of the cell and centre of the microsphere. The angle and distance parameters used are described and illustrated later in the Results (section 4.3.3.2).

To measure the coordinates of cells and microsphere within traps, each trap was considered separately, so that the top left corner of each trap was given the

coordinate value (0,0), allowing for later comparisons between traps (i.e., cells at the same location of different traps would share the same coordinates). Then, coordinates of all objects and cells were measured (from the objects centre point) using the built-in “Analyse particles” function within Fiji v1.51w software. Distances between microspheres and cells were calculated using these coordinates, using the equation:

$$\sqrt{(x_2 - x_1)^2 + (y_2 - y_1)^2}$$

Where X and Y are respective coordinates of each cell/object.

The angle between microspheres and cells was calculated using the mathematical function $\text{atan2}(y,x)$, which defined the angle (in radians) between the x axis and a straight line that passes through the cell and microsphere. These angles were converted into degrees and transformed, by addition or subtraction, to reflect the angle of the microspheres in relation to the trap opening, such that an angle of 0° represented a microsphere directly between the cell and trap opening, with negative angles representing microspheres behind the cell in relation to the trap opening.

4.2.6 Microscopy and imaging

All microscopy and imaging were conducted at the School of Life Science Imaging (SLIM) Centre, University of Nottingham. Soil micromodels were examined with a DeltaVision Elite Microscope (Applied Precision/GE Healthcare) equipped with a 20x, 0.85 NA objective. Fluorescence excitation was at 475 nm (bandwidth 28 nm) and emission measured at 525 nm (bandwidth 50 nm). Images were captured using a

CoolSnap HQ2 CCD camera (Photometrics) at 60 ms exposure. Brightfield transmitted light images were acquired with 10 ms exposure.

CellASIC microfluidics plates were examined using a Zeiss Exciter Widefield microscope equipped with a 20x, 0.50 NA objective. Fluorescence excitation was at 470 nm (bandwidth 40 nm) and emission recorded at 525 nm (bandwidth 50 nm). Fluorescence and brightfield images were captured using a Retiga R1 CCD camera at 60 and 10 ms exposure times, respectively.

On both systems, the cell chambers were imaged over multiple panels using a motorised stage to conduct multi-point visiting. This was controlled using Micro-Manager software V1.4 software, applying a 10% image overlap between panels to allow image stitching post acquisition. Both setups were contained within an environment control chamber, with ambient temperature controlled by a heater within the chamber. Microfluidics experiments and imaging were conducted at 30 °C unless otherwise specified.

4.2.7 Image analysis

4.2.7.1 General analysis

All image analysis was conducted using Fiji v1.51w software (Schindelin et al., 2012). Images from multi-point acquisition were assembled into one larger image using the Grid/Collection plugin V1.2 (Preibisch et al., 2009). Voronoi areas and greyscale distance maps were calculated using Fiji V.151w built-in plugins. Yeast cells were identified and selected manually, and fluorescence values calculated as mean intensity of pixels within each cell. For all microfluidics experiments, the same total

area for each yeast cell was measured at each timepoint, and cells which appeared to be doubling (determined visually) during the experiment were excluded from analysis.

4.2.7.2 Single cell spatial analysis

A method was developed to quantify a cell's local environmental structure, which related the distance from a cell to surrounding objects. This was achieved by generating Voronoi tessellations for each yeast cell. In short, this approach divides the open space between cell and object such that any point within a cell/object tessellation is closer to that cell than any other object (**Figure 4.5**). The areas of these Voronoi tessellations were used as a measure for the space surrounding individual cells. The Voronoi tessellations were generated in a semi-automated process in Fiji v1.51w using the "Voronoi" plugin.

In addition, linear greyscale distance mapping was used to give further detail to these Voronoi areas. Here, each pixel of a cell's "Voronoi area" was weighted linearly according to its distance from the cell centre, starting at a value of 1. For example, a pixel adjacent to the cell centre would be given a value of 1, whereas a cell 200 pixels from the cell centre is given a value of 201. This allows metrics such as the sum, median, and mean greyscale value to be tested for correlation with cell fluorescence values in a way that reflects how much of the space in a Voronoi area is close or far from the cell (this is important as Voronoi tessellations can have very different shapes around different cells, which 'area' alone does not capture). These values together with Voronoi measurements will henceforth be referred to as "spatial metrics".

4.2.7.3 *Fluid displacement analysis*

To measure the potential impact of microspheres present in the CellASIC cell traps on flow of fluid into the traps, 250 μM rhodamine 6G (Sigma-Aldrich) (a fluorescent dye) was introduced into either empty or microsphere filled traps, with fluorescence images taken for this duration using the same imaging parameters as before (section 4.2.6). To analyse the data in Fiji v1.51w, a “straight-line selection” was drawn from the trap opening to the back of the trap, and the mean fluorescence intensity along this line was measured at every 100 ms time interval using the “Plot profile” function, enabling a representative measurement of dye flow across the whole trap.

4.3 Results

4.3.1 Using fluorescent protein expression as a proxy for cellular exposure to stressor

In order to investigate relationships between single-cell stressor exposure and parameters of a cell's local environmental structure, it was first demonstrated that stressor exposure (copper or heat) could be assayed according to fluorescence of cells expressing GFP either under control of a copper inducible gene (*CUP1*) promoter, or as a GFP-tagged heat stress response protein (Hsp104).

S. cerevisiae SVY14 cells expressing *pCUP1*-GFP (the *CUP1* gene encodes the copper metallothionein and is strongly inducible by exogenous copper) showed a linear, positive correlation between the concentration of copper supplied to cells and cellular fluorescence, after either 1 hr or 2 hr incubation with final concentration of additional copper sulfate (CuSO_4) concentrations ranging from 25 to 300 μM ($R^2 = 0.939$ $p < 0.001$; $R^2 = 0.942$ $p < 0.001$ respectively). Including the no-copper control in this range gave a deviation from linearity, as it was noted that the fluorescence increase between 0 and 25 μM was larger than in subsequent increments of supplied copper concentration. The fluorescence increase of cells was greater at 2 hr exposure across all concentrations (**Figure 4.3**).

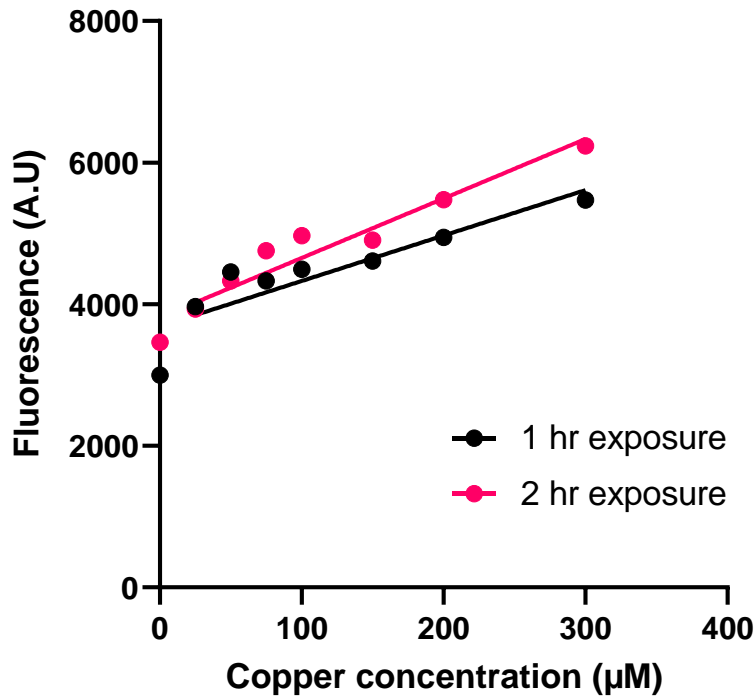


Figure 4.3- Expression of GFP under the CUP1 promoter correlates with copper concentration after 1 hr and 2 hr exposure

Fluorescence of single cells expressing GFP under the *CUP1* promoter and incubated in YNB medium with a range of supplemented copper sulfate concentrations were measured by flow cytometry (10^5 events) after either 1 or 2 hr exposure. Median fluorescence value is plotted from 100,000 cells per concentration. For 1 hr exposure $R^2 = 0.939$ $p < 0.001$, for 2 hr exposure $R^2 = 0.942$ $p < 0.001$, determined by linear regression applied to data for copper concentrations 25 to 300 μM . Data for the no-copper controls were excluded from the regression equation as these deviated from linearity.

S. cerevisiae cells expressing GFP-tagged Hsp104 under control of the native *HSP104* promoter showed an increase in fluorescence between 30 - 39°C at exposure times ranging from 15 - 120 minutes, with fluorescence decreasing at 42 and 45°C. The fluorescence difference between treatments was generally more pronounced at incubation times > 15 minutes (**Figure 4.4**).

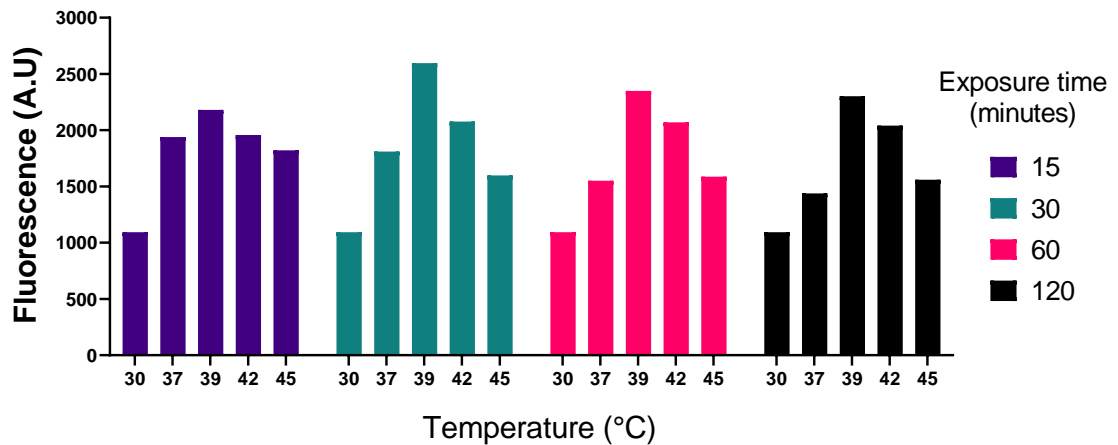


Figure 4.4- Temperature-dependent Hsp104-GFP expression under the native *HSP104* promoter

Fluorescence of exponential phase *S. cerevisiae* cells expressing Hsp104-GFP after exposure to temperatures ranging from 30–45 °C for 15–120 minutes (as indicated on the plot), determined by flow cytometry (10^5 events). Median fluorescence value is plotted from 100,000 cells per temperature and exposure time.

4.3.2 Use of defined “spatial metrics” to quantify a cell’s local environmental structure

After establishing a proxy to quantify single cell stressor exposure, a set of parameters were then considered for potential suitability as descriptors of the local physical surroundings of individual cells. Firstly, the use of Voronoi areas (described in section 4.2.7.2) to quantify the proximity between cells and surrounding objects was trialed. Voronoi areas are defined by tessellations that separate the open space between points, such that any space within a point’s Voronoi area is closer to that point than any other (illustrated in **Figure 4.5B**). A series of mock images were produced, starting with a single central point (representing a microbial cell) and object (representing an environmental structure), followed by the systematic

addition of objects at distances equal to one or two object diameters from the central cell (**Figure 4.5A**). This produced an array of spatial configurations for analysis. Voronoi areas were then calculated for each cell relative to its surrounding objects using Fiji V1.51w (see section 4.2.7.2) Subsequently each pixel within a Voronoi area was assigned a numerical value corresponding to its distance from the cell, represented as a greyscale distance map (with values from 1–255 representing white to black, respectively) (**Figure 4.5B**). This allowed Voronoi areas to be weighted in a way that reflected differing shapes, as Voronoi areas encompassing larger distances between the cell and area-perimeter included larger numerical values. Plotting cells' Voronoi areas or other parameters from the greyscale distance maps against the inferred, relative complexity of the different configurations trialled (**Figure 4.5A**) showed the anticipated trend. That is, either an increased number of objects around a cell or a reduced distance between objects and cell, reduced the Voronoi area and greyscale distance values, reflecting reductions in open space around the cell (**Figure 4.5C**). It should be noted that some measures, such as median greyscale value, showed this general trend but also showed deviation from the trend as the object number was increased.

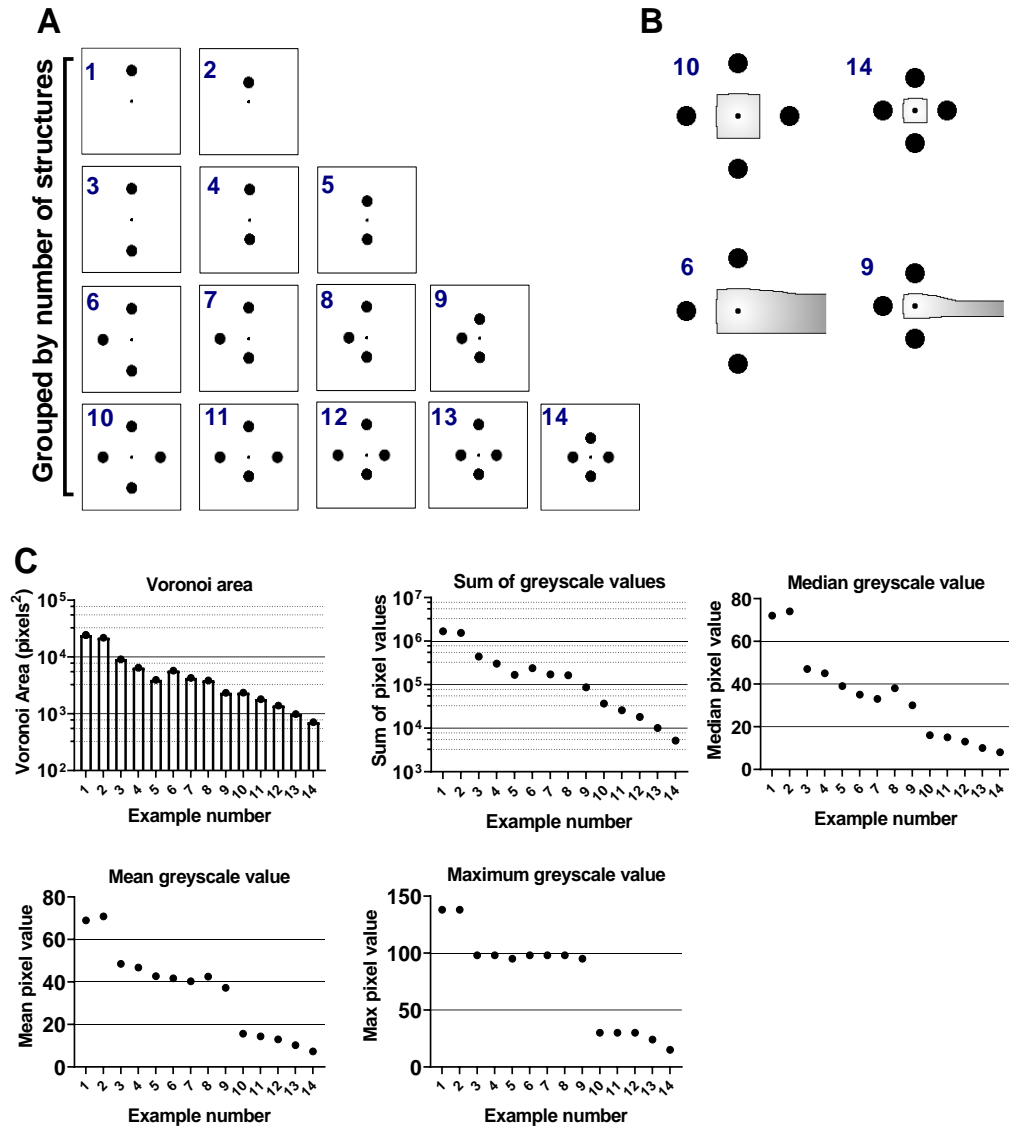


Figure 4.5- Exploring spatial metrics as a method of describing the spatial relationships between objects

(A) A systematic array of central points (smaller circle, representing a microbial cell) with an increasing number of objects (larger circles, representing a simple environmental structure) either one or two object diameters away from the central point. (B) Selected illustrations of Voronoi tessellation (black outline), around a central point, dividing the open space between objects. Each pixel within the tessellation is given a value corresponding to its distance from the central point, illustrated here as greyscale ranging from 1 (white) to 255 (black). The values of all measured parameters for each numbered example image in (A) are presented in panel (C).

4.3.3 Examining the relationship between environmental structure and microbial stress response

4.3.3.1 *Yeast stress response within soil micromodels does not correlate with their spatial metrics.*

Once spatial metrics and a proxy for cell stressor exposure had been established, experiments were conducted in microfluidics devices containing physical structures (soil micromodels - see section 4.2.4) to determine whether the introduction of physical environmental structure impacted microbial stress response. Cells were inoculated within soil micromodels by flowing a $750 \text{ cells } \mu\text{l}^{-1}$ cell suspension through them, resulting in approximately 100 cells per micromodel channel (with three identical replicate channels per model). See **Figure 4.6** for example images.

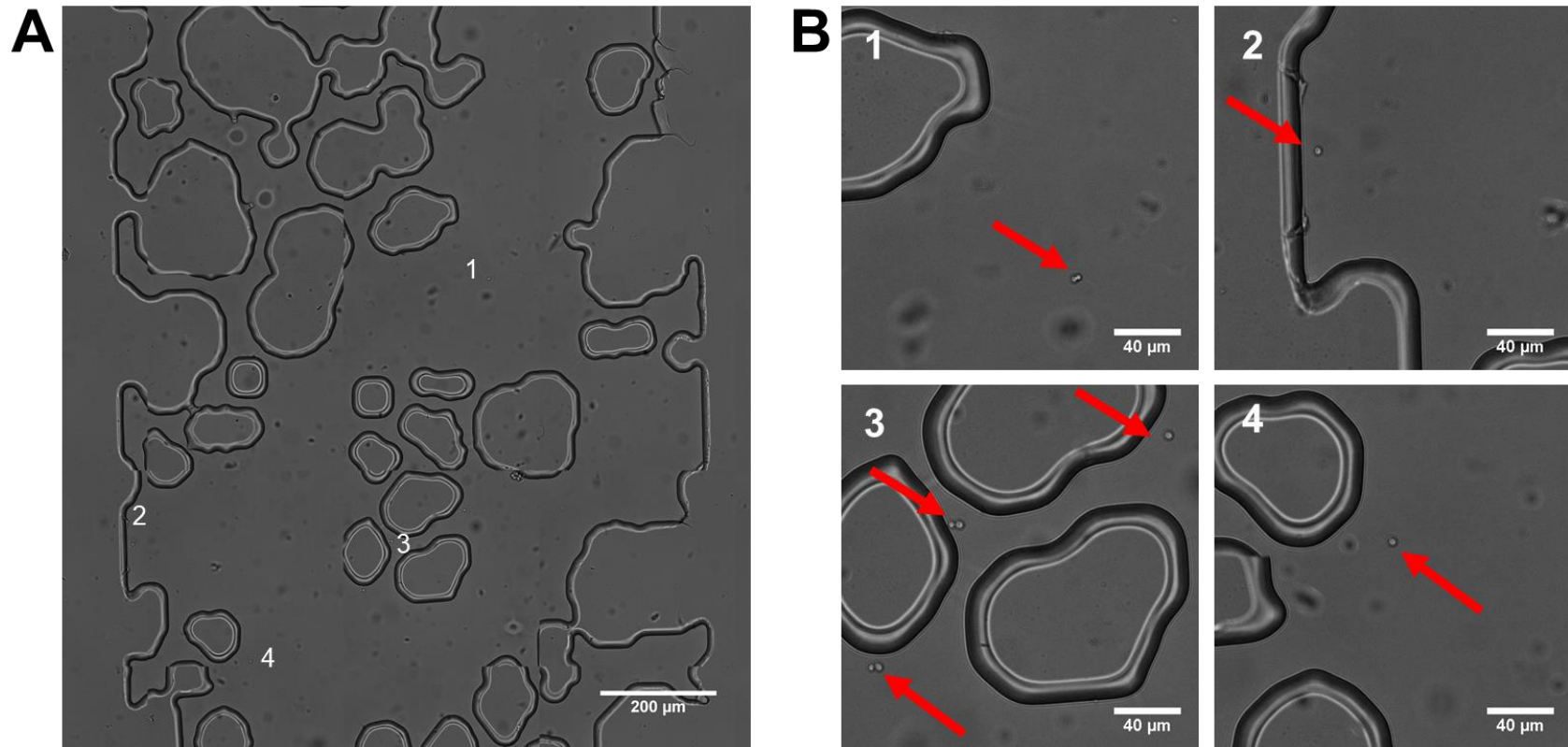
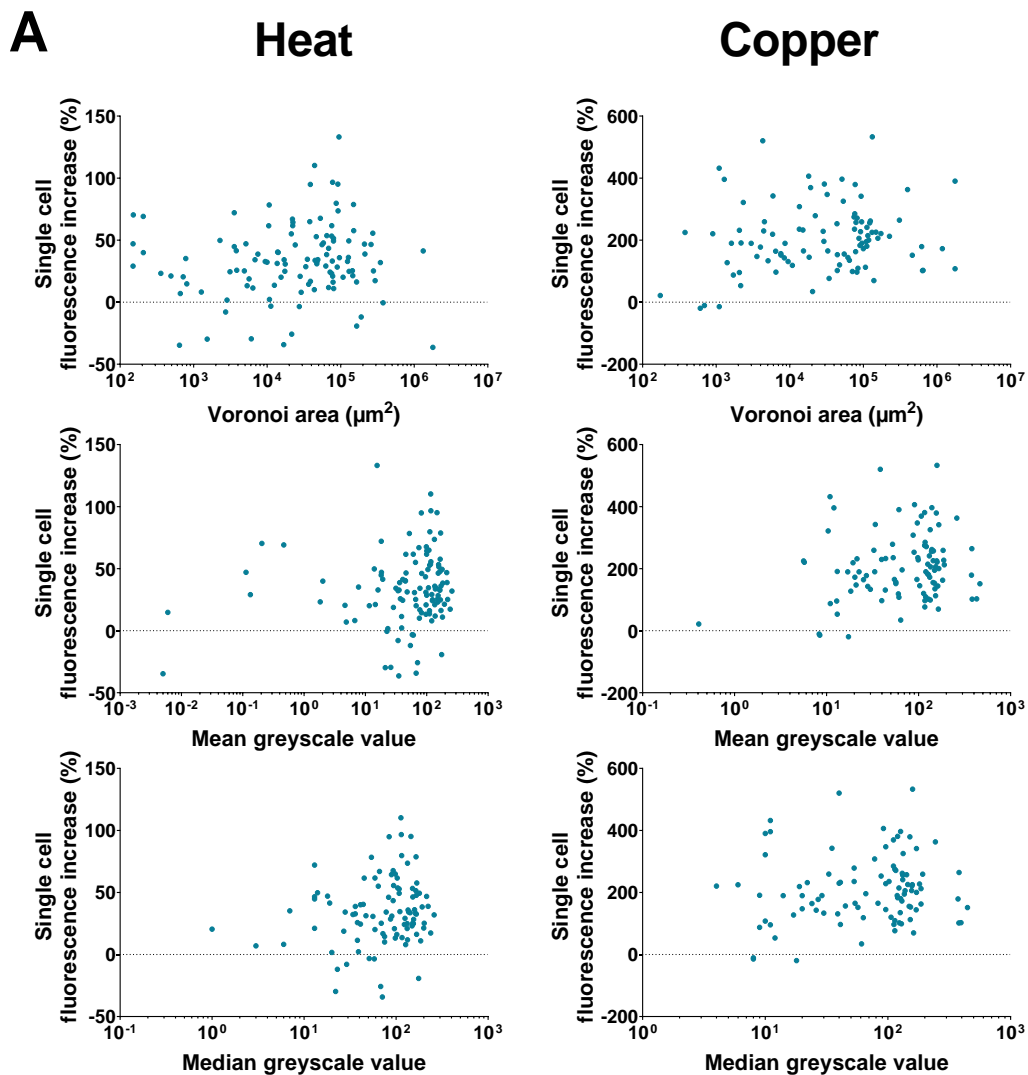


Figure 4.6- Representative microscopic images of soil micromodels

Soil-micromodel microfluidics devices contained solid PDMS structures within a channel 1 mm in diameter and 10 mm in length, presented in (A), with the direction of fluid flow from top to bottom of the image. Approximately one fifth of the channel length is presented. Cells are distributed randomly through the open pore space, with examples of cell locations highlighted in locations 1-4 in (A). Close-ups of each location and cell (red arrows) are presented in (B).

To determine whether a cell's local environmental structure influenced its exposure to each stressor, the percentage increase in single-cell fluorescence arising during exposure to each stressor was calculated and compared with the single-cell spatial metrics described above (**Figure 4.7A**). It was hypothesised that cells within more confined spaces (represented here as a smaller Voronoi area) would be shielded from copper stressor flow in comparison to cells in more open (exposed) spaces. Conversely, it was anticipated that heat stress would apply uniformly across the soil micromodel (as the entire chamber was heated externally) and would not correlate with any spatial metrics. However, no significant correlations between the spatial metrics and response were apparent for either copper- or heat-stress (see **Figure 4.7B** for Pearson's correlation and p-values).



B

Metric	Heat Stress		Copper Stress	
	Pearson r	p-value	Pearson r	p-value
Voronoi Area	-0.141	0.136	0.032	0.747
Greyscale Mean	0.127	0.178	0.072	0.481
Greyscale Median	0.130	0.169	0.075	0.460

Figure 4.7- The trialled spatial metrics do not predict cellular stress response

(A) Correlations between percentage increase in single-cell fluorescence (post- versus pre-stressor) and cell Voronoi area, or mean or median greyscale distance values of the Voronoi areas. These were determined after 1 hr of exposure of *S. cerevisiae* expressing *pCUP1*-GFP or Hsp104-GFP to either 200 μ M copper (left) or change from 30 $^{\circ}$ C to 39 $^{\circ}$ C (right), respectively, in soil micromodels. Pearson's correlation values and p-values for each linear regression analysis are listed in (B).

4.3.3.2 *Microsphere structures in CellASIC trap plates can impact microbial stress response*

Because the structures within the soil micromodels used above are complex and differences in cell fluorescence increase could not be accounted for by spatial metrics (**Figure 4.7**), a second experimental setup was designed with a simplified and modifiable environmental structure. The CellASIC microfluidics pad trap plate is a commercially available microfluidics device consisting of 4 polydimethylsiloxane (PDMS) chambers, each containing 104 barrier traps with dimensions 100 x 100 μm and ceiling heights of 4 μm (**Figure 4.8A**). Liquid flow can be introduced through the chamber with an external pressure system to create nutrient or stressor flow within the chamber in a controlled manner (see section 4.2.5 and **Figure 4.2**). By introducing 4- μm microspheres into the chamber, it was possible to create simple structured environments (**Figure 4.8B**) in which yeast cells could reside. Furthermore, by varying the concentration of microspheres added in each chamber, environments with varying degrees of structure could be created.

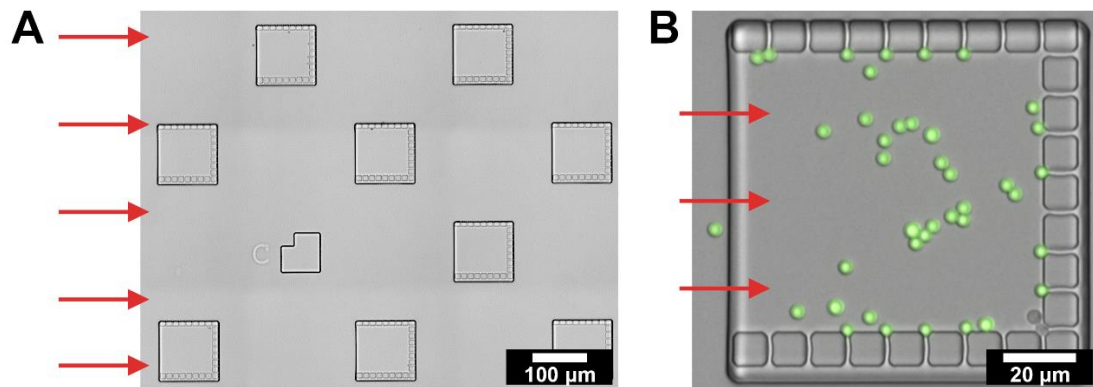


Figure 4.8- Illustration of CellASIC trap plates and environments with added microspheres for structure

Each of the four chambers within a microfluidics plate contains 104 individual 100 x 100 μm traps. A representative 9 traps from one chamber are pictured in A (note, the chamber is much larger than the crop shown), illustrating the alternating arrangement of traps. Red arrows indicate direction of fluid flow. Each individual trap (B) is composed of a U-shaped arrangement of pillars, with gaps between pillars sufficient to allow fluid flow but prevent cells from passing. Here, traps were inoculated with 4 μm microspheres (B, green spheres) to create individual structures within a trap. Yeast cell can be seen in the bottom-right corner of the trap in B. Red arrows indicate direction of fluid flow into the trap.

After introducing structure from microspheres within each trap of the microfluidics chambers, preliminary experiments were conducted to determine whether the microspheres may alter overall fluid flow within traps, potentially by blocking pores at the trap perimeter (seen in **Figure 4.8B**). By introducing a fluorescent dye (rhodamine 6G (R6G)) at 8 psi into traps with and without microspheres and measuring the movement of dye into traps over time, a decreased dye flow within the first ~2 seconds of introduction was observed in traps containing microspheres. However, after this initial difference in rate, the quantity of dye

within each trap type was similar after approximately 4 seconds as the dye level in the microsphere-free traps had plateaued earlier (**Figure 4.9**). This plateau was below the saturation limit of the camera (dotted line in **Figure 4.9**) indicating that it was not a saturation artefact. Based on these data, it was decided for subsequent stress-response experiments that medium containing copper would be introduced at 8 psi for ~10 seconds before continuing flow for 1 hr (at 2 psi) before analysis of cellular responses. Accordingly, kinetic differences in flow over the first 2–4 seconds of exposure (**Figure 4.9**) were negligible relative to the experimental timescales.

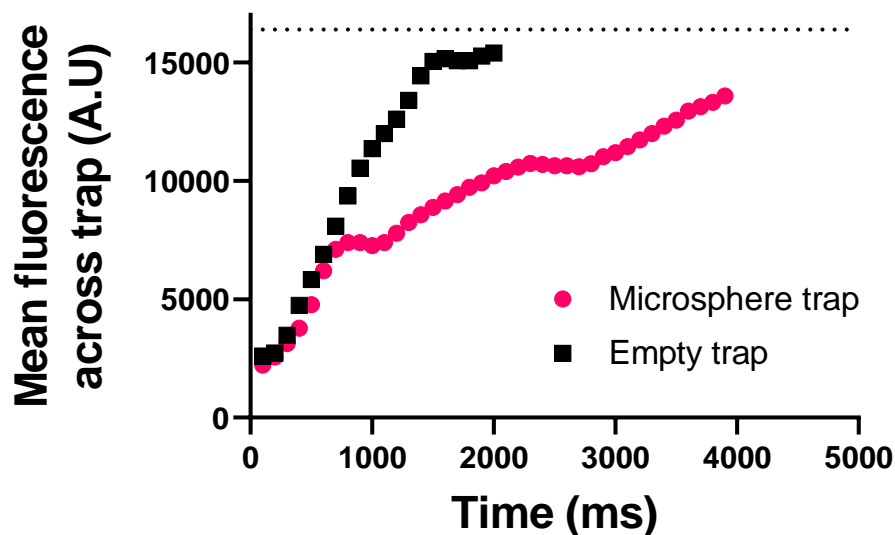


Figure 4.9- Examining flow rate differences in traps with and without microspheres

Rhodamine 6G was introduced to CellASIC trap plate traps either containing microspheres or not. The fluid flow into individual traps was compared using R6G fluorescence after R6G inflow was initiated, with fluorescence values across the length of the trap averaged at every time point. The dotted line at $Y = 16,383$ represents the saturation value of the camera.

Then, to investigate whether these micrometre-scale structured environments impacted microbial stress exposure, *S. cerevisiae* SVY14 cells (expressing *pCUP1*-GFP) were introduced to traps and exposed to 200 μ M copper sulfate for 1 hr under constant flow. By comparing mean fluorescence increase of cells (a proxy for stressor exposure) in unstructured chambers versus cells within chambers containing two different quantities of microspheres, a decreased relative response could be seen in the structured environments (**Figure 4.10**) (one-way ANOVA with Tukey's multiple comparisons, $p < 0.0001$ for both comparisons). These results suggest that introducing structure into these environments with microspheres suppresses microbial response (and, therefore, probably exposure) to copper.

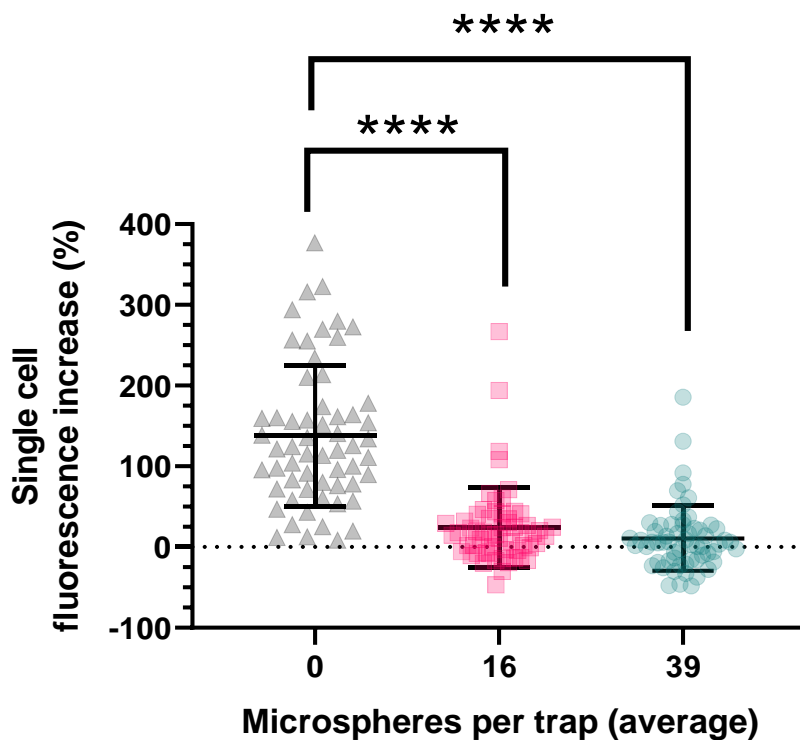


Figure 4.10- Increasing environmental structure density decreases cell stressor exposure

Comparison between average fluorescence increase of *S. cerevisiae* SVY14 cells across chambers with an average of either 0, 16 (± 5), or 39 (± 8) microspheres per trap after 1 hr exposure to 200 μM copper sulfate (****, $p < 0.0001$ according to one way ANOVA with Tukey's multiple comparisons,). Points represent individual cells, bars represent mean and standard deviation for 59, 58, and 62 cells, respectively, with every cell being located its own structured environment (trap).

To further understand the relationship between micrometre-scale structured environments and their impact on stress exposure and response, the same spatial analysis previously applied to cells in the soil micromodels was also applied to cells and microsphere structures in the microfluidic traps. When comparing the mean spatial metrics of cells at each of the two

microsphere densities tested, there was a significant reduction in average cell Voronoi area in comparison to the unstructured (microsphere-free) control (**Figure 4.11A**). This confirmed that cells within traps with more microspheres had reduced open space surrounding them. These spatial metrics showed a very similar trend as cellular response to copper inflow across the different structure densities (presented in **Figure 4.10**). Additionally, further analysis at the single cell level showed significant, positive correlation between an individual cell's Voronoi area and its fluorescence increase (Pearson's $r = 0.237$, $p = 0.0014$) (**Figure 4.11B**).

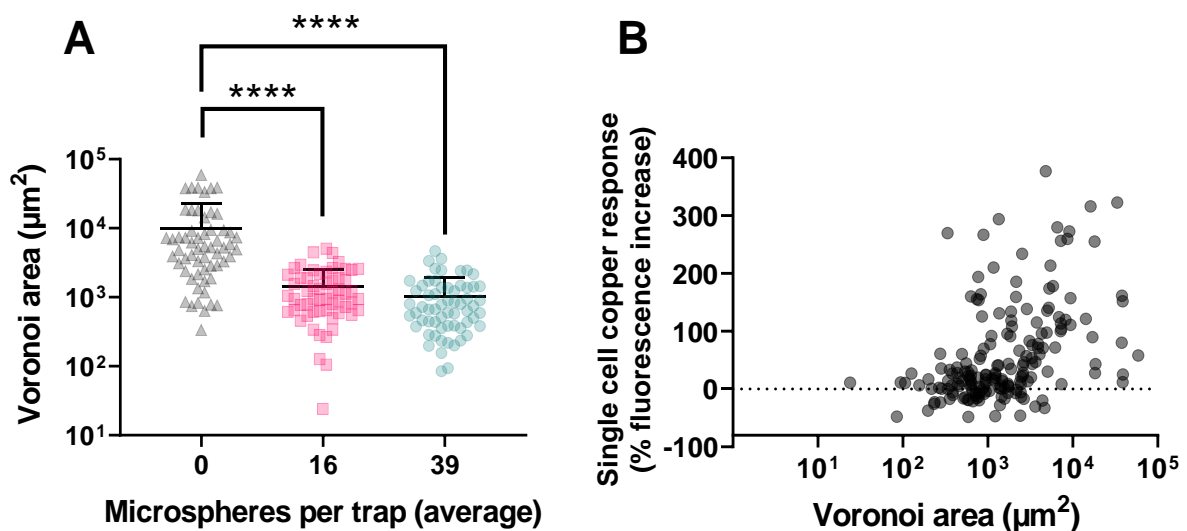


Figure 4.11- Comparison of single-cell spatial measures and copper responses between traps of different microsphere densities

(A) Comparison between cell Voronoi area across chambers with either 0, 16, or 39 microspheres per trap (on average) (****, $p < 0.0001$ according to one way ANOVA with Tukey's multiple comparisons). Bars represent mean and standard deviation of 59, 58, and 62 cells. (B) Correlation between single-cell Voronoi area and copper response (% fluorescence increase) when analysing cells across all three environments (Pearson's $r = 0.280$, $R^2 = 0.079$, $p < 0.0001$, $n=179$). For both figures, points represent individual cells, with each cell being located within its own structured environment (trap).

In a separate experiment omitting microspheres, manual reduction of the copper stressor flow rate by 50% using the CellASIC software reduced the response to copper by approximately 34% (**Figure 4.12**). Given this and the facts that the presence of microspheres also decreased the copper response of cells (by 80 – 90%) (**Figure 4.10**) but did not appear to substantially reduce overall flow into traps (**Figure 4.9**), it was reasoned that stressor flow rates could be locally decreased only within close proximity to microsphere structures, and potentially by more than the 50% trialled manually here. Accordingly, this would be expected to reduce the copper exposure of cells that are closest to the microspheres, and that is supported by the fact that reduced Voronoi area was associated with reduced response (**Figure 4.11B**). At the same time, the data do not eliminate a possibility that reduction in copper response in the structured environments is dependent on another parameter than flow.

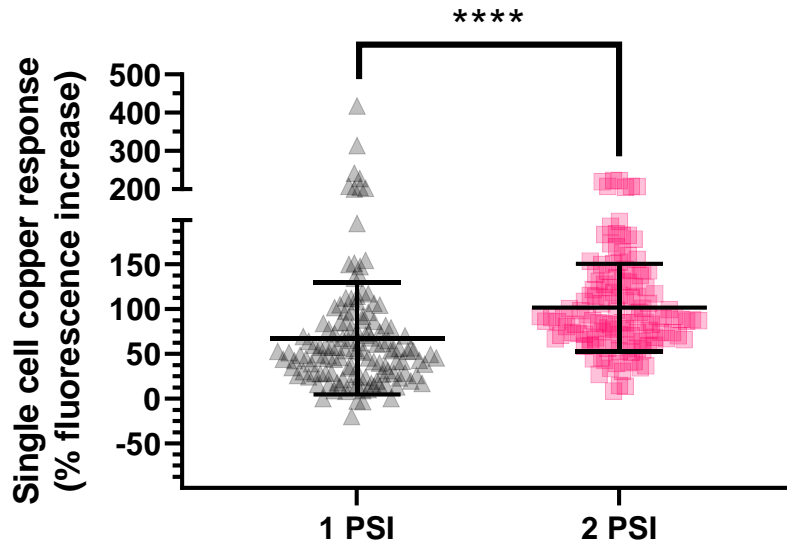


Figure 4.12- Reducing flow rate of copper-supplemented medium into the microfluidic traps reduces the cellular copper response

Cells in microfluidics traps were exposed to YNB supplemented with 200 μM copper nitrate at induced flow of either one or two psi (corresponding to ~ 2 and $4 \mu\text{L hr}^{-1}$, respectively). ****, $p < 0.0001$ (two-sample t -test).

To further test the hypothesis that cells within close proximity to structures were less exposed to stressors, microspheres associated with each cell were grouped into quartiles by distance from their relevant cell. Microspheres were then separated into three groups depending on the angle between the microsphere and cell, with respect to the trap opening (illustrated in **Figure 4.13A,B**)

Lastly, cells and associated beads were then grouped into quartiles based on cellular copper response (% fluorescence increase). The frequency of microspheres in each distance and angle grouping for each quartile of cells was visually compiled into a semicircle illustration,

with microsphere distance represented by distance from the semicircle centre and angle represented by three divisions, as illustrated in **Figure 4.13**.

This grouping of cells and microspheres provided a way of analysing the relationship between cell fluorescence increase (and hence stress exposure) and average distance and position of each microsphere in relation to the cell and source of stressor flow.

This analysis was conducted for the cells responding least and most to copper, defined as the lower and upper quartiles of cells based on copper responsiveness. Then, it was possible to compare the frequencies of microspheres in each of these distance-angle divisions between the two copper-response quartiles by subtracting the frequency of microspheres associated with the lowest responding cells from the frequencies of highest responding cells (**Figure 4.13C**) (see **Appendix D** for raw values). In this difference analysis, a positive number in a particular distance-angle location would indicate that more microspheres at this relative location were associated with cells responding strongly than weakly to copper. Overall, it was noted that more locations showed negative (red) than positive (green) difference values, indicating that the traps with the least copper-responsive cells were those that contain the most microspheres. This agrees with the previous Voronoi data, as cells in the most densely populated traps would be more likely to have smaller Voronoi area. However, there was evidence for a reversal of this overall trend at the closest proximities to cells (i.e., the inner segments of the semicircle), where more microspheres at some of these locations were associated with cells responding strongly than weakly to copper (**Figure 4.13C**). This effect was apparent in two independent replicate experiments.

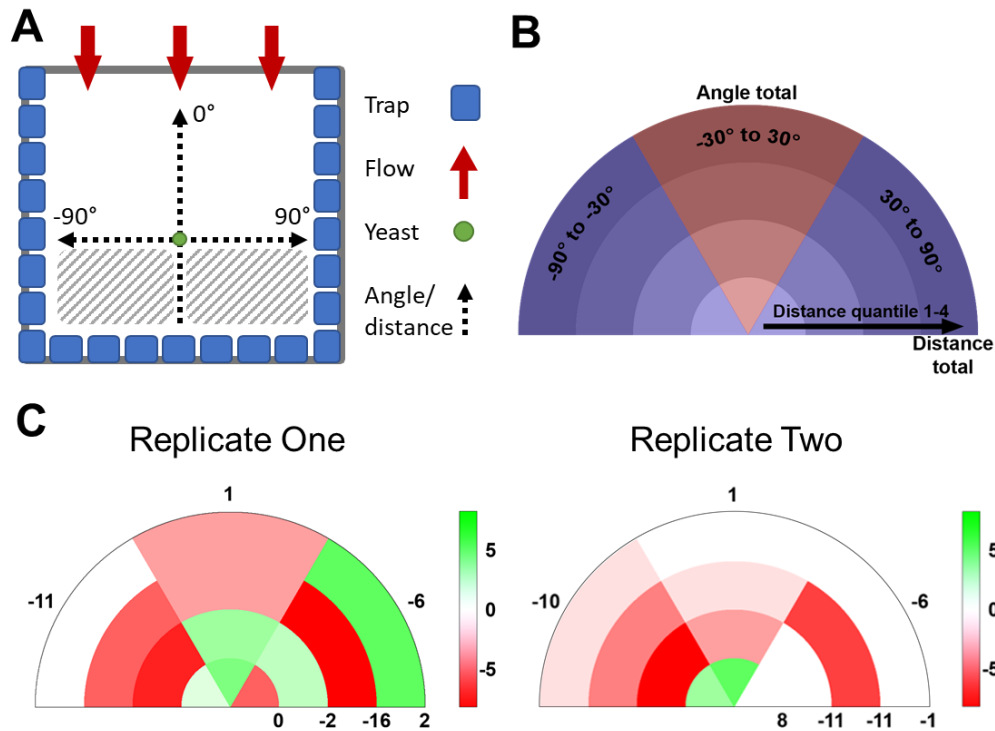


Figure 4.13- Differences in microsphere frequency at different angles and distances from the least and most copper-responsive fluorescent cells

The angle and distance of every microsphere from the yeast cell within each trap was calculated, with an angle of zero degrees representing a microsphere being located exactly perpendicular to the trap opening (i.e., directly between the trap opening where stressor is introduced and the yeast cell), and angles of 90° and -90° representing beads parallel with the cell relative to the trap opening (see dashed lines); this is illustrated in (A). The distance was calculated as linear distance between the centre of the cell and centre of the microsphere. Microspheres not between the trap opening and cell (i.e., behind the cell, relative to the stressor flow; hashed space in (A)) were not included in analysis. These angles and distances were then grouped into terciles and quartiles, respectively, to produce frequency counts of the number of microspheres in each of the angle-distance groupings. These data were visually compiled into a semicircle illustration, with microsphere distance represented by distance from the semicircle centre (where the yeast cell is positioned) and angle represented by three divisions (B). This analysis was conducted separately for the most and least fluorescent cells, represented by the fourth and first quartile of cells according to copper response. Differences in microsphere positioning between the most and least fluorescent cells were compared by subtracting the microsphere frequencies of the least copper-responsive cells from those associated with the most copper-responsive cells. Accordingly, a positive value (coloured green) indicated that more microspheres at a particular location were associated with cells responding strongly than weakly to copper. Microsphere frequencies after subtraction are represented with a red-white-green colour scale, with green representing more positive values, red representing more negative values, and white representing zero values. The data represented in (C) are from two independent experiments. Numbers in bold on the arc and straight line of the semicircle represent total difference in microsphere frequency summed across each angle tercile and distance quartile, respectively.

4.4 Discussion

This chapter aimed to examine the impact of micrometre-scale environmental structure on microbial stress exposure, as environments of such scale are common in the soil pore space (Zaffar and Lu, 2015) and other environments where microorganisms are found (e.g., medical and hygiene settings) (Verran et al., 2010). This was achieved by incorporating and stressing yeast cells, which express green fluorescent protein (GFP) proportionally to stressor exposure, in microfluidic devices which contained either structures that physically resembled soil particle sizes and shapes or small microspheres to create some simple physical structure. Spatial metrics were also developed and tested to quantify the proximity of a cell to its neighbouring environmental structures. Whereas these metrics were shown to quantify the distances between points and objects in an array of mock images, they were not sufficient to predict relationships between the physical structure around a yeast cell and its stress response in the soil micromodels. However, in a separate system, the proximity of a cell to a structure did correlate with its stress response, such that cells within more “open” spaces showed a greater induction of *pCUP1*-GFP (fluorescent reporter of copper response) during copper exposure.

4.4.1 Developing spatial metrics and experimental parameters

Initially, it was necessary to find a suitable reporter of cell exposure to stressor, such that fluorescence response was proportional to stressor concentration. For copper stress, *S. cerevisiae* strain SVY14 was deemed an appropriate reporter strain, expressing a genomic insert containing GFP under the control of the native *CUP1* promoter (which regulates copper induction of the Cup1 metallothionein in wild type cells (Koller et al., 2000, Mateus and Avery,

2000). In this strain, over the range 25–30 μM copper sulfate, a very strong correlation was observed between the concentration of supplied copper and fluorescence response of cells. For subsequent microfluidic experiments, 200 μM was used as the starting copper concentration. This was sub-inhibitory to growth but sufficient to eliciting a strong transcriptional response.

Regarding heat stress, *S. cerevisiae* expressing the translational fusion Hsp104-GFP under control of the native *HSP104* promoter was used to measure heat stress response. As with copper stress, fluorescence in this strain increased with increasing stressor (temperature). However, cells exposed to temperatures above 42°C showed a decline in fluorescence relative to 39°C. As GFP reportedly exhibits stability with limited loss of fluorescence up to temperatures as high as 65°C in vitro (Bokman and Ward, 1981), this fluorescence decrease was likely due to aberrant post-translational folding of the protein (Siemering et al., 1996). For subsequent soil micromodel experiments, 39°C was used as it elicited the highest fluorescence increase out of the tested temperatures.

For both stressors, a one-hour exposure was used in subsequent experiments because, although two hours exposure elicited a greater fluorescence response, the doubling time of *S. cerevisiae* in synthetic medium is approximately 140 minutes (Sherman, 2002). Therefore, one hour was chosen to reduce instances of cell division during the exposures, which may have skewed fluorescence intensity values and spatial metric analysis.

In conjunction with finding an appropriate stress reporter, a method of quantifying the space and structures surrounding a cell was established using Voronoi tessellations and greyscale distance mapping; used previously to describe distances between points in biological systems

(Chacon et al., 2018, Bar et al., 2020). By testing hypothetical environments with varying numbers of structures and distances from a cell, it was determined that the area of a Voronoi tessellation (defining the open space closer to a cell than another object) was predictably influenced by the number and proximity and objects around the cell. In addition, an approach was developed here to weight areas within a Voronoi tessellation, with increased weight for areas further away from the cell as it is nearby objects that are likely to have the strongest effect on cell response (the tessellations have different shapes and this approach helped to resolve whether average or minimum/maximum distance from cells to objects was a factor in stress response). However, it should be noted that the relationship between the number or distances of structures from the cell and the greyscale measurements was not always linear, as some changes to these parameters resulted in relatively large changes in greyscale values, sometimes resulting in two different structure configurations producing similar metric values (it may of course be possible for different structures to confer the same overall environmental properties). Other spatial statistics were also trialled during the study, such as the distance between a cell and nearest object, or the average of distances between several objects (data not shown). However, these measures did not reliably reflect observed differences in structure configurations and were hence not pursued further.

4.4.2 The impact of microscale environmental structure on stress response

Once suitable yeast strains and spatial metrics had been tested, soil micromodels were inoculated with fluorescent yeast strains and stressed in order to examine the impact of the structure on stress (exposure and) response. It was hypothesised that cells within more enclosed spaces would be less exposed to stressor flow, in comparison to cells within more open, exposed space. In soil micromodel experiments, differences in single cell fluorescence,

and hence heat or copper exposure, could not be correlated with differences in the spatial metric descriptors that were tested. This outcome may be expected for heat stress, as thermal conduction should be minimally impacted by such small-scale structures composed of the same material. However, these results were less expected in the case of exposure to copper stressor flowing through the micromodel, as it was anticipated that the flow may be obstructed and diverted by the structures within.

Several explanations may account for this apparent lack of influence of physical structure on stressor exposure in the soil micromodels. It is possible that the stressor was able to flow uniformly through the entire model regardless of physical structure. However, this is unlikely given that preliminary modelling of simulated fluid flow in these structures indicated that flow rates are expected to vary throughout the micromodel (see **Appendix E**) and a similar simulation output is reported in other structured microfluidic devices (Coyte et al., 2017). In addition, it was demonstrated in the CellASIC microfluidics system that the flow rate of dissolved copper could influence cellular copper response (**Figure 4.12**). Perhaps the most likely explanation is that the spatial metrics employed here do not describe the structural parameters responsible for any variation in stressor distribution (and cell response), although there is confidence from the systematic exploration of these metrics that they can be used to describe differences between spatial arrangements in a meaningful way.

While Voronoi areas have been used to describe some spatial parameters relevant to microbial activity, such as relating the distances between bacterial colonies to their interactions on agar plates (Chacon et al., 2018, Bar et al., 2020), the spatial dynamics of fluid flow in soil micromodel structures are likely to be more complex than in those examples.

Specifically, a factor unaccounted for in these metrics is that, because fluid flow is unidirectional from one end of the model to the other, the flow of stressor to each cell will be influenced by all structure before the cell (less-so for structures after cells). As the spatial metrics employed here assumes that each cell and structure is standalone and independent of other structures, the influence of structures further upstream or expected weaker influence expected of those downstream are not accounted for.

Additional experiments were conducted in a different, simpler, microfluidics system consisting of arrays of individual 100 x 100 μm traps to which microspheres (4 μm diameter) were introduced to produce different structured environments. Importantly, these traps are arranged to minimise the disruption of flow from one trap to the next, in contrast to the soil micromodel devices, as discussed above. In these microsphere experiments, there was a significant reduction in the copper response (correlating with copper exposure) for cells in the environments with an average of either 16 or 39 microspheres per trap, in comparison to cells in uniform trap environments lacking microspheres. In contrast to the soil micromodel environments, the differences in stress response between cells could be correlated positively with relative size of Voronoi area, suggesting that cells with more microspheres in closer proximity were less exposed to the stressor (and vice-versa). This was evident both in the average cell response of cells in chambers at different microsphere concentrations, or in the single-cell areas and responses across cells from all chambers. One possible reason for these contrasting outcomes between the two microfluidics systems, as indicated above, is that CellASIC plates are designed to minimise the influence of each trap on another, whereas stressor flow in soil micromodels is dependent on upstream structures. Whilst it is possible that a microsphere at the trap opening would alter the fluid flow into the trap, this

distribution would expectedly be less than that caused by an entire trap on another in the CellASIC system, or disruption by the much larger structures present in soil micromodels.

The relationship between cell and microsphere position was further analysed by grouping the position of microspheres in relation to the distance and angle from cells within the trap and comparing the frequency of microspheres at different positions between the least and most copper-responsive cells. This revealed a general apparent trend where beads were more commonly present in front of cells that responded relatively weakly to copper. This supporting the Voronoi analysis conclusions stated above, as cells with more distant structures would also have a larger Voronoi area. However, it was also noted that some cells showing the strongest copper response were more likely to be in very close proximity to a microsphere, with microspheres often positioned directly in front of the cell relative to trap opening.

In an attempt to rationalise why some of these highly responsive cells deviated from Voronoi trends, it was speculated that microspheres very close to a cell may disrupt the laminar fluid flow that is typical of microfluidic devices. This might create a turbulence behind the bead and in front of the cell relative to the trap opening, potentially replenishing more rapidly any localised copper depletion arising from copper uptake by the cell. However, such turbulent mixing is unlikely at the micrometre size and the low flow rate of the CellASIC system (Anandakrishnan and Varadarajulu, 1963). To further resolve this possibility, the Reynolds number was calculated. The Reynolds number is a ratio of the inertial forces relative to viscous forces within a fluid (Mosetti, 1984), and enables estimations of whether flow is laminar or turbulent in systems with fluid flow. Turbulent flow and small circular wakes begin

to occur at Reynolds numbers above ~ 17 (Jenson and Peierls, 1959) in viscous flow. The Reynolds number around microspheres here was estimated at approximately 1.24×10^{-12} (see **Appendix F** for equation), meaning that flow in this system is predominantly laminar and hence turbulent mixing is unlikely to explain the suggested increase in copper exposure experienced by cells immediately behind microspheres.

Whereas it can be difficult to identify relationships between complex structures and stressor exposure, as found here with the soil micromodels, more deterministic relationships were evident in the simplified artificial structure used in microfluidics chambers in this study. Stressor exposure was the primary focus of this thesis, but the results could be interpreted in the context of any soluble agent, such as nutrient or oxygen distribution within structured environments. However, this must be considered with caution, as the uptake of different substrates by the cell can vary in rate and extent alongside potential effects on cell growth (Gaensly et al., 2014, Einsele et al., 1979). In addition, given the complexity of the environmental structures in and around which microorganisms can naturally reside, such as in soils or other porous media, caution must be routinely employed when extrapolating these results to such environments. For example, many environments encompass semi-permeable structures, such as microbial extracellular polymeric substances (EPS) or biofilms that alter but not inhibit fluid movement (Nadell et al., 2017); or support fluid flow in several directions, such as water filtrating from aboveground and belowground in soils, which can alter fluid flow dynamics. These additional complexities could be incorporated into future microfluidic designs, such as by incorporating semi-permeable hydrogels into devices (Deng et al., 2015), or include multiple flow points in the devices to simulate semipermeable structures and more complex flow dynamics (Mahto and Rhee, 2012).

4.4.3 Conclusion

Ubiquitously, the environments of microorganisms have three-dimensional structure and create heterogeneous distributions of the space in which microorganisms reside. In this chapter, two alternative approaches are used to examine the impact of (micro)environmental structure on microbial stress response: using (i) micromodels containing soil-like structures and (ii) simple structures comprising microspheres within commercially available microfluidics devices. Taking the outcomes of both microfluidic setups together, it has been demonstrated that microscale structure can influence microbial stress exposure and hence response in some environments, but disentangling the impact of structure on microbial stress response can prove difficult in others. This was the case even in a controlled laboratory setup, in the absence of variability in other environmental factors such as nutrient and chemical distributions and seasonal/temporal transitions (Or et al., 2007). Future experiments could introduce some of these parameters to structured microfluidic devices, such as by fluctuation of stressor or nutrient exposure, or attempt to assess microbial adaptation in these environments over time — a consequence of living in any natural environment.

5 SUMMARY AND CONCLUDING REMARKS

5.1 Summary of Results

In Chapter 2, a method was developed to manufacture soil aggregates that mimic natural counterparts from the same parent soil material, sharing similar pore volume, pore-surface connectivity, and similar mean pore size to natural aggregates. Furthermore, yeasts (both laboratory strains and wild isolates) could be independently incorporated to, and recovered from, the aggregate interior or exterior fractions of the same aggregate. Using this new method, it was demonstrated that the degree of yeast heteroresistance (cell-cell variation in stress resistance) to lead nitrate did not differentially impact the survival of yeast in the aggregate interior or exterior. Additionally, yeast location did not impact resistance to lead nitrate or anoxia stress, regardless of heteroresistance, but yeast within the aggregate interior were more protected from acute heat stress in comparison to the aggregate exterior. Finally, it was demonstrated that this protective effect against temperature stress was increased when aggregates were mechanically compacted — a common perturbation in natural soil environments.

In chapter 3, the impact on stress resistance of larger, inter-particle pore sizes (analogous to the pore spaces that occur in between aggregates) was examined using an array of glass bead structures and 3D-printed lattices. A range of pore sizes and distributions were produced and characterised with X-ray CT. Yeast heteroresistance did not differentially impact lead resistance across structures with different levels of variation in pore sizes. However, a general trend was observed whereby survival (population-averaged) decreased with increasing pore

size in both bead and lattice structures. This effect could not be attributed to differences in cell concentration either in the pore spaces or adhered to surface areas, either in terms of lead depletion from the medium and overall survival.

In chapter 4, the impact of micrometre-scale structures yeast stress response was assessed. Several spatial metrics were developed to attempt to correlate a single cell's local environmental structure to stressor exposure (measured with a GFP reporter), both in soil micromodels and microfluidics devices with incorporated microspheres. These metrics did not correlate with stress exposure in soil micromodels, but it was demonstrated in microsphere chambers that cells within more open spaces showed a greater response to stressor. This suggested that even at the microscale, environmental physical structures can influence microbial exposure and response to stress.

5.2 Key Themes and Discussion

5.2.1 General relationships between stress resistance and environmental structure

In each experimental chapter presented in this thesis a different scale of (soil) environmental structure was incorporated into experiments assaying microbial survival of (or response to) stress. Throughout, it became evident that environmental structure could somewhat protect microorganisms from stressor exposure, either by cells being encompassed within a structure (in the case of soil aggregate experiments), or by being within relatively small pores, at both the millimetre and micrometre scale. The basis for this protection may be different for each structure experiment, and they could not be resolved clearly in structures with millimetre-scale pore sizes, but were likely to involve disruption of stressor flow in structures with

micrometre-scale pore sizes. The experiments emphasised the difficulty of fully disentangling the interactions between microbial processes and surrounding environment.

Whereas experiments within this thesis were conducted with soil physical structure in mind, micrometre and millimetre scale porous structures are common to many habitats in which microorganisms reside, such as on forest litter and deadwood (Schnee et al., 2016, Lladó et al., 2017), benthic systems (Richards et al., 1990), building materials (Verdier et al., 2014), medical devices (Francolini and Donelli, 2010), and hygienic surfaces (Verran et al., 2010). However, caution must be emphasised when extrapolating the results of this work to wider environments of microorganisms. This is because, by reducing the complexity of environmental structure to certain inert physical elements, other important components (e.g., affecting stressor distribution) such as particle/surface charge and long-term water influx/efflux have not been incorporated into experiments. In addition, the only biological component factored here was the yeast cells that were introduced. Now that the present experimental methods have been developed and validated, further elements of environmental structure could be introduced, as discussed in section below in 5.3 Future Work.

5.2.2 Microbial heteroresistance

In Chapters 2 and 3, stressor heteroresistance did not appear to influence yeast survival relative to variability of environmental structure, whether in relation to position within an aggregate, or in relation to pore-size distribution in glass bead structures. However, this does not necessarily suggest that heteroresistance does not confer an advantage for stress resistance at different spatial scales or environmental conditions not encompassed within this

thesis, as it has been previously found to be a selected trait in yeasts of natural polluted habitats (Holland et al., 2014) and potentially in non-uniform conditions such as temporal fluctuation between stressed and unstressed conditions (Luck et al., 2018). These additional types of heterogeneity may provide a focus for future work, as discussed below.

5.3 Future Work

Now that the methods described in this thesis have been developed, and a general influence of environmental structure on microbial stress response established, further research could explore extrapolation of the present data to more complex soil or other systems in several ways. Examples of this include the introduction of further environmental components such as charged particles and surfaces (commonly seen in soil minerals and clays); flowing stressor solutions through glass bead structures (experiments described here used static stress conditions); or by incorporating multiple microbial species, such as mixed biofilm-forming cultures, into structured environments for subsequent stress response experiments. There are also of course other environmentally relevant phenotypes to consider besides stress-survival that was the focus here, such as nutrient availability and assimilation or protection from predation.

Furthermore, it should be considered that most environments, and especially soils, are in a constant state of flux, as opposed to the snapshot considered in these experiments. Fluctuating stressor exposure over longer experimental durations may draw out potential benefits of heteroresistance, as suggested in other studies (Luck et al., 2018). Additionally, fluctuating stress and non-stress conditions may result in stressor accumulation in some parts of a structure more so than others, such as the accumulation of lead nitrate in smaller pores

of soil aggregates that are harder to flush out once saturated. This would more closely mimic real environments as they change over time. These structures could also be incorporated into evolution-based experiments, such as by examining the impact of long-term exposure to nutrient or stressor fluxes on microorganisms inside and outside of a soil aggregate, or within different bead structures.

APPENDIX A

ImageJ macro used to automate colony area measurements from agar plates.

```
dir = getDirectory("Choose a Directory ");
list = getFileList(dir);
dir2 = dir+"Results"+File.separator;
File.makeDirectory(dir2);

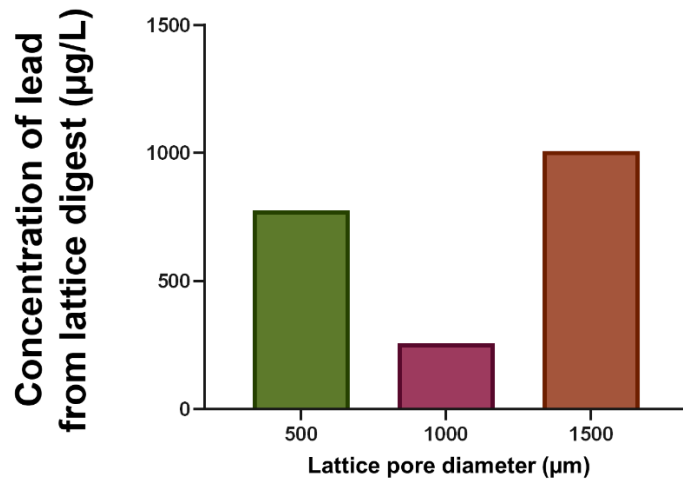
for (i=0; i<list.length; i++) {
    path = dir+list[i];
    print(i+" "+path);
    showProgress(i, list.length);
    if (endsWith(list[i], "/") == 0) {
        open(path);

run("Clear Results");
roiManager("Reset");
title=getTitle();

delimiters = ".";
stringResult = split(title, delimiters);
title2=stringResult[0];
run("Set Scale...", "distance=660.9098 known=90 pixel=1 unit=mm
global");
    selectWindow(title);
    s=nSlices();
    run("Specify...", "width=520.32 height=520.32 x=250 y=250
oval");
    setTool("Oval");
    //waitForUser("Select measurement region, then press
OK."); //Use this to check each plates selection region
separately, but can be removed by adding \\ to beginning of line
    run("Duplicate...", "title="+title2+"_mask duplicate
range=1");
    run("8-bit");
    run("Despeckle");
    run("Subtract Background...", "rolling=200");
    run("Auto Threshold", "method=IsoData ignore_black
ignore_white white");
    run("Restore Selection");
    run("Set Measurements...", "area standard median");
    run("Invert");
    run("Watershed");
    run("Analyze Particles...", "size=0.3-3 circularity=0.7-
1.00 show=Outlines display exclude add");
```

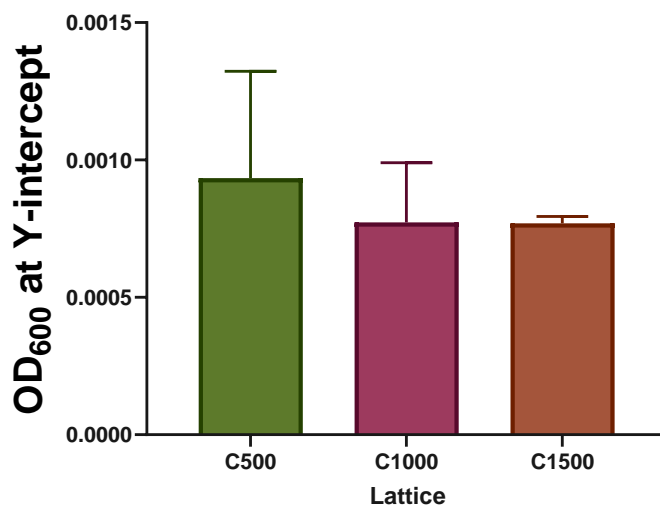
```
selectWindow("Results");  
saveAs("Text", dir2+title+"Results.xls"); } }  
run("Close");  
showStatus ("Done");
```

APPENDIX B



Lead digested from lattices exposed to lead nitrate in the absence of cells demonstrates lead is adsorbed to the lattice material.

APPENDIX C

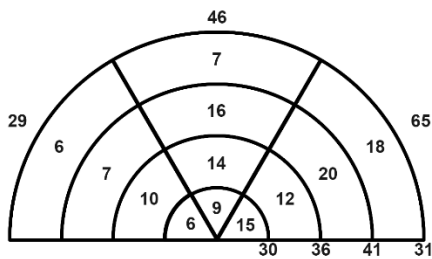


Outgrowth of cells from lattices in no-stress conditions is similar across structures with 500, 100, or 1500 µm pore sizes

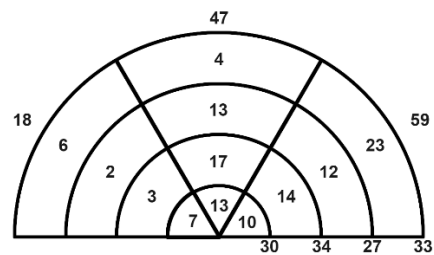
APPENDIX D

Replicate One

Least fluorescent cells

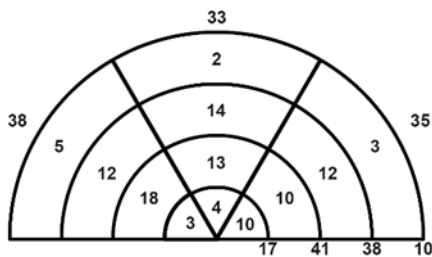


Most fluorescent cells

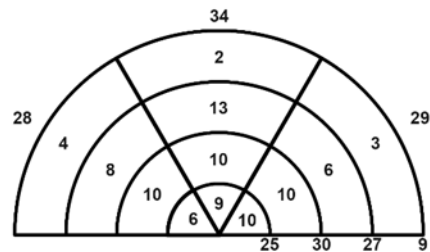


Replicate Two

Least fluorescent cells

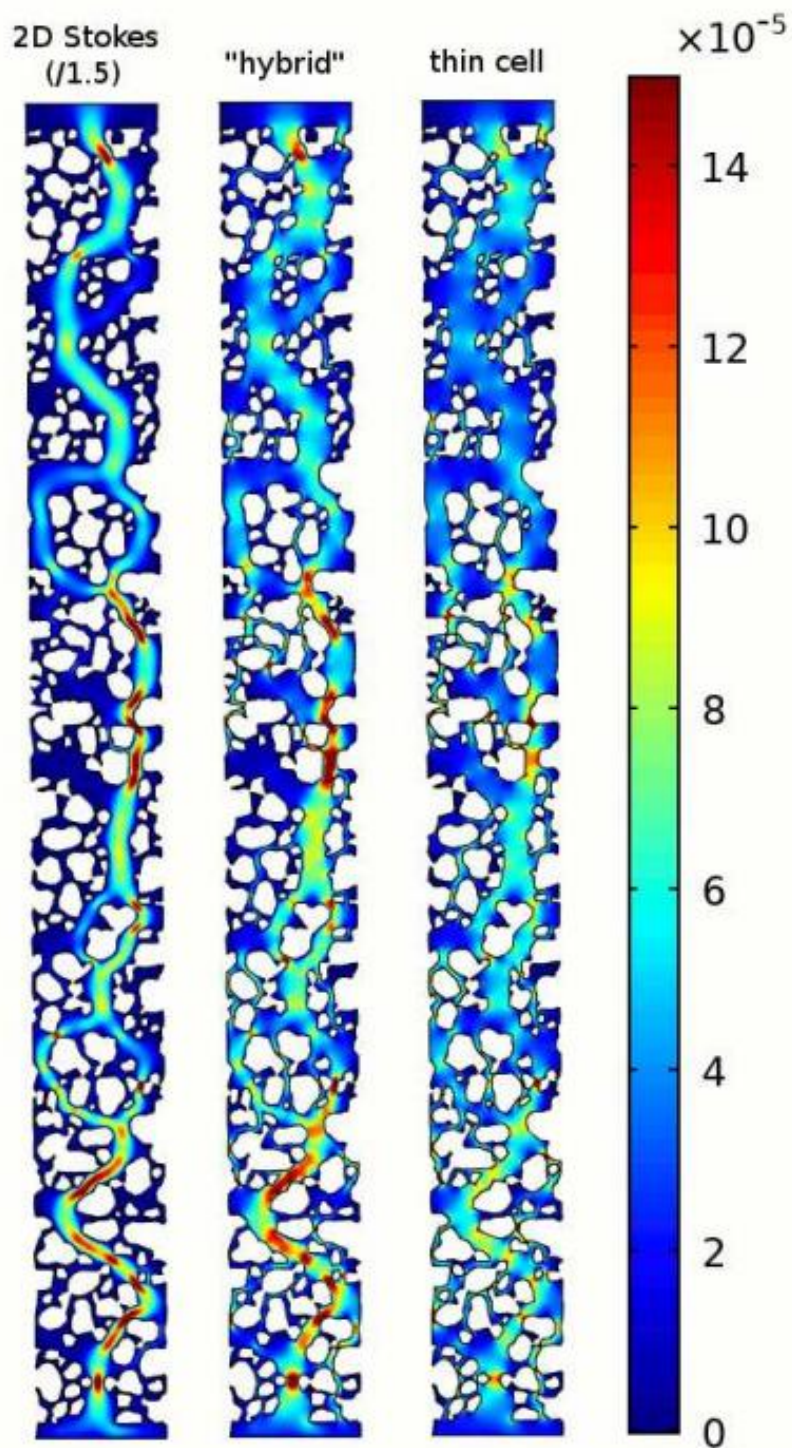


Most fluorescent cells

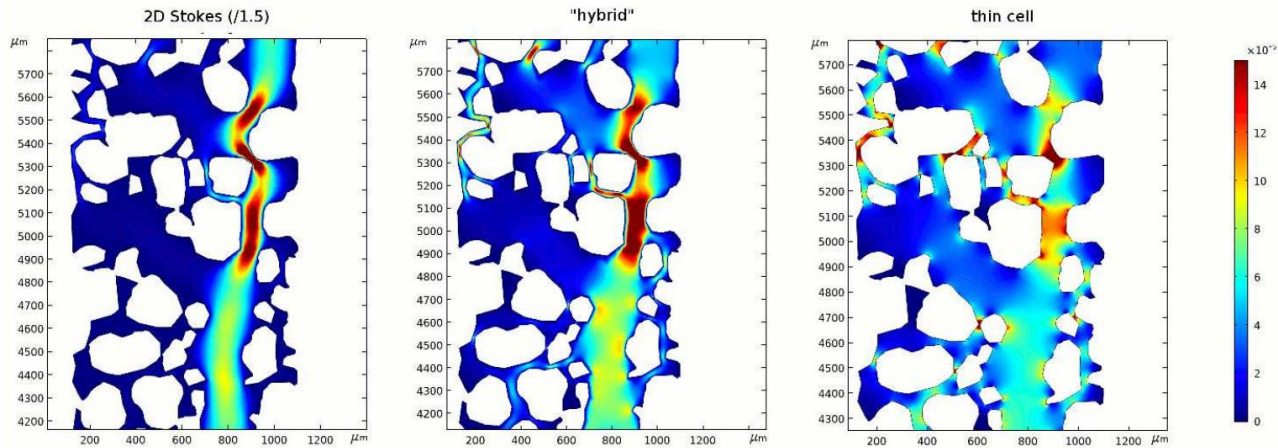


Raw frequencies of microspheres used to calculate the difference between cells with the the least and most fluorescent increase in repsonse to copper. Values were rounded before subtraction for simplicity.

APPENDIX E



Preliminary fluid flow simulation through soil micromodels, with each section representing a different modelling approach to account for large pores (left) and small pores (right), with the middle simulation a hybrid equation of the left and right model. The colour scale represents flow rate in metres per second. The micromodel channel measures 1×10 mm.



Here, a small section of each model has been isolated to show the details and differences of each modelling approach. The left axis shows the scale in micrometres and the colour scale represents flow rate in metres per second.

To determine whether stressor flow rate (and hence cell exposure) at cell locations within soil micromodel correlated with Cup1-GFP expression in SVY14 cells, computational fluid dynamics (CFD) modelling was conducted by Dr Mykyta Chubynsky, University of Warwick, using COSMOL Multiphysics V5.6. A hybrid equation was produced to account for flow rates in both wide and narrow pores (where pore width was wider or narrower than the ceiling height of 32 μm) in the form:

$$\nabla_{\perp} p = \mu \left(\nabla_{\perp}^2 \bar{v} - \frac{12}{h^2} \bar{v} \right)$$

Where p is momentum, μ is, \bar{v} is mean flow speed, and h is the height of the model.

Then, the average vertical flow velocity was calculated at the distance from each cell at which the transport mechanism of copper ions moves from advection to diffusion (averaging approximately 7 μm across all cells). This was calculated by dividing the estimated diffusivity of Cu (II) ions ($7 \times 10^{-6} \text{ cm}^2 \text{ s}^{-1}$) by the vertically averaged flow speed across the model (10^{-4} m s^{-1}). The average flow velocity for each cell around this distance was then calculated for correlation with microscopy data.

APPENDIX F

Calculating Reynolds number for flow around 4 μm microspheres in CellASIC using the equation

$$Re = \frac{\rho u L}{\mu}$$

Where ρ is fluid density, u is flow speed, L is particle diameter, and μ is fluid viscosity.

Fluid density was measured as 1011.2 Kg/m^3

Flow speed was approximately $5.5 \times 10^{-13} \text{ m}^3/\text{s}$

Particle diameter is $4 \times 10^{-6} \text{ m}$

Fluid viscosity was measured as $1.179 \times 10^{-3} \text{ Pa.s}$

Therefore,

$$Re = \frac{1011.2 \times 5.5 \times 10^{-13} \times 4 \times 10^{-6}}{1.79 \times 10^{-3}} = 1.24 \times 10^{-12}$$

REFERENCES

- ABDUL SALAM, J., LAKSHMI, V., DAS, D. & DAS, N. 2013. Biodegradation of lindane using a novel yeast strain, *Rhodotorula sp.* VITJzN03 isolated from agricultural soil. *World Journal of Microbiology and Biotechnology*, 29, 475-487.
- ACKERMANN, M. 2015. A functional perspective on phenotypic heterogeneity in microorganisms. *Nature Reviews Microbiology*, 13, 497-508.
- AHMED, I. M., HELAL, A. A., EL AZIZ, N. A., GAMAL, R., SHAKER, N. O. & HELAL, A. A. 2019. Influence of some organic ligands on the adsorption of lead by agricultural soil. *Arabian Journal of Chemistry*, 12, 2540-2547.
- ALEKLETT, K., OHLSSON, P., BENGTSSON, M. & HAMMER, E. C. 2021. Fungal foraging behaviour and hyphal space exploration in micro-structured Soil Chips. *The ISME Journal*, 15, 1782-1793.
- ALMÅS, Å. R., MULDER, J. & BAKKEN, L. R. 2005. Trace metal exposure of soil bacteria depends on their position in the soil matrix. *Environmental Science & Technology*, 39, 5927-5932.
- ALTAMIRANO, S., SIMMONS, C. & KOZUBOWSKI, L. 2018. Colony and single cell level analysis of the heterogeneous response of *Cryptococcus neoformans* to fluconazole. *Frontiers in Cellular and Infection Microbiology*, 8, 203.
- ANANDAKRISHNAN, M. & VARADARAJULU, G. H. 1963. Laminar and turbulent flow of water through sand. *Journal of the Soil Mechanics and Foundations Division*, 89, 1-16.
- ANANYEVA, K., WANG, W., SMUCKER, A. J. M., RIVERS, M. L. & KRAVCHENKO, A. N. 2013. Can intra-aggregate pore structures affect the aggregate's effectiveness in protecting carbon? *Soil Biology and Biochemistry*, 57, 868-875.
- ANOVITZ, L. M. & COLE, D. R. 2015. Characterization and analysis of porosity and pore structures. *Reviews in Mineralogy and Geochemistry*, 80, 61-164.
- BAHRAM, M., HILDEBRAND, F., FORSLUND, S. K., ANDERSON, J. L., SOUDZILOVSKAIA, N. A., BODEGOM, P. M., BENGTSSON-PALME, J., ANSLAN, S., COELHO, L. P., HAREND, H., HUERTA-CEPAS, J., MEDEMA, M. H., MALTZ, M. R., MUNDRA, S., OLSSON, P. A., PENT, M., POLME, S., SUNAGAWA, S., RYBERG, M., TEDERSOO, L. & BORK, P. 2018. Structure and function of the global topsoil microbiome. *Nature*, 560, 233-237.
- BANKOLE, P. O., ADEKUNLE, A. A., OBIDI, O. F., OLUKANNI, O. D. & GOVINDWAR, S. P. 2017. Degradation of indigo dye by a newly isolated yeast, *Diutina rugosa* from dye wastewater polluted soil. *Journal of Environmental Chemical Engineering*, 5, 4639-4648.
- BAR, J., BOUMASMOUD, M., KOUYOS, R. D., ZINKERNAGEL, A. S. & VULIN, C. 2020. Efficient microbial colony growth dynamics quantification with ColTapp, an automated image analysis application. *Scientific Reports*, 10, 16084.
- BAVEYE, P. C., OTTEN, W., KRAVCHENKO, A., BALSEIRO-ROMERO, M., BECKERS, E., CHALHOUB, M., DARNAULT, C., EICKHORST, T., GARNIER, P., HAPCA, S., KIRANYAZ, S., MONGA, O., MUELLER, C. W., NUNAN, N., POT, V., SCHLUTER, S., SCHMIDT, H. & VOGEL, H. J. 2018. Emergent properties of microbial activity

- in heterogeneous soil microenvironments: different research approaches are slowly converging, yet major challenges remain. *Frontiers in Microbiology*, 9, 1929.
- BERDY, B., SPOERING, A. L., LING, L. L. & EPSTEIN, S. S. 2017. In situ cultivation of previously uncultivable microorganisms using the ichip. *Nature Protocols*, 12, 2232-2242.
- BEVEN, K. & GERMANN, P. 1982. Macropores and water flow in soils. *Water Resources Research*, 18, 1311-1325.
- BEZIAT, A. 1988. Effect of compaction pressure and water content on the thermal conductivity of some natural clays. *Clays and Clay Minerals*, 36, 462-466.
- BHATTACHARJEE, T. & DATTA, S. S. 2019. Bacterial hopping and trapping in porous media. *Nature Communications*, 10, 2075.
- BIESGEN, D., FRINDTE, K., MAARASTAWI, S. & KNIEF, C. 2020. Clay content modulates differences in bacterial community structure in soil aggregates of different size. *Geoderma*, 376, 114544.
- BISHOP, A. L., RAB, F. A., SUMNER, E. R. & AVERY, S. V. 2007. Phenotypic heterogeneity can enhance rare-cell survival in 'stress-sensitive' yeast populations. *Molecular Microbiology*, 63, 507-520.
- BLAUD, A., CHEVALLIER, T., VIRTO, I., PABLO, A.-L., CHENU, C. & BRAUMAN, A. 2014. Bacterial community structure in soil microaggregates and on particulate organic matter fractions located outside or inside soil macroaggregates. *Pedobiologia*, 57, 191-194.
- BOA, E. 2004. Wild edible fungi: a global overview of their use and importance to people. *Non-Wood Forest Products* 17, Fao Press, Rome, Italy.
- BOKMAN, S. H. & WARD, W. W. 1981. Renaturation of Aequorea green-fluorescent protein. *Biochemical and Biophysical Research Communications*, 101, 1372-1380.
- BORER, B., TECON, R. & OR, D. 2018. Spatial organization of bacterial populations in response to oxygen and carbon counter-gradients in pore networks. *Nature Communications*, 9, 769.
- Botha, A. 2006. Yeasts in soils. In: C.A. Rosa, and G. Péter, editors, *The yeast handbook: Biodiversity and ecophysiology of yeasts*. Springer, Berlin. p. 221–240.
- BRADLEY, R. S., ROBINSON, I. K. & YUSUF, M. 2017. 3D X-ray nanotomography of cells grown on electrospun scaffolds. *Macromolecular Bioscience*, 17, 1600236.
- BREWER, R. 1964. *Fabric and Mineral Analysis of Soil*, John Wiley & Sons, New York.
- CAO, J., YANG, G., MAI, Q., ZHUANG, Z. & ZHUANG, L. 2020. Co-selection of antibiotic-resistant bacteria in a paddy soil exposed to As(III) contamination with an emphasis on potential pathogens. *Science of The Total Environment*, 725, 138367.
- CARSON, J. K., GONZALEZ-QUINONES, V., MURPHY, D. V., HINZ, C., SHAW, J. A. & GLEESON, D. B. 2010. Low pore connectivity increases bacterial diversity in soil. *Applied Environmental Microbiology*, 76, 3936-42.
- CHACON, J. M., MOBIUS, W. & HARCOTBE, W. R. 2018. The spatial and metabolic basis of colony size variation. *The ISME Journal*, 12, 669-680.

- CHAIT, R., RUESS, J., BERGMILLER, T., TKACIK, G. & GUET, C. C. 2017. Shaping bacterial population behavior through computer-interfaced control of individual cells. *Nature Communications*, 8, 1535.
- CHAN, K. Y. 2011. Climate Change on Soil Structure and Soil Health: Impacts and Adaptation. In: Singh B., Cowie A., Chan K. (eds) *Soil Health and Climate Change*. Soil Biology, vol 29. Springer, Berlin, Heidelberg.
- CHANDRAN, P. & DAS, N. 2012. Role of plasmid in diesel oil degradation by yeast species isolated from petroleum hydrocarbon-contaminated soil. *Environmental Technology*, 33, 645-652.
- CHAU, J. F., BAGTZOGLU, A. C. & WILLIG, M. R. 2011. The effect of soil texture on richness and diversity of bacterial communities. *Environmental Forensics*, 12, 333-341.
- CIAIS, P., SABINE, C., BALA, G., BOPP, L., BROVKIN, V., CANADELL, J., CHHABRA, A., DEFRIES, R., GALLOWAY, J., HEIMANN, M., JONES, C., LE QUÉRE, C., MYNENI, R. B., PIAO, S. & THORNTON, P. 2013. Carbon and Other Biogeochemical Cycles. In: STOCKER, T. F., QIN, D., PLATTNER, G.-K., TIGNOR, M., ALLEN, S. K., BOSCHUNG, J., NAUELS, A., XIA, Y., BEX, V. & MIDGLEY, P. M. (eds.) *Climate Change 2013: The Physical Science Basis. Contribution of Working Group I to the Fifth Assessment Report of the Intergovernmental Panel on Climate Change*. Cambridge, United Kingdom and New York, NY, USA: Cambridge University Press.
- COYTE, K. Z., TABUTEAU, H., GAFFNEY, E. A., FOSTER, K. R. & DURHAM, W. M. 2017. Microbial competition in porous environments can select against rapid biofilm growth. *Proceedings of the National Academy of Sciences of the United States of America*, 114, E161-E170.
- CRAWFORD, J. W., DEACON, L., GRINEV, D., HARRIS, J. A., RITZ, K., SINGH, B. K. & YOUNG, I. 2012. Microbial diversity affects self-organization of the soil-microbe system with consequences for function. *Journal of the Royal Society Interface*, 9, 1302-10.
- DAL CO, A., ACKERMANN, M. & VAN VLIET, S. 2019. Metabolic activity affects the response of single cells to a nutrient switch in structured populations. *Journal of the Royal Society Interface*, 16, 20190182.
- DE GRYZE, S., SIX, J. & MERCKX, R. 2006. Quantifying water-stable soil aggregate turnover and its implication for soil organic matter dynamics in a model study. *European Journal of Soil Science*, 57, 693-707.
- DE MOURA, M. S., SILVA, B. M., MOTA, P. K., BORGHI, E., RESENDE, A. V. D., ACUÑA-GUZMAN, S. F., ARAÚJO, G. S. S., DA SILVA, L. D. C. M., DE OLIVEIRA, G. C. & CURTI, N. 2021. Soil management and diverse crop rotation can mitigate early-stage no-till compaction and improve least limiting water range in a Ferralsol. *Agricultural Water Management*, 243.
- DE OLIVEIRA, R. A., RAMOS, M. M. & DE AQUINO, L. A. 2015. In: Santos F, Borem A, Caldas C (eds) *Sugarcane*. Elsevier, Amsterdam, pp 161–183
- DELEON-RODRIGUEZ, N., LATHAM, T. L., RODRIGUEZ, R. L., BARAZESH, J. M., ANDERSON, B. E., BEYERSDORF, A. J., ZIEMBA, L. D., BERGIN, M., NENES, A. & KONSTANTINIDIS, K. T. 2013. Microbiome of the upper troposphere: species composition and prevalence, effects of tropical storms, and atmospheric

- implications. *Proceedings of the National Academy of Sciences of the United States of America*, 110, 2575-80.
- DENG, J., ORNER, E. P., CHAU, J. F., ANDERSON, E. M., KADILAK, A. L., RUBINSTEIN, R. L., BOUCHILLON, G. M., GOODWIN, R. A., GAGE, D. J. & SHOR, L. M. 2015. Synergistic effects of soil microstructure and bacterial EPS on drying rate in emulated soil micromodels. *Soil Biology and Biochemistry*, 83, 116-124.
- DONLAN, R. M. 2002. Biofilms: microbial life on surfaces. *Emerging Infectious Diseases*, 8, 881-90.
- DORAU, K., LUSTER, J. & MANSFELDT, T. 2018. Soil aeration: the relation between air-filled pore volume and redox potential. *European Journal of Soil Science*, 69, 1035-1043.
- DOWNIE, H. F., VALENTINE, T. A., OTTEN, W., SPIERS, A. J. & DUPUY, L. X. 2014. Transparent soil microcosms allow 3D spatial quantification of soil microbiological processes in vivo. *Plant Signaling and Behaviour*, 9, e970421.
- DUCHICELA, J., SULLIVAN, T. S., BONTTI, E., BEVER, J. D. & WAN, S. 2013. Soil aggregate stability increase is strongly related to fungal community succession along an abandoned agricultural field chronosequence in the Bolivian Altiplano. *Journal of Applied Ecology*, 50, 1266-1273.
- DULLIEN, F. 1992. *Porous Media: Fluid Transport and Pore Structure*, Academic Press.
- EBRAHIMI, A. & OR, D. 2016. Microbial community dynamics in soil aggregates shape biogeochemical gas fluxes from soil profiles - upscaling an aggregate biophysical model. *Global Change Biology*, 22, 3141-56.
- EINSELE, A., RISTROPH, D. L. & HUMPHREY, A. E. 1979. Substrate uptake mechanisms for yeast cells. *European journal of applied microbiology and biotechnology*, 6, 335-339.
- EKELUND, F., RØNN, R. & CHRISTENSEN, S. 2001. Distribution with depth of protozoa, bacteria and fungi in soil profiles from three Danish forest sites. *Soil Biology and Biochemistry*, 33, 475-481.
- EKWUE, E. I., STONE, R. J. & BHAGWAT, D. 2006. Thermal conductivity of some compacted trinidadian soils as affected by peat content. *Biosystems Engineering*, 94, 461-469.
- FALCONER, R. E., BATTIAIA, G., SCHMIDT, S., BAVEYE, P., CHENU, C. & OTTEN, W. 2015. Microscale heterogeneity explains experimental variability and non-linearity in soil organic matter mineralisation. *PLoS One*, 10, e0123774.
- FARR, R. S. & GROOT, R. D. 2009. Close packing density of polydisperse hard spheres. *Journal of Chemical Physics*, 131, 244104.
- FAY, J. C. & BENAVIDES, J. A. 2005. Evidence for domesticated and wild populations of *Saccharomyces cerevisiae*. *PLoS Genetics*, 1, 66-71.
- FEDOTOV, G. N., SHOBA, S. A., FEDOTOVA, M. F., STEPANOV, A. L. & STRELETSKY, R. A. 2017. Soil yeasts and their role in seed germination. *Eurasian Soil Science*, 50, 573-579.
- FICHTNER, A., VON OHEIMB, G., HÄRDTLE, W., WILKEN, C. & GUTKNECHT, J. L. M. 2014. Effects of anthropogenic disturbances on soil microbial communities in oak forests persist for more than 100 years. *Soil Biology and Biochemistry*, 70, 79-87.

- FIERER, N., BREITBART, M., NULTON, J., SALAMON, P., LOZUPONE, C., JONES, R., ROBESON, M., EDWARDS, R. A., FELTS, B., RAYHAWK, S., KNIGHT, R., ROHWER, F. & JACKSON, R. B. 2007. Metagenomic and small-subunit rRNA analyses reveal the genetic diversity of bacteria, archaea, fungi, and viruses in soil. *Applied Environmental Microbiology*, 73, 7059-66.
- FISCHER, K. & BIPP, H. P. 2002. Removal of heavy metals from soil components and soils by natural chelating agents. *Water, Air, and Soil Pollution*, 138, 271-288.
- FOWLER, D., COYLE, M., SKIBA, U., SUTTON, M. A., CAPE, J. N., REIS, S., SHEPPARD, L. J., JENKINS, A., GRIZZETTI, B., GALLOWAY, J. N., VITOUSEK, P., LEACH, A., BOUWMAN, A. F., BUTTERBACH-BAHL, K., DENTENER, F., STEVENSON, D., AMANN, M. & VOSS, M. 2013. The global nitrogen cycle in the twenty-first century. *Philosophical Transactions of The Royal Society B Biological Sciences*, 368, 20130164.
- FRANCOLINI, I. & DONELLI, G. 2010. Prevention and control of biofilm-based medical-device-related infections. *FEMS Immunology and Medical Microbiology*, 59, 227-238.
- FREY, S. D., DRIJBER, R., SMITH, H. & MELILLO, J. 2008. Microbial biomass, functional capacity, and community structure after 12 years of soil warming. *Soil Biology and Biochemistry*, 40, 2904-2907.
- GADD, G.M. (2005). Microorganisms in toxic metal polluted soils. In: *Microorganisms in Soils: Roles in Genesis and Functions*. Eds: F. Buscot and A. Varma, pp. 325-356. Springer-Verlag, Berlin.
- GADHAVE, K. R., DEVLIN, P. F., EBERTZ, A., ROSS, A. & GANGE, A. C. 2018. Soil Inoculation with *Bacillus spp.* modifies root endophytic bacterial diversity, evenness, and community composition in a context-specific manner. *Microbial Ecology*, 76, 741-750.
- GAENSLY, F., PICHETH, G., BRAND, D. & BONFIM, T. M. B. 2014. The uptake of different iron salts by the yeast *Saccharomyces cerevisiae*. *Brazilian Journal of Microbiology*, 45, 491-494.
- GARBUZ, S. A., YAROSLAVTSEVA, N. V. & KHOLODOV, V. A. 2016. Enzymatic activity inside and outside of water-stable aggregates in soils under different land use. *Eurasian Soil Science*, 49, 367-375.
- GRAHAM, J. K., SMITH, M. L. & SIMONS, A. M. 2014. Experimental evolution of bet hedging under manipulated environmental uncertainty in *Neurospora crassa*. *Proceedings of the Royal Society B: Biological Sciences*, 281, 20140706.
- GRINELL, J. 1917. The niche relationships of the California Thrasher. *The Auk*, 34, 427-433.
- GUEVEN, I., FRIJTERS, S., HARTING, J., LUDING, S. & STEEB, H. 2017. Hydraulic properties of porous sintered glass bead systems. *Granular Matter*, 19, 28.
- HARVEY, H. J., WILDMAN, R. D., MOONEY, S. J. & AVERY, S. V. 2020a. Challenges and approaches in assessing the interplay between microorganisms and their physical micro-environments. *Computational and Structural Biotechnology Journal*, 18, 2860-2866.
- HARVEY, H. J., WILDMAN, R. D., MOONEY, S. J. & AVERY, S. V. 2020b. Soil aggregates by design: Manufactured aggregates with defined microbial composition for

- interrogating microbial activities in soil microhabitats. *Soil Biology and Biochemistry*, 148, 107870.
- HE, B., BURKE, B. J., ZHANG, X., ZHANG, R. & REGNIER, F. E. 2001. A picoliter-volume mixer for microfluidic analytical systems. *Analytical Chemistry*, 73, 1942-1947.
- HELIOS RYBICKA, E., CALMANO, W. & BREEGER, A. 1995. Heavy metals sorption/desorption on competing clay minerals; an experimental study. *Applied Clay Science*, 9, 369-381.
- HELLING, C. S., CHESTERS, G. & COREY, R. B. 1964. Contribution of organic matter and clay to soil cation-exchange capacity as affected by the pH of the saturating solution. *Soil Science Society of America Journal*, 28, 517-520.
- HELLIWELL, J. R., MILLER, A. J., WHALLEY, W. R., MOONEY, S. J. & STURROCK, C. J. 2014. Quantifying the impact of microbes on soil structural development and behaviour in wet soils. *Soil Biology and Biochemistry*, 74, 138-147.
- HEWITT, S. K., FOSTER, D. S., DYER, P. S. & AVERY, S. V. 2016. Phenotypic heterogeneity in fungi: Importance and methodology. *Fungal Biology Reviews*, 30, 176-184.
- HILLEL, D. 2003. *Introduction to Environmental Soil Physics*, USA, Academic Press.
- HINGLEY-WILSON, S. M., MA, N., HU, Y., CASEY, R., BRAMMING, A., CURRY, R. J., TANG, H. L., WU, H., BUTLER, R. E., JACOBS, W. R., JR., ROCCO, A. & MCFADDEN, J. 2020. Loss of phenotypic inheritance associated with ydcl mutation leads to increased frequency of small, slow persisters in *Escherichia coli*. *Proceedings of the National Academy of Sciences of the United States of America*, 117, 4152-4157.
- HIRSCH, P. R., GILLIAM, L. M., SOHI, S. P., WILLIAMS, J. K., CLARK, I. M. & MURRAY, P. J. 2009. Starving the soil of plant inputs for 50 years reduces abundance but not diversity of soil bacterial communities. *Soil Biology and Biochemistry*, 41, 2021-2024.
- HIRSCH, P. R., JHURREEA, D., WILLIAMS, J. K., MURRAY, P. J., SCOTT, T., MISSELBROOK, T. H., GOULDING, K. W. T. & CLARK, I. M. 2016. Soil resilience and recovery: rapid community responses to management changes. *Plant and Soil*, 412, 283-297.
- HO, W. H., TSHIMANGA, I. J., NGOEPE, M. N., JERMY, M. C. & GEOGHEGAN, P. H. 2020. Evaluation of a desktop 3D printed rigid refractive-indexed-matched flow phantom for piv measurements on cerebral aneurysms. *Cardiovascular Engineering Technology*, 11, 14-23.
- HOL, F. J., ROTEM, O., JURKEVITCH, E., DEKKER, C. & KOSTER, D. A. 2016. Bacterial predator-prey dynamics in microscale patchy landscapes. *Proceedings of the Royal Society B: Biological Sciences*, 283, 20152154.
- HOLLAND, S. L., READER, T., DYER, P. S. & AVERY, S. V. 2014. Phenotypic heterogeneity is a selected trait in natural yeast populations subject to environmental stress. *Environmental Microbiology*, 16, 1729-1740.
- HOONDEE, P., WATTANAGONNIYOM, T., WEERAPHAN, T., TANASUPAWAT, S. & SAVARAJARA, A. 2019. Occurrence of oleaginous yeast from mangrove forest in Thailand. *World Journal of Microbiol Biotechnol*, 35, 108.
- HOVER, B. M., KIM, S. H., KATZ, M., CHARLOP-POWERS, Z., OWEN, J. G., TERNEI, M. A., MANIKO, J., ESTRELA, A. B., MOLINA, H., PARK, S., PERLIN, D. S. & BRADY,

- S. F. 2018. Culture-independent discovery of the malacidins as calcium-dependent antibiotics with activity against multidrug-resistant Gram-positive pathogens. *Nature Microbiology*, 3, 415-422.
- IDOWU, O. J. 2011. Relationships between aggregate stability and selected soil properties in humid tropical environment. *Communications in Soil Science and Plant Analysis*, 34, 695-708.
- ILG, K., WILCKE, W., SAFRONOV, G., LANG, F., FOKIN, A. & KAUPENJOHANN, M. 2004. Heavy metal distribution in soil aggregates: a comparison of recent and archived aggregates from Russia. *Geoderma*, 123, 153-162.
- IPCC 2013. *Climate Change 2013: The Physical Science Basis. Contribution of Working Group I to the Fifth Assessment Report of the Intergovernmental Panel on Climate Change*, Cambridge, United Kingdom and New York, NY, USA, Cambridge University Press.
- JACKSON, R. S. 2014. Wine Science. Amsterdam: Academic Press, an imprint of Elsevier. 240-266.
- JACOBY, R., PEUKERT, M., SUCCURRO, A., KOPRIVOVA, A. & KOPRIVA, S. 2017. The role of soil microorganisms in plant mineral nutrition-current knowledge and future directions. *Frontiers in Plant Science*, 8, 1617.
- JANSSENS, G. E. & VEENHOFF, L. M. 2016. The natural variation in lifespans of single yeast cells is related to variation in cell size, ribosomal protein, and division time. *PLoS One*, 11, e0167394.
- JANSSON, J. K. & HOFMOCKEL, K. S. 2020. Soil microbiomes and climate change. *Nature Reviews Microbiology*, 18, 35-46.
- JAROSLAWIECKA, A. & PIOTROWSKA-SEGET, Z. 2014. Lead resistance in microorganisms. *Microbiology*, 160, 12-25.
- JENSON, V. G. & PEIERLS, R. E. 1959. Viscous flow round a sphere at low Reynolds numbers (<40). *Proceedings of the Royal Society of London. Series A. Mathematical and Physical Sciences*, 249, 346-366.
- JONES, C. A. 1983. Effect of soil texture on critical bulk densities for root growth. *Soil Science Society of America Journal*, 47, 1208.
- JORGENSEN, P., NISHIKAWA, J. L., BREITKREUTZ, B. J. & TYERS, M. 2002. Systematic identification of pathways that couple cell growth and division in yeast. *Science*, 297, 395-400.
- JUYAL, A., OTTEN, W., BAVEYE, P. C. & EICKHORST, T. 2020. Influence of soil structure on the spread of *Pseudomonas fluorescens* in soil at microscale. *European Journal of Soil Science*. 72, 141-153
- KEILUWEIT, M., GEE, K., DENNEY, A. & FENDORF, S. 2018. Anoxic microsites in upland soils dominantly controlled by clay content. *Soil Biology and Biochemistry*, 118, 42-50.
- KEILUWEIT, M., WANZEK, T., KLEBER, M., NICO, P. & FENDORF, S. 2017. Anaerobic microsites have an unaccounted role in soil carbon stabilization. *Nature Communications*, 8, 1771.
- KOLLER, A., VALESCO, J. & SUBRAMANI, S. 2000. The CUP1 promoter of *Saccharomyces cerevisiae* is inducible by copper in *Pichia pastoris*. *Yeast*, 16, 651-656.

- KOO, B. J., ADRIANO, D. C., BOLAN, N. S. & BARTON, C. D. 2005. ROOT EXUDATES AND MICROORGANISMS. In: HILLEL, D. (ed.) *Encyclopedia of Soils in the Environment*. Oxford: Elsevier.
- KUSHWAHA, A., HANS, N., KUMAR, S. & RANI, R. 2018. A critical review on speciation, mobilization and toxicity of lead in soil-microbe-plant system and bioremediation strategies. *Ecotoxicology and Environmental Safety*, 147, 1035-1045.
- LAL, R. 2004. Soil carbon sequestration impacts on global climate change and food security. *Science*, 304, 1623-1627.
- LAMAN TRIP, D. S. & YOUK, H. 2020. Yeasts collectively extend the limits of habitable temperatures by secreting glutathione. *Nature Microbiology*, 5, 943-954.
- LAMANDÉ, M., SCHJØNNING, P., DAL FERRO, N. & MORARI, F. 2020. Soil pore system evaluated from gas measurements and CT images: A conceptual study using artificial, natural and 3D-printed soil cores. *European Journal of Soil Science*, 72, 769-781.
- LEVY, S. F., ZIV, N. & SIEGAL, M. L. 2012. Bet hedging in yeast by heterogeneous, age-correlated expression of a stress protectant. *PLoS Biology*, 10, e1001325.
- LEYGEBER, M., LINDEMANN, D., SACHS, C. C., KAGANOVITCH, E., WIECHERT, W., NOH, K. & KOHLHEYER, D. 2019. analyzing microbial population heterogeneity-expanding the toolbox of microfluidic single-cell cultivations. *Journal of Molecular Biology*, 431, 4569-4588.
- LI, C. H. & TAM, P. K. S. 1998. An iterative algorithm for minimum cross entropy thresholding. *Pattern Recognition Letters*, 19, 771-776.
- LING, L. L., SCHNEIDER, T., PEOPLES, A. J., SPOERING, A. L., ENGELS, I., CONLON, B. P., MUELLER, A., SCHABERLE, T. F., HUGHES, D. E., EPSTEIN, S., JONES, M., LAZARIDES, L., STEADMAN, V. A., COHEN, D. R., FELIX, C. R., FETTERMAN, K. A., MILLETT, W. P., NITTI, A. G., ZULLO, A. M., CHEN, C. & LEWIS, K. 2015. A new antibiotic kills pathogens without detectable resistance. *Nature*, 517, 455-459.
- LINN, D. M. & DORAN, J. W. 1984. Aerobic and anaerobic microbial populations in no-till and plowed soils. *Soil Science Society of America Journal*, 48, 794-799.
- LLADÓ, S., LÓPEZ-MONDÉJAR, R. & BALDRIAN, P. 2017. Forest soil bacteria: diversity, involvement in ecosystem processes, and response to global change. *Microbiology and Molecular Biology Reviews*, 81, e00063-16
- LONHIENNE, T., MASON, M. G., RAGAN, M. A., HUGENHOLTZ, P., SCHMIDT, S. & PAUNGFLOO-LONHIENNE, C. 2014. Yeast as a biofertilizer alters plant growth and morphology. *Crop Science*, 54, 785.
- LUCK, A., KLIMMASCH, L., GROSSMANN, P., GERMERODT, S. & KALETA, C. 2018. Computational investigation of environment-noise interaction in single-cell organisms: the merit of expression stochasticity depends on the quality of environmental fluctuations. *Scientific Reports*, 8, 333.
- LUPATINI, M., KORTHALS, G. W., DE HOLLANDER, M., JANSSENS, T. K. & KURAMAE, E. E. 2016. Soil microbiome is more heterogeneous in organic than in conventional farming system. *Frontiers in Microbiology*, 7, 2064.

- MA, W., PENG, D., WALKER, S. L., CAO, B., GAO, C. H., HUANG, Q. & CAI, P. 2017. *Bacillus subtilis* biofilm development in the presence of soil clay minerals and iron oxides. *NPJ Biofilms and Microbiomes*, 3, 4.
- MAHDAVI, S. M., NEYSHABOURI, M. R. & FUJIMAKI, H. 2016. Assessment of some soil thermal conductivity models via variations in temperature and bulk density at low moisture range. *Eurasian Soil Science*, 49, 915-925.
- MAHTO, S. K. & RHEE, S. W. 2012. A multi-inlet microfluidic device fabricated for in situ detection of multiple cytotoxicity endpoints. *BioChip Journal*, 6, 48-55.
- MAIRE, E. & WITHERS, P. J. 2013. Quantitative X-ray tomography. *International Materials Reviews*, 59, 1-43.
- MALISZEWSKA, W., DEC, S., WIERZBICKA, H., & WOZNIAKOWSKA, A. 1985. The influence of various heavy metal compounds on the development and activity of soil microorganisms. *Environmental Pollution A*, 37, 195-215.
- MANGALASSERY, S., MOONEY, S. J., SPARKES, D. L., FRASER, W. T. & SJÖGERSTEN, S. 2015. Impacts of zero tillage on soil enzyme activities, microbial characteristics and organic matter functional chemistry in temperate soils. *European Journal of Soil Biology*, 68, 9-17.
- MARTIN, J. P., MARTIN, W. P., PAGE, J. B., RANEY, W. A. & DE MENT, J. D. 1955. Soil Aggregation. *Advances in Agronomy*, 7, 1-37.
- MASKERY, I., AREMU, A. O., PARRY, L., WILDMAN, R. D., TUCK, C. J. & ASHCROFT, I. A. 2018. Effective design and simulation of surface-based lattice structures featuring volume fraction and cell type grading. *Materials & Design*, 155, 220-232.
- MATEUS, C. & AVERY, S. V. 2000. Destabilized green fluorescent protein for monitoring dynamic changes in yeast gene expression with flow cytometry. *Yeast*, 16, 1313-23.
- MCTEE, M., BULLINGTON, L., RILLIG, M. C. & RAMSEY, P. W. 2019. Do soil bacterial communities respond differently to abrupt or gradual additions of copper? *FEMS Microbiological Ecology*, 95, fiy212 .
- MESTRE, M. C., ROSA, C. A., SAFAR, S. V., LIBKIND, D. & FONTENLA, S. B. 2011. Yeast communities associated with the bulk-soil, rhizosphere and ectomycorrhizosphere of a *Nothofagus pumilio* forest in northwestern Patagonia, Argentina. *FEMS Microbiology Ecology*, 78, 531-41.
- METWALY, M., KHALIL, M., AL-SAYED, E.-S. & OSMAN, S. 2006. A hydrogeophysical study to estimate water seepage from northwestern Lake Nasser, Egypt. *Journal of Geophysics and Engineering*, 3, 21-27.
- MORRISON-WHITTLE, P., LEE, S. A. & GODDARD, M. R. 2017. Fungal communities are differentially affected by conventional and biodynamic agricultural management approaches in vineyard ecosystems. *Agriculture, Ecosystems & Environment*, 246, 306-313.
- MOSETTI, F. 1984. Reynold's number. In: SCHWARTZ, M. (ed.) *Beaches and Coastal Geology*. New York, NY: Springer US.
- MOSS, A. J. & GREEN, P. 1975. Sand and silt grains: Predetermination of their formation and properties by microfractures in quartz. *Journal of the Geological Society of Australia*, 22, 485-495.

- MUMMEY, D. L. & STAHL, P. D. 2004. Analysis of soil whole- and inner-microaggregate bacterial communities. *Microbial Ecology*, 48, 41-50.
- MUSAT, N., HALM, H., WINTERHOLLER, B., HOPPE, P., PEDUZZI, S., HILLION, F., HORREARD, F., AMANN, R., JORGENSEN, B. B. & KUYPERS, M. M. 2008. A single-cell view on the ecophysiology of anaerobic phototrophic bacteria. *Proceedings of the National Academy of Sciences of the United States of America*, 105, 17861-17866.
- MUSTAFA, A., MINGGANG, X., ALI SHAH, S. A., ABRAR, M. M., NAN, S., BAOREN, W., ZEJIANG, C., SAEED, Q., NAVEED, M., MEHMOOD, K. & NUNEZ-DELGADO, A. 2020. Soil aggregation and soil aggregate stability regulate organic carbon and nitrogen storage in a red soil of southern China. *Journal of Environmental Management*, 270, 110894.
- MUTLU, A., TRAUTH, S., ZIESACK, M., NAGLER, K., BERGEEST, J. P., ROHR, K., BECKER, N., HOFER, T. & BISCHOF, I. B. 2018. Phenotypic memory in *Bacillus subtilis* links dormancy entry and exit by a spore quantity-quality tradeoff. *Nature Communications*, 9, 69.
- NADELL, C. D., RICAURTE, D., YAN, J., DRESCHER, K. & BASSLER, B. L. 2017. Flow environment and matrix structure interact to determine spatial competition in *Pseudomonas aeruginosa* biofilms. *Elife*, 6.
- NAVAS, M., PÉREZ-ESTEBAN, J., TORRES, M. A., HONTORIA, C. & MOLINER, A. 2020. Taxonomic and functional analysis of soil microbial communities in a mining site across a metal(loid) contamination gradient. *European Journal of Soil Science*, 72, 1190-1205.
- NEAL, A. L., BACQ-LABREUIL, A., ZHANG, X., CLARK, I. M., COLEMAN, K., MOONEY, S. J., RITZ, K. & CRAWFORD, J. W. 2020. Soil as an extended composite phenotype of the microbial metagenome. *Scientific Reports*, 10, 10649.
- NGO, T. D., KASHANI, A., IMBALZANO, G., NGUYEN, K. T. Q. & HUI, D. 2018. Additive manufacturing (3D printing): A review of materials, methods, applications and challenges. *Composites Part B: Engineering*, 143, 172-196.
- NGUYEN, L. D., KALACHOVA, L., NOVOTNA, J., HOLUB, M., KOFRONOVA, O., BENADA, O., THOMPSON, C. J. & WEISER, J. 2005. Cultivation system using glass beads immersed in liquid medium facilitates studies of *Streptomyces* differentiation. *Applied Environmental Microbiology*, 71, 2848-52.
- NICHOLS, D., CAHOON, N., TRAKHTENBERG, E. M., PHAM, L., MEHTA, A., BELANGER, A., KANIGAN, T., LEWIS, K. & EPSTEIN, S. S. 2010. Use of ichip for high-throughput in situ cultivation of "uncultivable" microbial species. *Applied Environmental Microbiology*, 76, 2445-2450.
- NIKOLIC, N., SCHREIBER, F., DAL CO, A., KIVIET, D. J., BERGMILLER, T., LITTMANN, S., KUYPERS, M. M. M. & ACKERMANN, M. 2017. Cell-to-cell variation and specialization in sugar metabolism in clonal bacterial populations. *PLoS Genetics*, 13, e1007122.
- NIMMO, J. R. 2005a. aggregation: physical aspects, in Hillel, D., ed., *Encyclopedia of Soils in the Environment*: London, Academic Press.
- NIMMO, J. R. 2005b. Porosity and pore size distribution, in Hillel, D., ed., *Encyclopedia of Soils in the Environment*. London: Academic Press.

- NOVOTNY, J. & FORET, F. 2017. Fluid manipulation on the micro-scale: Basics of fluid behavior in microfluidics *Journal of Separation Science*, 40, 383-394.
- NUNAN, N. 2017. The microbial habitat in soil: Scale, heterogeneity and functional consequences. *Journal of Plant Nutrition and Soil Science*, 180, 425-429.
- OR, D., SMETS, B. F., WRAITH, J. M., DECHESNE, A. & FRIEDMAN, S. P. 2007. Physical constraints affecting bacterial habitats and activity in unsaturated porous media – a review. *Advances in Water Resources*, 30, 1505-1527.
- ORROÑO, D. I. & LAVADO, R. S. 2015. Distribution of extractable heavy metals in different soil fractions. *Chemical Speciation & Bioavailability*, 21, 193-198.
- OTTEN, W., PAJOR, R., SCHMIDT, S., BAVEYE, P. C., HAGUE, R. & FALCONER, R. E. 2012. Combining X-ray CT and 3D printing technology to produce microcosms with replicable, complex pore geometries. *Soil Biology and Biochemistry*, 51, 53-55.
- OZBUDAK, E. M., THATTAI, M., KURTSEY, I., GROSSMAN, A. D. & VAN OUDENAARDEN, A. 2002. Regulation of noise in the expression of a single gene. *Nature Genetics*, 31, 69-73.
- PAGLIAI, M., VIGNOZZI, N. & PELLEGRINI, S. 2004. Soil structure and the effect of management practices. *Soil and Tillage Research*, 79, 131-143.
- PALMER, R. C. & SMITH, R. P. 2013. Soil structural degradation in SW England and its impact on surface-water runoff generation. *Soil Use and Management*, 29, 567-575.
- POURRUT, B., SHAHID, M., DUMAT, C., WINTERTON, P. & PINELLI, E. 2011. Lead uptake, toxicity, and detoxification in plants. *Reviews of Environmental Contamination and Toxicology*, 213, 113-36.
- PREIBISCH, S., SAALFELD, S. & TOMANCAK, P. 2009. Globally optimal stitching of tiled 3D microscopic image acquisitions. *Bioinformatics*, 25, 1463-5.
- RABBI, S. M., DANIEL, H., LOCKWOOD, P. V., MACDONALD, C., PEREG, L., TIGHE, M., WILSON, B. R. & YOUNG, I. M. 2016. Physical soil architectural traits are functionally linked to carbon decomposition and bacterial diversity. *Scientific Reports*, 6, 33012.
- RASER, J. M. & O'SHEA, E. K. 2004. Control of stochasticity in eukaryotic gene expression. *Science*, 304, 1811-4.
- RIAH-ANGLET, W., TRINSOUTROT-GATTIN, I., MARTIN-LAURENT, F., LAROCHE-AJZENBERG, E., NORINI, M.-P., LATOUR, X. & LAVAL, K. 2015. Soil microbial community structure and function relationships: A heat stress experiment. *Applied Soil Ecology*, 86, 121-130.
- RICHARDS, K. J., CHARNOCK, H., EDMOND, J. M., MCCAVE, I. N., RICE, A. L. & WILSON, T. R. S. 1990. Physical processes in the benthic boundary layer. *Philosophical Transactions of the Royal Society of London. Series A, Mathematical and Physical Sciences*, 331, 3-13.
- RILLIG, M. C., MULLER, L. A. & LEHMANN, A. 2017. Soil aggregates as massively concurrent evolutionary incubators. *The ISME Journal*, 11, 1943-1948.
- RUBINSTEIN, R. L., KADILAK, A. L., COUSENS, V. C., GAGE, D. J. & SHOR, L. M. 2015. Protist-facilitated particle transport using emulated soil micromodels. *Environmental Science Technology*, 49, 1384-1391.

- SASAL, M. C., ANDRIULO, A. E. & TABOADA, M. A. 2006. Soil porosity characteristics and water movement under zero tillage in silty soils in Argentinian Pampas. *Soil and Tillage Research*, 87, 9-18.
- SAUVÉ, S., MCBRIDE, M. & HENDERSHOT, W. 1998. Soil solution speciation of lead(II): effects of organic matter and pH. *Soil Science Society of America Journal*, 62, 618-621.
- SCHELER, O., MAKUCH, K., DEBSKI, P. R., HORKA, M., RUSZCZAK, A., PACOCHA, N., SOZANSKI, K., SMOLANDER, O. P., POSTEK, W. & GARSTECKI, P. 2020. Droplet-based digital antibiotic susceptibility screen reveals single-cell clonal heteroresistance in an isogenic bacterial population. *Scientific Reports*, 10, 3282.
- SCHINDELIN, J., ARGANDA-CARRERAS, I., FRISE, E., KAYNIG, V., LONGAIR, M., PIETZSCH, T., PREIBISCH, S., RUEDEN, C., SAALFELD, S., SCHMID, B., TINEVEZ, J. Y., WHITE, D. J., HARTENSTEIN, V., ELICEIRI, K., TOMANCAK, P. & CARDONA, A. 2012. Fiji: an open-source platform for biological-image analysis. *Nature Methods*, 9, 676-682.
- SCHLÜTER, S., HENJES, S., ZAWALLICH, J., BERGAUST, L., HORN, M., IPPISCH, O., VOGEL, H.-J. & DÖRSCH, P. 2018. Denitrification in soil aggregate analogues-effect of aggregate size and oxygen diffusion. *Frontiers in Environmental Science*, 6, 17.
- SCHMIDT, P. A., SCHMITT, I., OTTE, J., BANDOW, C., ROMBKE, J., BALINT, M. & ROLSHAUSEN, G. 2018. Season-long experimental drought alters fungal community composition but not diversity in a grassland soil. *Microbial Ecology*, 75, 468-478.
- SCHNEE, L. S., KNAUTH, S., HAPCA, S., OTTEN, W. & EICKHORST, T. 2016. Analysis of physical pore space characteristics of two pyrolytic biochars and potential as microhabitat. *Plant and Soil*, 408, 357-368.
- SCHULZE, I., HANSEN, S., GROßHANS, S., RUDSZUCK, T., OCHSENREITHER, K., SYLDATK, C. & NEUMANN, A. 2014. Characterization of newly isolated oleaginous yeasts - *Cryptococcus podzolicus*, *Trichosporon porosum* and *Pichia segobiensis*. *AMB Express*, 4, 24.
- SEATON, F. M., GEORGE, P. B. L., LEBRON, I., JONES, D. L., CREER, S. & ROBINSON, D. A. 2020. Soil textural heterogeneity impacts bacterial but not fungal diversity. *Soil Biology and Biochemistry*, 144, 107766.
- SEU, K. J., PANDEY, A. P., HAQUE, F., PROCTOR, E. A., RIBBE, A. E. & HOVIS, J. S. 2007. Effect of surface treatment on diffusion and domain formation in supported lipid bilayers. *Biophysical Journal*, 92, 2445-50.
- SEXSTONE, A. J., REVSBECH, N. P., PARKIN, T. B. & TIEDJE, J. M. 1985. Direct measurement of oxygen profiles and denitrification rates in soil aggregates. *Soil Science Society of America Journal*, 49, 645-651.
- SHARMA, R. K. & AGRAWAL, M. 2005. Biological effects of heavy metals: an overview. *Journal of Environmental Biology*, 26, 301-13.
- SHEARER, T., BRADLEY, R. S., HIDALGO-BASTIDA, L. A., SHERRATT, M. J. & CARTMELL, S. H. 2016. Three-dimensional visualisation of soft biological structures by X-ray computed micro-tomography. *Journal of Cell Science*, 129, 2483-92.

- SHERMAN, F. 2002. Getting started with yeast. *In: GUTHRIE, C. & FINK, G. R. (eds.) Methods in Enzymology*. Academic Press.
- SIEMERING, K. R., GOLBIK, R., SEVER, R. & HASELOFF, J. 1996. Mutations that suppress the thermosensitivity of green fluorescent protein. *Current Biology*, 6, 1653-1663.
- SIX, J., ELLIOTT, E. T. & PAUSTIAN, K. 2000. Soil macroaggregate turnover and microaggregate formation: a mechanism for C sequestration under no-tillage agriculture. *Soil Biology and Biochemistry*, 32, 2099-2103.
- SLEGEL, D. L. & DAVIS, L. R. 1977. Transient Heat and Mass Transfer in Soils in the Vicinity of Heated Porous Pipes. *Journal of Heat Transfer*, 99, 541-546.
- SMITH, M. C., SUMNER, E. R. & AVERY, S. V. 2007. Glutathione and Gts1p drive beneficial variability in the cadmium resistances of individual yeast cells. *Molecular Microbiology*, 66, 699-712.
- SMITH, T. 2000. Antibiotics from soil bacteria. *Nature Structural Biology*, 7, 189-90.
- SOUFAN, R., DELAUNAY, Y., GONOD, L. V., SHOR, L. M., GARNIER, P., OTTEN, W. & BAVEYE, P. C. 2018. Pore-scale monitoring of the effect of microarchitecture on fungal growth in a two-dimensional soil-like micromodel. *Frontiers in Environmental Science*, 6, 68.
- STEELS, H., JAMES, S. A., ROBERTS, I. N. & STRATFORD, M. 2000. Sorbic acid resistance: the inoculum effect. *Yeast*, 16, 1173-1183.
- STOCK, S. R. 2013. Recent advances in X-ray microtomography applied to materials. *International Materials Reviews*, 53, 129-181.
- STOCKHOLM, D., BENCHAOUIR, R., PICOT, J., RAMEAU, P., NEILDEZ, T. M., LANDINI, G., LAPLACE-BUILHE, C. & PALDI, A. 2007. The origin of phenotypic heterogeneity in a clonal cell population in vitro. *PLoS One*, 2, e394.
- STRATFORD, M., STEELS, H., NEBE-VON-CARON, G., AVERY, S. V., NOVODVORSKA, M. & ARCHER, D. B. 2014. Population heterogeneity and dynamics in starter culture and lag phase adaptation of the spoilage yeast *Zygosaccharomyces bailii* to weak acid preservatives. *International Journal of Food Microbiology*, 181, 40-47.
- STRELETSKII, R. A., KACHALKIN, A. V., GLUSHAKOVA, A. M., DEMIN, V. V. & CHERNOV, I. Y. 2016. Quantitative determination of indole-3-acetic acid in yeasts using high performance liquid chromatography—tandem mass spectrometry. *Microbiology*, 85, 727-736.
- SUMNER, E. R., AVERY, A. M., HOUGHTON, J. E., ROBINS, R. A. & AVERY, S. V. 2003. Cell cycle- and age-dependent activation of Sod1p drives the formation of stress resistant cell subpopulations within clonal yeast cultures. *Molecular Microbiology*, 50, 857-70.
- SUMNER, E. R. & AVERY, S. V. 2002. Phenotypic heterogeneity: differential stress resistance among individual cells of the yeast *Saccharomyces cerevisiae*. *Microbiology*, 148, 345-51.
- SUMNER, M. E. 2000. *Handbook of Soil Science*, Boca Raton, CRC Press.
- TAKAHASHI, M. & FUJI, M. 2002. Synthesis and fabrication of inorganic porous materials: from nanometer to millimeter sizes. *kona powder and particle journal*, 20, 84-97.

- TIWARI, S. & LATA, C. 2018. Heavy metal stress, signaling, and tolerance due to plant-associated microbes: an overview. *Frontiers in Plant Science*, 9, 452.
- TOTH, G., HERMANN, T., DA SILVA, M. R. & MONTANARELLA, L. 2016. Heavy metals in agricultural soils of the European Union with implications for food safety. *Environmental International*, 88, 299-309.
- UPTON, R. N., BACH, E. M. & HOFMOCKEL, K. S. 2019. Spatio-temporal microbial community dynamics within soil aggregates. *Soil Biology and Biochemistry*, 132, 58-68.
- VAGASKA, B., BACAKOVA, L., FILOVA, E. & BALIK, K. 2010. Osteogenic cells on bio-inspired materials for bone tissue engineering. *Physiological Research*, 59, 309-22.
- VAN DEN BERGH, B., SWINGS, T., FAUVART, M. & MICHIELS, J. 2018. Experimental design, population dynamics, and diversity in microbial experimental evolution. *Microbiology Molecular Biology Reviews*, 82, e00008-e000018.
- VERDIER, T., COUTAND, M., BERTRON, A. & ROQUES, C. 2014. A review of indoor microbial growth across building materials and sampling and analysis methods. *Building and Environment*, 80, 136-149.
- VERRAN, J., PACKER, A., KELLY, P. & WHITEHEAD, K. A. 2010. The retention of bacteria on hygienic surfaces presenting scratches of microbial dimensions. *Letters in Applied Microbiology*, 50, 258-63.
- WAKSMAN, S. A. & GREGORY, F. J. 1954. Actinomycin. II. Classification of organism producing different forms of actinomycin. *Antibiotic Chemotherapy (Northfield)*, 4, 1050-1056.
- WANG, X., KANG, Y., LUO, C., ZHAO, T., LIU, L., JIANG, X., FU, R., AN, S., CHEN, J., JIANG, N., REN, L., WANG, Q., BAILLIE, J. K., GAO, Z. & YU, J. 2014. Heteroresistance at the single-cell level: adapting to antibiotic stress through a population-based strategy and growth-controlled interphenotypic coordination. *MBio*, 5, e00942-13.
- WANG, Y., SHI, J., WANG, H., LIN, Q., CHEN, X. & CHEN, Y. 2007. The influence of soil heavy metals pollution on soil microbial biomass, enzyme activity, and community composition near a copper smelter. *Ecotoxicology and Environmental Safety*, 67, 75-81.
- WATTS, C. W., WHALLEY, W. R., BROOKES, P. C., DEVONSHIRE, B. J. & WHITMORE, A. P. 2005. Biological and physical processes that mediate micro-aggregation of clays. *Soil Science*, 170, 573-583.
- WHITAKER, S. 1986. Flow in porous media i: a theoretical derivation of darcy's law. *Transport in Porous Media*, 1, 3-25.
- WHITE T J, BRUN T, LEE S, TAYLOR J. 1990. Amplification and direct sequencing of fungal ribosomal RNA genes for phylogenetics. In: Innis M A, Gelfand D H, Sninsky J J, White T J, eds., PCR Protocols. A Guide to Methods and Applications. Academic Press, San Diego, USA. pp. 315–320.
- WHITTAKER JA, JOHNSON RI, FINNIGAN TJA, AVERY SV, DYER PS. The biotechnology of Quorn mycoprotein: past, present and future challenges. In: Nevalainen H, editor. Grand challenges in fungal biotechnology. Cham: Springer; 2020. pp. 59–79.

- WOHLGEMUTH, F., GOMES, R. L., SINGLETON, I., RAWSON, F. J. & AVERY, S. V. 2020. Top-down characterization of an antimicrobial sanitizer, leading from quenchers of efficacy to mode of action. *Frontiers in Microbiology*, 11, 575157.
- WUBS, E. R., VAN DER PUTTEN, W. H., BOSCH, M. & BEZEMER, T. M. 2016. Soil inoculation steers restoration of terrestrial ecosystems. *Nature Plants*, 2, 16107.
- YAN, N., MARSCHNER, P., CAO, W., ZUO, C. & QIN, W. 2015. Influence of salinity and water content on soil microorganisms. *International Soil and Water Conservation Research*, 3, 316-323.
- YANG, C., LIU, N. & ZHANG, Y. 2019. Soil aggregates regulate the impact of soil bacterial and fungal communities on soil respiration. *Geoderma*, 337, 444-452.
- YOUNG, I. M. & CRAWFORD, J. W. 2004. Interactions and self-organization in the soil-microbe complex. *Science*, 304, 1634-1637.
- YURKOV, A. M. 2018. Yeasts of the soil - obscure but precious. *Yeast*, 35, 369-378.
- ZAFFAR, M. & LU, S.-G. 2015. Pore size distribution of clayey soils and its correlation with soil organic matter. *Pedosphere*, 25, 240-249.
- ZHANG, S., CAO, K., WANG, C., WANG, X., DENG, G. & WEI, P. 2020. Influence of the porosity and pore size on the compressive and splitting strengths of cellular concrete with millimeter-size pores. *Construction and Building Materials*, 235.
- ZHAO, Y. P., LIN, S., CHU, L., GAO, J., AZEEM, S. & LIN, W. 2016. Insight into structure dynamics of soil microbiota mediated by the richness of replanted *Pseudostellaria heterophylla*. *Scientific Reports*, 6, 26175.
- ZIMMERMANN, M., ESCRIG, S., LAVIK, G., KUYPERS, M. M. M., MEIBOM, A., ACKERMANN, M. & SCHREIBER, F. 2018. Substrate and electron donor limitation induce phenotypic heterogeneity in different metabolic activities in a green sulphur bacterium. *Environmental Microbiology Reports*, 10, 179-183.